SCUOLA INTERNAZIONALE SUPERIORE STUDI AVANZATI (SISSA)
INTERNATIONAL SCHOOL FOR ADVANCED STUDIES
PhD COURSE IN FUNCTIONAL AND STRUCTURAL GENOMICS
NEUROSCIENCE AREA
Trieste, Italy



RNA therapeutics of neuropathogenic haploinsufficiencies

THESIS SUBMITTED FOR THE DEGREE OF "DOCTOR PHILOSOPHIAE"
Academic Year 2015/2016

Candidate:
Cristina Fimiani

Supervisor:
Prof. Antonello Mallamaci

ABSTRACT

Artificial transactivation of endogenous genes ad libitum is a desirable goal for a number of basic and applied research purposes. For this purpose, we recently developed a fully synthetic ribonucleoproteic transactivator prototype. Kept together via an MS2 coat protein/RNA interface, it includes a fixed, polypeptidic transactivating domain and a variable RNA domain that recognizes the desired gene. Thanks to this device, we specifically upregulated five genes, in cell lines and primary cultures of murine pallial precursors. Even if gene upregulation was small, however it was sufficient to inhibit neuronal differentiation. Our transactivator activity was restricted to cells in which the target gene is normally transcribed. These features make our prototype a promising tool for clean rescue of gene haploinsufficiencies, since it could lead to a specific overstimulation of the spared gene allele in its physiological expression domain.

On the other hand, we are interested in stimulating transcription of endogenous genes by small activating RNAs (saRNAs). These are miRNA/siRNA-like molecules, supposed to destabilize transcription-inhibiting ncRNAs or facilitate the recruitment of transcription transactivating complexes to chromatin. The expression gain they elicit is small; however it may be sufficient to modify the behaviour of cells in a robust way. They comply with endogenous gene tuning. Moreover, silent genes generally do not respond to them. As such, also saRNAs are a promising tool for therapeutic stimulation of gene transcription. We selected a number of saRNAs able to stimulate haploinsufficient genes involved in CNS morphogenesis and physiology. We reconstructed their mechanism of action. We provided proof-of-principle they can be exploited for in vivo correction of defective gene expression.

INDEX

1.Introduction 1

1.1 Neuropathological haploinsufficiencies 1

1.2 Genetic treatment of haploisufficiencies 2

1.2.1 Zinc-finger-based genomic manipulations 3

1.2.2 Transcription activator-like effectors (TALEs) 5

1.2.3 The clustered regularly interspaced short palindromic repeats CRISPR/Cas9 system 9

1.2.4 Novel RNA-programmable transcription factors (NMHV) 13

1.2.5 RNA activation (RNAa) 14

1.3 Choice of haploinsufficient genes 16

1.3.1 *FOXG1* and Rett syndrome 17

1.3.2 *FRATAXIN* and Friedreich's ataxia 21

1.3.3 *SCN1A* and Dravet syndrome 28

2. Materials and Methods 33

3. Aim of the work 45

4. Results 46

4.1 Upregulating endogenous genes by an RNA-programmable artificial transactivator 46

4.1.1 Upregulation of endogenous genes by artificial, non-CRISPR, RNA-programmable transactivator 46

4.1.2 Specific upregulation of brain patterning genes in pallial precursors by dedicated RNA-programmable transactivators and its biological consequences 53

4.1.3 Shortening the baits and assessing mismatch tolerance of our device 60

4.2 RNA activation of haploinsufficient Foxg1 gene in murine neocortex 62

4.2.1 Selecting miRNA-like saRNAs upregulating *Foxg1*-mRNA 62

4.2.2 Compliance of RNAa with endogenous tuning of *Foxg1*-mRNA 66

4.2.3 Molecular mechanisms underlying *Foxg1*-RNAa 68

4.2.4 In vivo *Foxg1*-RNAa 71

4.3 Portability of RNA activation (RNAa) to other haploinsufficient genes 74

4.3.1 Selecting miRNA-like saRNAs upregulating *FXN*-mRNA 74

4.3.2 Combination of *FXN*-saRNAs with HDAC inhibitors 78
4.3.3 Molecular mechanisms underlying *FXN*-RNAa: a preliminary assessment 81
4.3.4 Selecting miRNA-like saRNAs upregulating *Scn1a*-mRNA 83
4.3.5 Combinatorial transcriptional/translational stimulation of *Scn1a* gene 84
5. Discussion 86
6. Supplementary figures & tables 97
7. Bibliography 122

1. INTRODUCTION

1.1 Neuropathological haploinsufficiencies

An increasing number of neurodevelopmental disorders with relatively high prevalence in the general population, including autism spectrum disorders (1%), epilepsy (0.8%), schizophrenia (1%) and intellectual disability (2%), as well as neurodegenerative diseases, have been recently associated to copy number variations and, in some cases, to haploinsufficiency for specific genes (van Bokhoven, 2011).

Organisms heterozygous for a loss-of-function allele often have no discernible phenotype. This observation has been attributed to the metabolic theory of dominance described over 30 years ago. Briefly, this model states that the phenotypic consequences of heterozygous loss-of-function alleles are masked by the presence of one wild-type allele due to the redundancy of cellular physiology (Kacser and Burns, 1981). There are, however, exceptions to this rule where deletion of a single gene copy leads to an abnormal phenotype. Such haploinsufficiency is observed in all eukaryotes from yeast to humans. In yeast, the phenomenon has been characterized in gene-by-gene analyses of, for example, cytoskeletal components such as actin (*ACT1*) (Drubin et al., 1993), tubulin (*TUB1*) (Schatz et al., 1986), and components of the spindle pole body (*NDC1*) (Chial et al., 1999) . An explanation for the observation of reduced fitness in these heterozygous strains is provided by biochemical studies showing that a balance of protein levels is required to maintain cytoskeletal integrity.

The relevance of haploinsufficiency to human disease has become increasingly apparent. Many of the haploinsufficient mutations in humans are observed in transcription factors including *TWIST* (Johnson et al., 1998) and *GATA3* (Muroya et al., 2001). It is not surprising that such haploinsufficiencies are detrimental, as they should result in multiple transcription defects of diverse downstream targets (Seidman and Seidman, 2002). Haploinsufficiency has also been implicated in cancer: heterozygous mutations in

both *ATM* (Spring et al., 2002) and *BLM* (Goss et al., 2002) result in increased cancer susceptibility.

1.2 Genetic treatment of haploisufficiencies

Nowadays, different approaches to rescue the correct gene dosage may be employed:

(1) delivering a miniaturized extra-copy of the missing allele, a so-called mini-gene, comprising all the regulatory sequences normally present in the gene locus;

(2) entering a faithful copy of the missing allele into the defective chromosome, by means of artificial, engineered endonucleases (EENs) and endogenous DNA repair machineries;

(3) stimulating the spared, haploinsufficient allele, in order to restore the corresponding physiological protein level even in an hemizygous scenario.

As for (1), it is hardly feasible. Our genes often undergo a complex modulation of their expression, locked to metabolic and functional fluctuations of the cell in order and possibly instrumental to their proper articulation. That expecially applies to *neuronal genes*. Therefore, firstly, building a therapeutically plausible minigene will require a deep and accurate knowledge of all the mechanisms governing natural expression of every single gene. That is neither simple nor cheap. Moreover, it will require the recapitulation of these mechanisms in a small, deliverable transgenic cassette, which may result extremely difficult or impossible at all.

As for (2), homologous recombination (HR)-mediated correction of the defective chromosome/gene, triggered by an EEN and relying on an editor DNA, is hardly applicable to rescue of haploinsufficiencies, since DNA repair via non-homologous end joining (NHEJ) often

overcomes DNA repair via HR, in particular in neuronal cells (Orii 2006, Yang, 2013). Moreover, the large size of editor DNA needed for these manipulations (often in the range of Mb) hardly fits the commonly used devices for central nervous system gene delivery.

Alternatively (3), the haploinsufficiency problem might be solved relying on the spared allele, under the control of the whole array of cis- and trans-activg regulatory elements which normally influence its expression. This last approach might be implemented thanks to different effectors, able to stimulate transcription of endogenous genes. These include: (a) established artificial transactivators, such as Zinc-Finger (ZF)-type-, Transcription activator-like effectors (TALEs)-type- and Clustered Regularly Interspaced Short Palindromic Repeats (CRISPR)/Cas9-type-transactivators; (b) novel, ad hoc developed, RNA-programmable transcription factors; (c) small activating RNAs (saRNAs), giving "small-RNA-driven transcriptional activation" (RNAa).

1.2.1 Zinc finger-based genetic manipulation

The Cys_2–His_2 zinc-finger domain is among the most common types of DNA-binding motifs found in eukaryotes and represents the second most frequently encoded protein domain in the human genome. An individual zinc-finger consists of approximately 30 amino acids in a conserved ββα configuration (Beerli and Barbas, 2002). Several amino acids on the surface of the α-helix typically contact 3 bp in the major groove of DNA, with varying levels of selectivity. The modular structure of zinc-finger proteins has made them an attractive framework for the design of custom DNA-binding proteins. Key to the application of zinc-finger proteins for specific DNA recognition was the development of unnatural arrays that contain more than three zinc-finger domains. This advance was facilitated by the structure-based discovery of a highly conserved linker sequence that enabled construction of synthetic zinc-finger proteins that recognized DNA sequences 9–18 bp in length (Liu et al., 1997). Because 18 bp of DNA sequence can confer specificity within 68 billion bp of DNA, this method allowed for specific sequences to be targeted in the human genome for the first time (Beerli et al., 1998, 2000). Although initially controversial (Kim et al., 2011), this design

has proven to be the optimal strategy for constructing zinc-finger proteins that recognize contiguous DNA sequences that are specific in complex genomes (Beerli and Barbas, 2002; Liu et al., 1997; Beerli et al., 2000, 1998; Segal et al., 2006; Neuteboom et al., 2006; Bhakta et al., 2013; Kim et al., 2011; Gonzalez et al., 2010) (Figure 1.1).

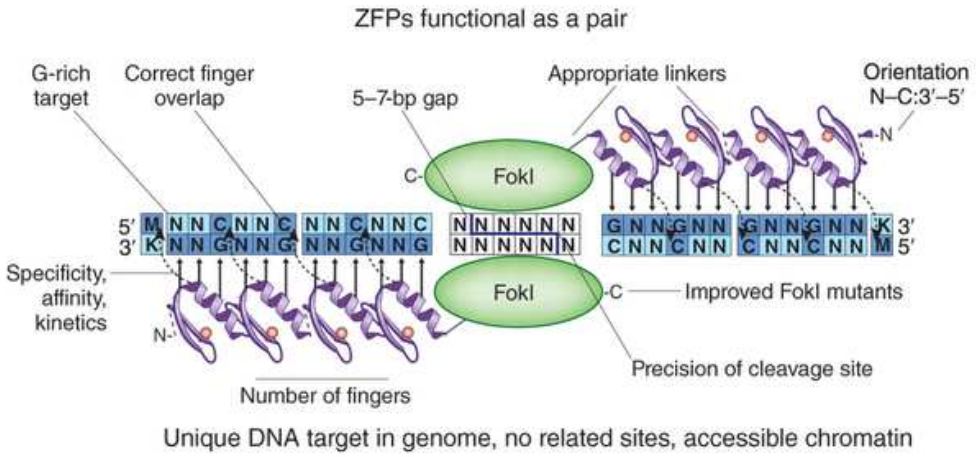


Figure 1.1. **Schematics of a canonical zinc-finger nuclease (ZFN).** The two four-finger pairs bind to DNA in a canonical mode and the main engineering constraints and considerations are highlighted. Zinc-finger binding sites are shaded in blue (darker for the main contacted DNA bases). Adapted from Isalan, 2011

Following this proof-of-principle work, several methods for constructing zinc-finger proteins with unique DNA-binding specificity were developed. The 'modular assembly' approach involves the use of a preselected library of zinc-finger modules generated by selection of large combinatorial libraries or by rational design (Beerli and Barbas, 2002; Segal et al., 1999). Because zinc-finger domains have been developed that recognize nearly all of the 64 possible nucleotide triplets, preselected zinc-finger modules can be linked together in tandem to target DNA sequences that contain a series of these DNA triplets (Beerli and Barbas, 2002; Beerli et al., 1998; Bhakta et al., 2013; Kim et al., 2011; Gonzalez et al., 2010; Beerli et al., 2000). Alternatively, selection-based approaches, such as oligomerized pool

engineering (OPEN) can be used to select for new zinc-finger arrays from randomized libraries that take into consideration context-dependent interactions between neighboring fingers (Maeder et al., 2008). Approaches have also been developed that combine the methods described above, utilizing zinc-finger modules preselected for context-dependency to assemble longer arrays by modular assembly (Sander et al., 2011; Gupta et al., 2012). Broadly, zinc-finger protein technology enables targeting of virtually any sequence.

ZF-architectures with DNA-recognition functions may be incorporated into chimaeric proteins, including different effector modules. One of them is the FokI-nuclease domain, originating from the corresponding bacterial restrictase and able to cut double-strand DNA upon dimerization. Acting as heterodimers, ZF_n-FokI chimaeras are among the earliest EENs employed to specifically cut genomic DNA in vivo. Coupled to endogenous HR-machinery and an exogenous editor DNA, they may effectively prime precise genome editing in the surroundings of their cutting site (Urnov et al., 2005; Klug, 2010). As such, they might theoretically support the entering of the missing allele of a haploinsufficient gene into the corresponding defective chromosome (Klug, 2010). Alternatively, a ZF_narray recognizing the surroundings of the haploinsufficient gene transcriptional start site (TSS) may be joined to a transactivating domain (e.g. VP16), so resulting into an artificial chimaeric transactivator, stimulating gene transcription (Klug, 2010).

1.2.2. Transcription activator-like effectors (TALE)

Transcription activator-like effectors (TALEs) are proteins secreted by *Xanthomonas* bacteria to aid the infection of plant species. TALEs assist infections by binding to specific host DNA sequences and activating the expression of host genes (Römer et al., 2007). TALEs have a modular DNA-binding domain (DBD) consisting of repetitive sequences of residues; each repeat region consists of 34 amino acids (Kay et al., 2007; Muñoz Bodnar et al., 2013). A pair of residues at the 12th and 13th position of each repeat region determines the nucleotide specificity and is referred to as the repeat variable diresidue (RVD) (Boch et al., 2009). The last repeat region, termed the half-repeat, is typically

truncated to 20 amino acids (Bogdanove and Voytas, 2011). Combining these repeat regions allows synthesizing sequence-specific synthetic TALEs (Garg et al., 2012; Carlson et al., 2012). The C-terminus typically contains a nuclear localization signal (NLS), which directs a TALE to the nucleus, as well as a functional domain that modulates transcription, such as an acidic activation domain (AD) (Boch et al., 2009; Schornack et al., 2008; Gürlebeck et al., 2005; Kay et al., 2005). The endogenous NLS can be replaced by an organism-specific localization signal. For example, an NLS derived from the simian virus 40 large T-antigen can be used in mammalian cells (Zhang et al., 2011a). The RVDs HD, NG, NI, and NN target C, T, A, and G/A (Bogdanove and Voytas, 2011; Cong et al., 2012; Moscou and Bogdanove, 2009), respectively. Recent studies suggest that NH has a higher specificity for G than NN and results in stronger TALE binding (Cong et al., 2012). This basic code enables DNA targeting where each RVD corresponds to a specific nucleotide. Out of the RVDs that have close to a one-to-one correspondence, HD and NH bind more strongly to DNA and target C and G, respectively (Cong et al., 2012) (Figure 1.2).

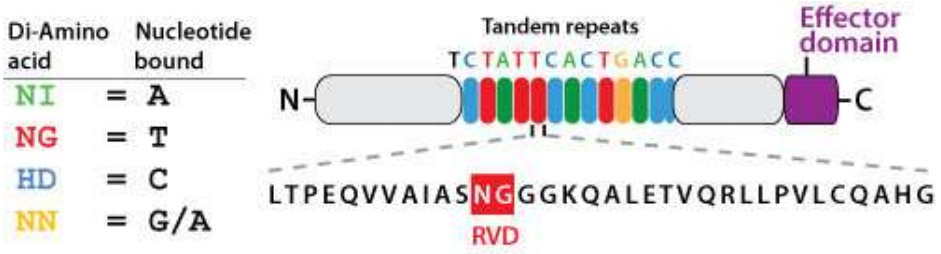


Figure 1.2. Schematics of a transcription-activator-like effector. The corresponding RVD for each nucleotide is shown. he DNA binding domain of the TALE protein includes several repeat modules of 34 residues flanked by an N and C-terminus, which may include mammalian NLS or functional domains. Adapted from https://www.systembio.com

Multiple examples of engineered TALE have been reported (Figure 1.3). TALE nucleases (TALEN) utilize a C-terminal fusion with the type II restriction enzyme FokI to create a heterodimer which produces a double-stranded break (DSB) in DNA (Christian et al., 2010). Nuclease-induced DSBs are repaired by nonhomologous end joining (NHEJ) or

homologous directed repair (HDR), where homologous recombination (HR) is the most important type of HDR. NHEJ is an error-prone mechanism that results in a functional gene knockout by creating small insertions or deletions (indels) while HR, in combination with a template donor DNA sequence, results in a gene insertion or direct nucleotide exchange (Moore et al., 2012; Orlando et al., 2010).

The majority of the repression examples rely on fusing the TALE with a functional domain known to interfere with the RNA Polymerase II complex. TALEs with either the KRAB domain (Peng et al., 2000) or the mSin3 interacting domain inhibit mammalian transcription (Cong et al., 2012; Li et al., 2012). Furthermore, TALE repressors in combination with post-transcriptional repressors such as shRNA show virtually complete repression in mammalian cells (Garg et al., 2012).

For activation, fusing the herpes simplex virus derived VP-16 or VP-64 activation domains to a TALE can cause an increase in transcription (Zhang et al., 2011a; Perez-Pinera et al., 2013). Weaker activation domains such as the one of human NF-κB add to the variety of options for gene activation (Li et al., 2012). Furthermore, as shown on endogenous promoters (Maeder et al., 2013), combinations of TALE activators can be used to introduce synergistic effects.

Moreover, TALE-recombinases (TALER) have been developed in order to allow to site-specific recombinases (SSRs) the possibility of integrate, excise, invert specific DNA segments (Mercer et al., 2012). Fusion of LSD1 demethylase to TALE was recently used to demonstrate epigenetic control in mammalian cells. The TALE-LSD1 fusion altered the chromatin at enhancers and modified gene expression (Mendenhall et al., 2013).

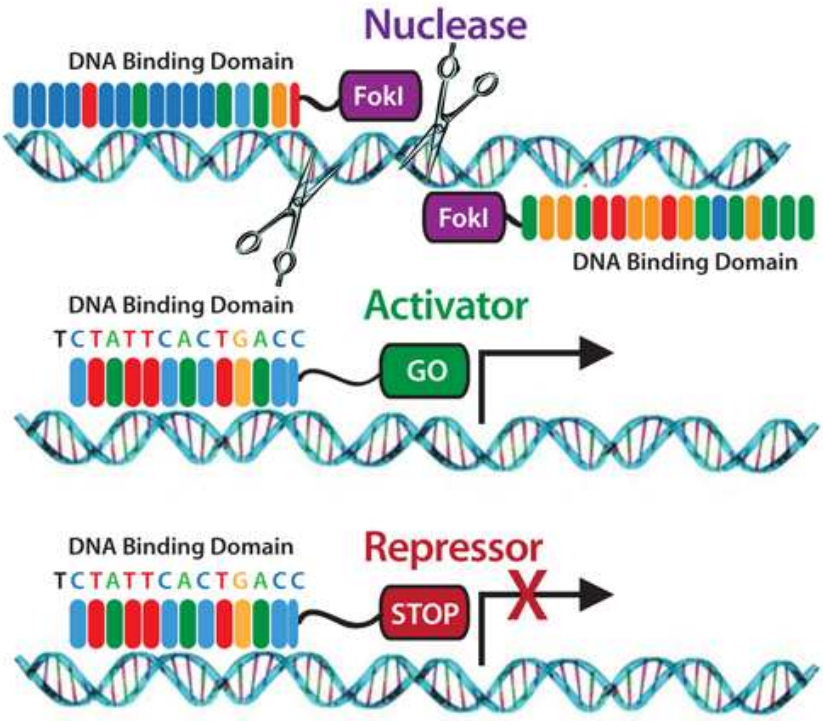


Figure 1.3. Examples of TALE-driven effectors. TALE DNA binding domain can drive nuclease activity, as well as gene-transactivating activity and gene-repression. Adapted from http://www.ozyme.fr/

1.2.3 The Clustered Regularly Interspaced Short Palindromic Repeats CRISPR-Cas9 system

First applied in mammalian cells in 2013 (Cong et al., 2013; Mali et al., 2013a), the clustered regularly interspaced short palindromic repeats CRISPR/Cas9 genome editing tool is adapted from microbial adaptive immune defense system. The type II CRISPR from *Streptococcus pyogenes* encodes a RNA-guided endonuclease protein, Cas9 (including RuvC and HNH domains), which was shown to use only two small RNAs (a mature crRNA and a *trans*-acting tracrRNA) for sequence-specific DNA recognition and cleavage (Jinek et al., 2012; Deltcheva et al., 2011; Sapranauskas et al., 2011). Furthermore, a chimeric crRNA-tracrRNA single guide RNA (sgRNA) recapitulated the structure and function of the tracrRNA:crRNA complex, which could efficiently direct Cas9 to induce DSBs *in vitro* (Jinek et al., 2012). The rules used by Cas9 to recognize target DNA are based on Watson-Crick base paring: a 20-nucleotide (nt) sequence on the sgRNA matches the target DNA, but it requires the presence of a DNA protospacer adjacent motif (PAM), adjacent to the complementary region (Jinek et al., 2012; Marraffini and Sontheimer, 2010).

Once directed to the target locus, Cas9 generates site-specific DNA double-strand breaks (DSBs) that are subsequently repaired by homologous directed repair (HDR) if homologous sequences are available or, otherwise, by non-homologous end joining (NHEJ) (Cong et al., 2013; Mali et al., 2013a; Doudna and Charpentier, 2014). HDR leads to precise gene correction or replacement whereas NHEJ is error prone and may induce small insert or delete (in-del) mutations (Figure 1.4). Like in cases of ZFNs and TALEN, targeted, sgRNA/Cas9-driven restriction of a diseased chromosome, associated to HR-mobilization of an exogenous editor DNA, might in principle allow for reintegration of the defective gene allele into its natural genomic landscape.

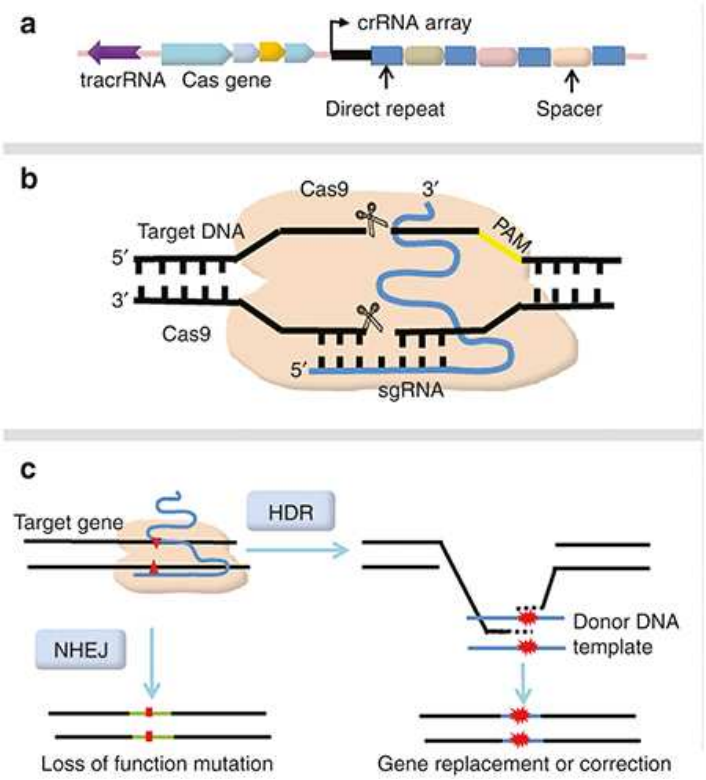


Figure 1.4. Schematic representation of CRISPR-Cas9- mediated genome editing. (**a**) Schematic of CRISPR locus (from *Streptococcus pyogenes*). (**b**) Site-specific DNA cleavage by nuclease Cas9 directed by complementary between a single guide RNA (sgRNA) and the target sequence upon the presence of a protospacer-adjacent motif (PAM) on the opposite strand. (**c**) The resultant double-strand breaks (DSBs) are subsequently repaired either by non-homologous end-joining (NHEJ) or by homology directed repair (HDR) upon the existence of a donor template. NHEJ is more efficient than HDR but is error prone and may produce in-del mutations, whereas HDR can provide a precise gene modification.

Additionally, Cas9 can be reprogrammed into nickase (nCas9), which cleaves on strand of DNA, by inactivating either RuvC or HNH (Ran et al., 2013), or into catalytically inactive Cas9 (termed dead Cas9, or dCas9) by inactivating both of them (Qi et al., 2013). dCas9 can be repurposed as a site-specific DNA-binding domain, transporting various functional domains to the target locus. In bacteria, the dCas9 protein was sufficient to

induce strong sequence-specific gene repression, simply by sterically hindering the transcriptional activity of RNA polymerase (Qi et al., 2013; Peters et al., 2016). In eukaryotic cells, fusing dCas9 to transcriptional effector proteins allowed for more efficient RNA-guided transcriptional modulation for both gene interference (CRISPRi) and activation (CRISPRa) (Maeder et al., 2013; Gilbert et al., 2014, 2013; Konermann et al., 2015) (Figure 1.5).

By fusing dCas9 to transcriptional repressors, such as the Kruppel-associated box (KRAB) domain, CRISPRi can efficiently repress coding and noncoding genes, such as miRNAs and large intergenic noncoding RNAs (lincRNAs) in mammalian cells (Gilbert et al., 2014, 2013; Larson et al., 2013; Zhao et al., 2014). Compared with complete loss-of-function using Cas9, CRISPRi can use different sgRNAs that bind to different genomic loci for tunable and titratable gene repression (Gilbert et al., 2014). While complete knockout is useful for studying gene function in many cases, tunable repression of a gene to different levels offers advantages when knocking out a gene leads to lethality of cells or an organism (Peters et al., 2016).

Earlier work using dCas9 fused to a peptide containing multiple VP16 domains (VP64 or VP128) could only activate endogenous genes mildly (Gilbert et al., 2013; Perez-Pinera et al., 2013; Cheng et al., 2013); therefore, several strategies have been developed to improve CRISPRa efficiency. These include recruiting multiple copies of the VP64 domain via a multimeric peptide array (SunTag), wherein each peptide domain could bind to a single-chain variable fragment (scFv) fused to VP64 (Tanenbaum et al., 2014); fusing dCas9 to a synergistic tripartite activator system containing VP64, the activation domain of p65 (p65AD), and Epstein-Barr virus R transactivator (Rta) (Chavez et al., 2015); and combining dCas9-VP64 with a modified sgRNA engineered with two copies of an MS2 RNA hairpin that could recruit p65AD and the human heat shock factor 1 (HSF1) activation domain via interaction with the MS2-binding protein (Konermann et al., 2015). A systematic comparison of the efficacy of these methods revealed that these systems perform comparably but are dependent on the genomic and cellular context (Chavez et al., 2016), suggesting that activation efficiency varies for different genes and in different types of cell. To repurpose

more complex gene regulation, sgRNA was engineered as a class of 'scaffold' RNAs (scRNAs) that directly recruit transcription effectors without protein fusion (Zalatan et al., 2015). scRNAs are generated by fusing RNA hairpins to the sgRNA, which interact with the cognate protein to recruit activators or repressors.

Moreover, Cas9 fused to epigenetic-modifying enzymes (such as p300, lysine demethylase 1 and DNA methyltransferase 3A) has been used to introduce locus-specific epigenetic modifications in the genome (Hilton et al., 2015; Kearns et al., 2015; Thakore et al., 2015; Vojta et al., 2016). Up to now, CRISPR-Cas9 system has been used for a variety of purposes, such as large-scale functional genomics studies (Zhou et al., 2014), generation of animal models (Yang et al., 2013) and genome imaging (Deng et al., 2015; Nelles et al., 2016)(Figure 1.5).

Of course, both dCas9-based transactivators and some dCas9-based epigenetic effectors are potentially avaliable to stimulate the spared allele of a haploinsufficient gene.

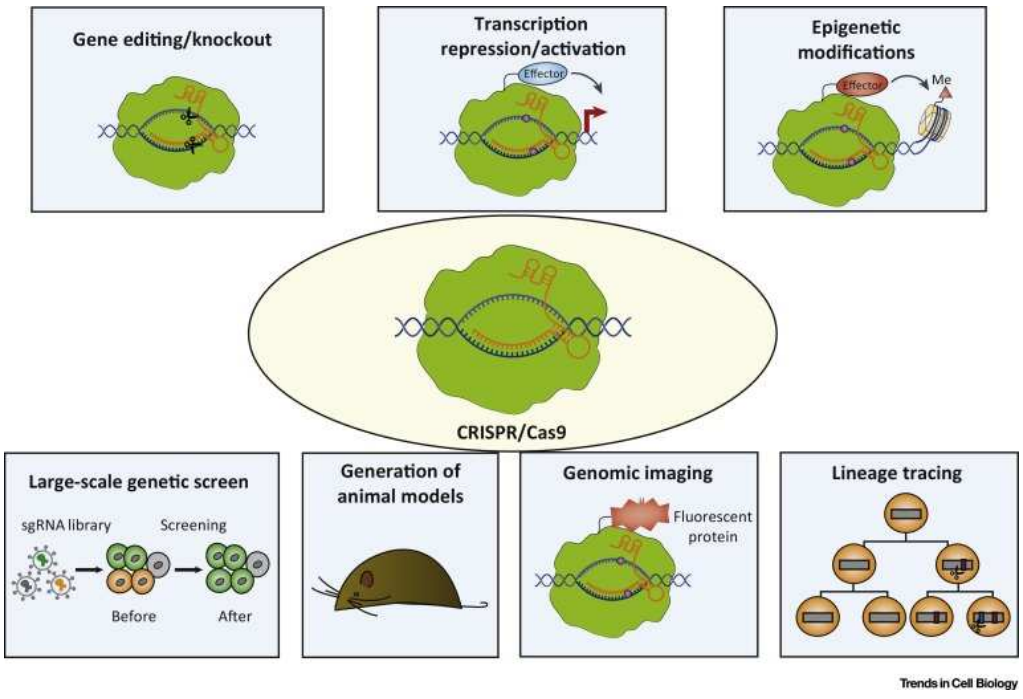


Figure 1.5. Applications of Clustered Regularly Interspaced Short Palindromic Repeats (CRISPR)/CRISPR-Associated Protein 9 (Cas9) to Cell Biology Research. CRISPR/Cas9 technology has been used for gene editing, transcriptional regulation, epigenetic regulation, large-scale genetic screens, generation of animal models, and genomic imaging. Abbreviation: sgRNA, single guide RNA. Adapted from Wang and Qi, 2016.

1.2.4 Novel RNA-programmable transcription factors (NMHV)

We recently developed a novel class of artificial transactivators, named NMHV (an acronym standing for Nuclear localization signal - MS2 coat protein RNA interacting domain - HA epitope - (3x) VP16 transactivating domain) (Fimiani et al., 2015). This transactivator is seven-fold smaller then CRISPR transactivator and, moreover, is active only where genes are normally expressed. Hence, it avoids potentially detrimental ectopic gene activation and this feature makes it feasible for clean treatment of gene haploisufficiencies.

I will describe the development of this new artificial transactivator in a dedicated chapter of Results.

1.2.5 RNA activation (RNAa)

The first report of transcriptional stimulation by small RNAs, termed RNA activation (RNAa) was described by Li et al (Li et al., 2006), where siRNA-like molecules targeting the promoter of Cadherin E, p21 and VEGF, were able to elicit a specific and prolonged stimulation of their transcription in human cells. After that, a crescent number of reports confirmed these findings (Janowski et al., 2007; Place et al., 2008; Faghihi et al., 2010; Portnoy et al., 2011; Diodato et al., 2013).

Different small RNA types may trigger RNAa: they are commonly referred as small activating RNAs (saRNAs). Bioactive saRNAs may be directed against transcription start sites (TSS) (Li et al., 2006; Schwartz et al., 2008), against conserved, cis active elements of the gene of interest (Diodato et al., 2013) or against the transcribed region of the gene (Liu et al., 2013) and they may be sense oriented or antisense oriented (Diodato et al., 2013).

The dynamics underlying RNAa are currently under investigation. At least two classes of molecular mechanisms may exist. On one hand, saRNAs can act by destabilizating ncRNAs which normally inhibit cognate mRNA transcription. This phenomenon has been documented in a numbers of examples (Morris et al., 2008; Faghihi et al., 2010; Modarresi et al., 2012). Alternatively, saRNAs may convey transactivating macromolecular complexes to gene locus (Morris et al., 2008; Schwartz et al., 2008; Matsui et al., 2013) (Figure 1.6). A limited number of mismatches between the saRNA and the target sequence might be tolerated, unless the mismatch is located at saRNA 5’ end (Li et al., 2006).

The differentiative state of cells and their functional state might influence their responsivity to saRNAs. A reduced basal expression of the gene may favour RNA activation (Yue et al., 2010). It was reported that RNAa is restricted to cells that normally express the gene of interest (Li et al., 2006; Diodato et al., 2013).

mRNA upregulation achieved is small, often <5-folds, usually within the physiological range of gene expression level. Such small changes in target gene expression level are not

negligible. They can impact functional state of cells and give rise to clear biological effects (Diodato et al., 2013; Janowski et al., 2007).

Interestingly, moderate power and small size of saRNAs make them a promising tool for treatment of neural haploinsufficiencies. We designed saRNAs targeting genes involved in neurodevelopmental pathologies and we assess their biological effectiveness, specificity and compliance with endogenous gene tuning.

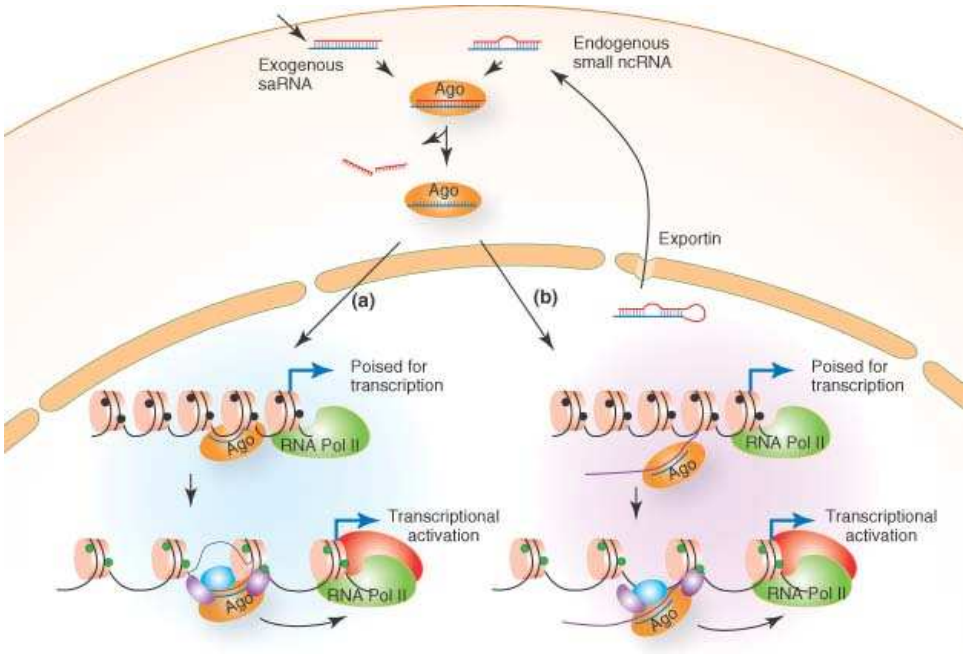


Figure 1.6. Mechanism for RNA activation. An exogenously introduced or naturally occurring saRNA/agRNA is loaded into an Ago protein (e.g., Ago2) where the passenger strand is cleaved and discarded, resulting in an active Ago–RNA complex. This complex gains access to the nuclear compartment by either passive transport when the nuclear envelope disappears during mitosis or active transport mechanisms. The complex may then bind to (a) complementary DNA sequences or (b) nascent cognate transcripts in promoters or 3' flanking regions and further recruit histone modifiers, leading to an open chromatin structure and active transcription. Ago, Argonaut proteins; agRNA, antigene RNA; ncRNA, noncoding RNA; saRNA, small activating RNA. Adapted from Portnoy et al., 2011.

1.3 Choice of haploisufficient genes

Among haploinsufficient neuropathogenic genes potentially suitable for experimental therapeutic stimulation, we focused our attention on some fullfilling certain key criteria:

(1) such genes display a clear and established causal relationship between the hemizygous state and the occurrence of the neuropathological condition;

(2) easily quantifiable biological outcomes of gene expression levels are known, which allow us to get a fast and straightforward response after therapeurtic manipulations;

(3) mouse models recapitulating the haploinsufficient phenotype are available, for an in depth evaluation of our therapeutic intervention in a pathologically plausible scenario.

1.3.1 *FOXG1* and Rett syndrome

Rett syndrome (RTT) is a severe neurodevelopmental disorder that affects 1 in 10,000 females and it is characterized by cognitive impairment, autism-like features, stereotypic hand movements, hypotonia, microcephaly and often epilepsy . About 90% of typical RTT cases are attributable to mutations in the methyl-CpG-binding protein 2 (*MECP2*), located on X chromosome (Amir et al., 1999) and for this reason female are prevalently affected. However, mutational analysis conducted for RTT patients without *MECP2* abnormalities have revealed mutations in the cyclin-dependent kinase-like 5 gene (*CDKL5*) on X chromosome (Scala et al., 2005) or mutations in the forkhead box G1 gene (*FOXG1*) on chromosome 14q12 (Neul et al., 2010; Kortüm et al., 2011; Florian et al., 2012).

Heterozygous mutations (missense and nonsense) and microdeletions of FOXG1 have been identified, accounting for 0.6% of patients with RTT (Ariani et al., 2008; Papa et al., 2008; Mencarelli et al., 2009; Pintaudi et al., 2010; Florian et al., 2012). In particular, mutations in *FOXG1* give rise to the congenital variant that shows classic RTT features but earlier onset (Yeung et al., 2009; Brunetti-Pierri et al., 2011). Patients with FOXG1 alterations show a complex pattern of clinical features that includes postnatal growth deficiency, severe postnatal microcephaly, developmental delay with absent speech, defective social contact resembling autism, poor sleep, stereotyped movements in combination with dyskinesia. Although these features overlap with RTT, patients with FOXG1 alteration may have unique characteristics, including distinct epilepsy phenotypes (Guerrini and Parrini, 2012; Fehr et al., 2013; Seltzer and Paciorkowski, 2014). Brain MRI reveals a combination of frontal gyral simplification with severe myelination delay most prominent in both frontal region and corpus callosum (Bahi-Buisson et al., 2010; Le Guen et al., 2011; Kortüm et al., 2011; Guerrini and Parrini, 2012).

The FOXG1 gene (also known as Brain-restricted transcription Factor-1, BF1) belongs to the forkhead family and FOX genes are known to encode a subgroup of the helix-turn-helix class of protein (Clark et al., 1993). Currently, they are divided into 17 subclasses (A to

Q), according to the amino acid sequence of their conserved forkhead domains (Kaestner et al., 1993). Human FOXG1 gene is located on chromosome 14q12 and contains only 1 coding exon (exon 1) (Bredenkamp et al., 2007). Four alternative transcripts (exon 2 to 5) have been identified in fetal brain (Shoichet et al., 2005) (Figure 1.7).

The FOXG1 protein (50KDa) consists of a 100-residue forkhead DNA-binding domain (FHD), highly conserved across all members of the FOX family. FOXG1 recruits transcriptional corepressor proteins, a histone demethylase and Groucho (Gro), via two further protein-binding domains, the 10-residue KDM5B (previously JARID1B)-binding domain (JBD) and the about 20-residue Gro-binding domain (GBD), respectively. Structurally, the FHD consists of 3 alpha helices and 1 beta hairpin (2 beta strands and 1 loop), whereas the GBD and JBD are random coiled. It has been reported that mutations in FOXG1 gene may impaired the DNA binding properties as well as cause the loss of JBD interaction domain and the misfolding of the motif responsible for GBD (Ariani et al., 2008). Moreover, mutations that produce truncated FOXG1 protein have been described (Le Guen et al., 2011).

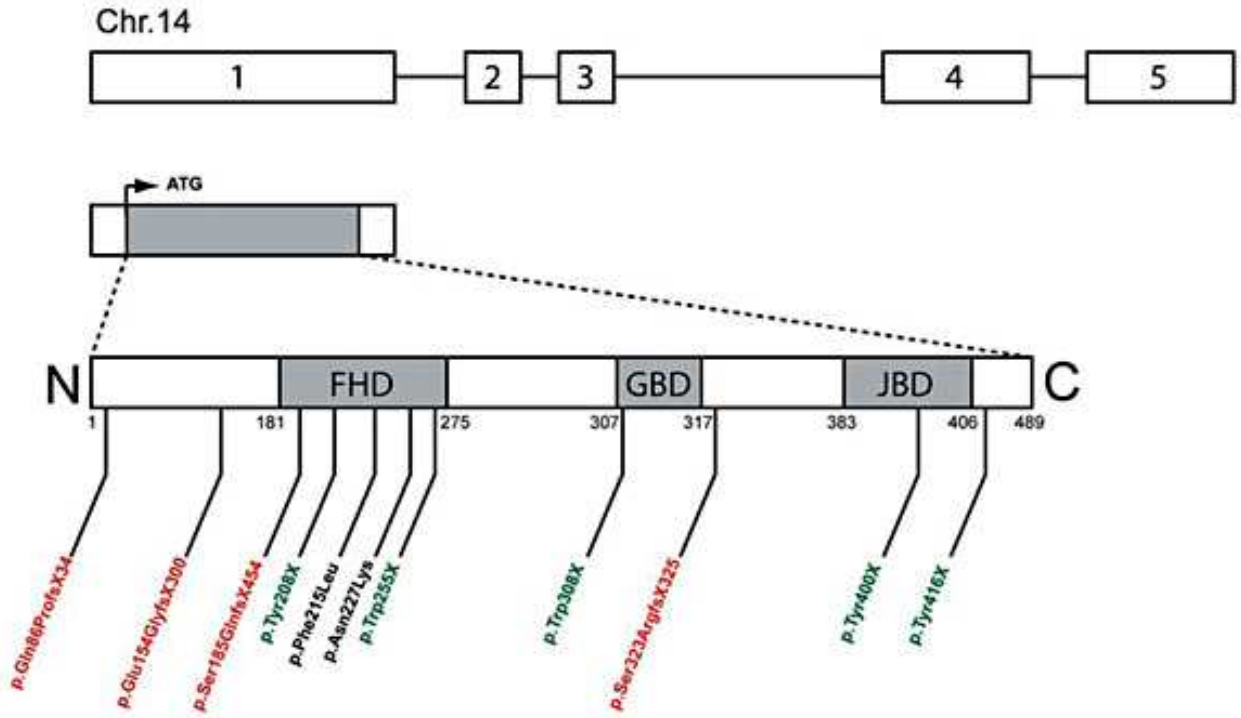


Figure 1.7. Schematic representation of human *FOXG1* gene and its deleterious mutations. The 489-amino-acid-long FOXG1 transcription factor (ARN NM_005249) is encoded by the intronless *FOXG1* coding region (exon 1). Shaded regions indicate the 3 functional domains of the protein, i.e. the DNA-binding forkhead domain (FHD) (amino acids 181–275), the Gro-binding domain (GBD) (amino acids 307–317) and the KDM5B (formerly JARID1B) binding domain (JBD) (amino acids 383–406). Three different mutations reported in *FOXG1* exon 1 are represented: frameshift mutations (red), stop codon mutations (green) and missense mutations (black). Amino acid numbers are indicated below the protein representation. Adapted from Florian et al., 2011

Murine *Foxg1* is a conserved transcriptional repressor that regulates telencephalon development from the early embryonic to adult stages through multiple mechanisms (Roth et al., 2010). It is expressed in the telencephalon since early stages of its development (Tao and Lai, 1992) in a rostro/ventral^{high} to caudo/dorsal^{low} fashion (Acampora et al., 2001). The Foxg1 protein is strongly expressed in progenitor cells of the ventricular zone, in early postmitotic neurons in the developing telencephalon, and in visual structures (Bourguignon et al., 1998; Tao and Lai, 1992).

As demonstrated by analysis of constitutive, murine *Foxg1*-null mutants, *Foxg1* promotes differential specification of the telencephalic vs the diencephalic field (Hanashima et al., 2007) and is necessary for morphogenesis of basal ganglia (Martynoga et al., 2005; Xuan et al., 1995). Within the pallial field, it antagonizes specification of Cajal-Retzius cells (Hanashima et al., 2002, 2004; Muzio and Mallamaci, 2005) and restricts the hippocampal program to the dorso-medialmost telencephalon (Muzio and Mallamaci, 2005). *Foxg1* increases the size of neural proliferating pools, delaying the exit of neural elements from cell cycle (Martynoga et al., 2005). Hence, *Foxg1* early ablation results into dramatic telencephalic hypoplasia (Xuan et al., 1995). More recently, *Foxg1* was associated with the control of the developmental progression from cortico-cerebral neural stem cells (NSC), through neuronal and glial progenitors (NPs and GPs, respectively), up to neurons, astrocytes and oligodendrocytes (Brancaccio et al., 2010). In particular, when overexpressed in NSCs

and NPs, *Foxg1* antagonizes commitment of neural stem cells to glial fates and promotes neuritic overgrowth, respectively (Mallamaci et al, unpublished data).

Mouse mutants heterozygous for *Foxg1* were originally reported to be normal (Xuan et al., 1995). Actually, *Foxg1* dosage causes specific neocortical dysmorphologies, reminiscent of defects found in human patients. These include: thickening of frontal areas, hypoplasia of upper neocortical layers, a reduction of corpus callosum and myelination defects (Eagleson et al., 2007; Shen et al., 2006), all possibly arising from reduced self-renewal of the cortical proliferating pool (Siegenthaler et al., 2008). Moreover, the dentate gyrus, almost normal at birth, undergoes progressive hypoplasia, possibly reflecting an anticipated exhaustion of the hippocampal proliferting pool and reduced cell survival (Shen et al., 2006). *Foxg1+/-* mutants show defective habituation in the open field test, as well as a severe deficit in contextual fear conditioning (Shen et al., 2006).

1.3.2 *FRATAXIN* and Friedreich's ataxia

Friedreich's ataxia (FRDA) is a multisystemic autosolmal recessive disorder. Patients affected by FRDA display neurodegeneration of large sensory neurons of dorsal root ganglia (DRG) as well as of Betz pyramidal neurons of cerebral cortex. Atrophy of the sensory pathways leads to sensory loss, afferent ataxia and loss of tendon reflex (Pandolfo and Manto, 2013; Koeppen and Mazurkiewicz, 2013). Degeneration of deep cerebellar nuclei causes cerebellar ataxia, dysarthria and fixation instability. Cardiomyopathy may cause premature death in 59% of FRDA patients, due to heart failure and arrhythmias (Tsou et al., 2011). FRDA is the most common hereditary ataxia, with a prevalence of 1 in 29,000 in the Caucasian population and a carrier frequency of 1 in 85 (Khonsari et al., 2016).

In 96% of patients affected by FRDA, a homozygous GAA triplet repeat expansion is found in the first intron of the frataxin (*FXN*) gene. *FXN* is located on chromosome 9q21 and it includes, normally, from 10 to 66 GAA-triplet repeats the the first intron. A number of repeats ranging from 70 to 1000 triggers epigenetic changes in the gene, which eventually causes frataxin transcriptional repression (Campuzano et al., 1996; Herman et al., 2006; Rai et al., 2008) (Figure 1.8). On one hand, GAA repeats expansion may mediate frataxin gene silencing via the formation of abnormal non B-DNA structures. The GAA(TTC) tract in FRDA is recognised as poly-purine/poly-pyrimidine sequence which may adopt various unusual nucleic acid structures, including triple helices (Frank-Kamenetskii and Mirkin, 1995). Triplex or sticky DNA may inhibit transcription, possibly by sequestering RNA polymerase (Sakamoto et al., 2001). Moreover, it has been demonstrated that *FXN* gene transcription leads to the formation of a persistent RNA/DNA hybrid *in vitro* (Grabczyk et al., 2007). As the RNA polymerase moves, nascent RNA transcript anneals to the template strand. It was found that RNA/DNA hybrids formed can span the GAA repeat and this is associated with arrest of the RNA polymerase during the transcription of such repeats (Grabczyk et al., 2007; Wells, 2008; Rajeswari, 2012).

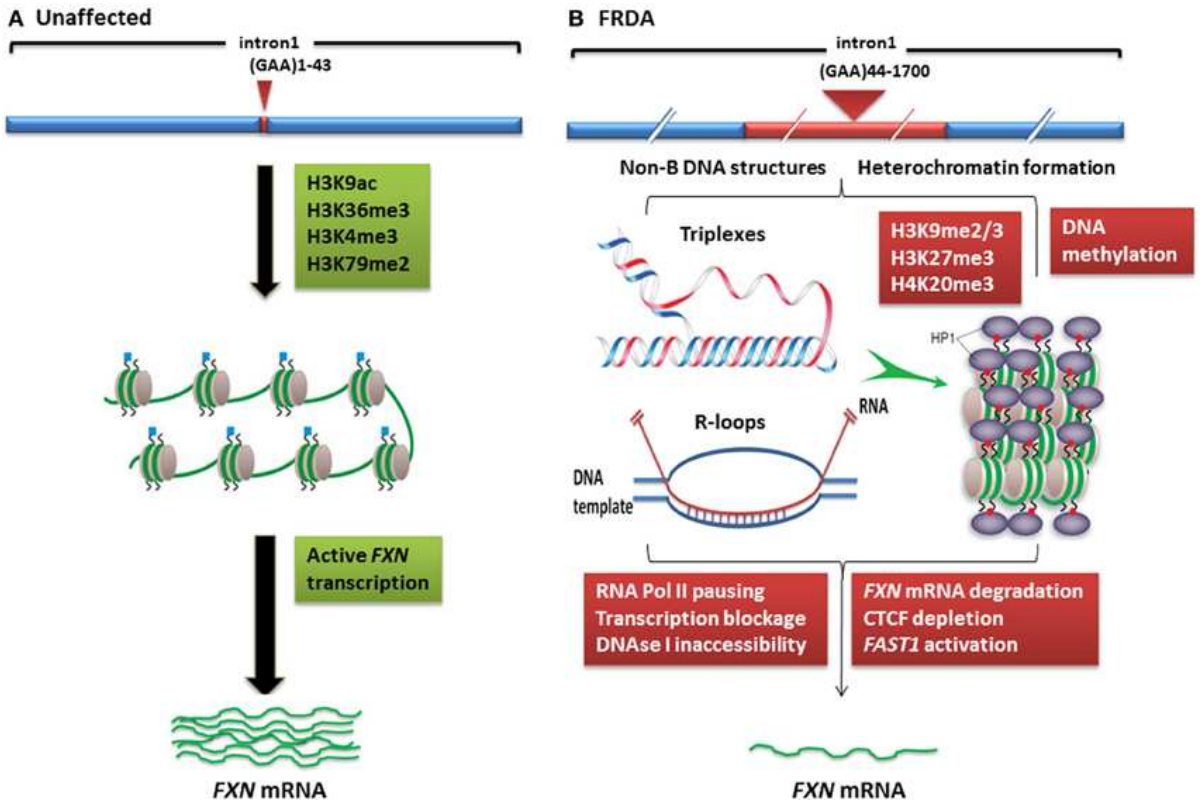


Figure 1.8. Models of *FXN* gene silencing in FRDA. (a) Unaffected individuals, who carry up to 43 GAA•TTC repeats, contain active histone marks of gene transcription initiation and elongation at the *FXN* promoter and intron 1 regions. **(b)** In FRDA patients, the presence of large GAA•TTC repeat expansion leads to *FXN* gene silencing by two potential mechanisms: (i) the GAA•TTC repeat may adopt abnormal non-B DNA structures (triplexes) or DNA•RNA hybrid structures (R loops), which impede the process of RNA polymerase and thus reduce *FXN* gene transcription, (ii) increased levels of DNA methylation and HP1 and significant enrichment of repressive histone marks at the *FXN* gene trigger heterochromatin formation that may lead to more pronounced *FXN* gene silencing. Adapted from Sandi et al., 2014.

On the other hand, it has been demonstrated that GAA repeat expansions can lead to heterochromatin-mediated frataxin gene silencing. These events include DNA methylation and hydroxymethylation, histone deacetylation and histone methylation (Sandi et al., 2014) (Figure 1.8). Hypermethylation of specific CpG sites upstream of the GAA repeat sequence in

FRDA patient-derived cells and tissues was reported (Greene et al., 2005; Al-Mahdawi et al., 2008). Interestingly, the degree of methylation correlates whith the length of GAA repeats (Castaldo et al., 2008). Several reports demonstrate that some post-translational histone modifications at frataxin locus occur most frequently in FRDA patients compared to unaffected individuals. In particular low levels of acetylated H3 and H4 lysine residues as well as increased H3K9me2, H3K9me3 and H3K27me3 were reported at frataxin promoter, 5'UTR, upstream and downstream GAA regions (Herman et al., 2006; Greene et al., 2005; Al-Mahdawi et al., 2008). Elevated levels of heterochromatin protein 1 (HP1) were also observed (De Biase et al., 2009). Conversely, decreased levels of H3K4me3, H3K36me3 and H3K79me3 (normally associated with a more open chromatin state and active gene expression) at the upstream and downsteam GAA repeat regions of the *FXN* gene in FRDA cells were described (Punga and Bühler, 2010; Kim et al., 2010; Kumari et al., 2011) (Figure 1.8).

Moreover, heterochromatin formation has been suggested to be related with the CCCTC-binding factor (CTCF) protein which, normally, can prevent the spreading of DNA methylation (Filippova et al., 2005; Engel et al., 2006). CTCF has binding sites in the repeat expansion flanking regions of several trinucleotide expansion disorders, such as FRAXA (Ladd et al., 2007), DM1 (Filippova et al., 2001), and SCA7 (Libby et al., 2008), and loss of CTCF binding at triplet expansion is associated with the spread of heterochromatin and DNA methylation (Cho et al., 2005). Significant increased levels of a frataxin antisense transcript 1 (*FAST1*) in FRDA patient cells, associated with depletion of CTCF binding at the 5' UTR region of the *FXN* gene has been reported (De Biase et al., 2009; Al-Mahdawi et al., 2008) (Figure 1.9).

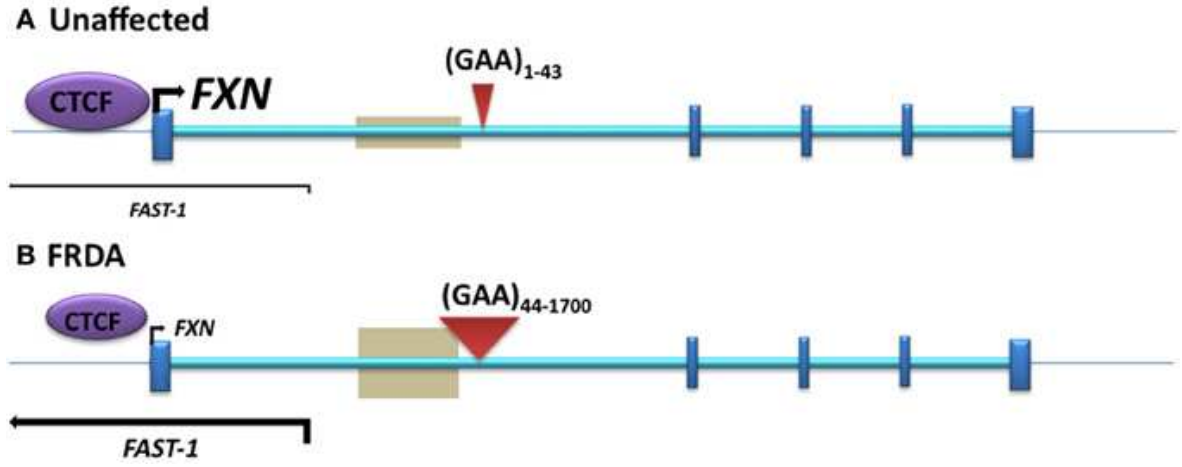


Figure 1.9. The position of DNA methylation, hydroxymethylation, and CTCF binding sites within the *FXN* gene. (a) Unaffected: normal-sized GAA repeat; **(b)** FRDA: GAA repeat expansion. Gray boxes represent regions of disease-associated DNA methylation and hydroxymethylation. Arrow marks represent the directions and levels of transcription for *FXN* and *FAST-1*. Blue bars represent exons of the *FXN* gene. Red triangles indicate GAA repeats within intron 1 of the *FXN* gene. Adapted from Sandi et al., 2014

Frataxin protein levels are, hence, reduced by more than 70% of normal levels. In homozygous individuals, levels of frataxin correlate with the length of GAA repeats (Montermini et al., 1997; Campuzano et al., 1996), which, in turn, correlates with the age of onset and the severity of the disease (Montermini et al., 1997; Dürr et al., 1996; Reetz et al., 2015). Heterozygous carriers, characterized by 50% of frataxin levels, do not show disease symptoms (Plasterer et al., 2013).

The *FXN* gene is composed of seven exons and spans 95 Kb of genomic DNA. The main functional messenger RNA is 1.3 kb long and arises from the first five exons and encodes a 210 amino acid protein. In addition, by alternative splicing, a 171 amino acid protein can be also produced (Campuzano et al., 1996). Two major transcription start sites (TSS) were identified in the frataxin gene: TSS1 is located 221bp upstream of the ATG translation start site (Campuzano et al., 1996) and TTS2 was identified 62bp upstream the ATG (Kumari et al., 2011). The region between TSS1 and the first exon is thought to be a

TATA-less downstream promoter. Moreover, binding sites for transcription factors were identified, such as TFAP2 and EGR3 (Tourtellotte and Milbrandt, 1998) as well as for the insulator protein CCCTC-binding factor (CTCF) (De Biase et al., 2009). Apart from (GAA)n repeats, a number of repetitive DNA elements have been identified at FXN locus, such as L2 (LINE) (Greene et al., 2005) and Alu (SINE) elements as well as MIRb and mariner DNA transposon (Campuzano et al., 1996; Cossée et al., 1997), although their precise function in frataxin regulation is not known (Greene et al., 2005).

Frataxin protein is highly conserved in most organisms from bacteria to mammals (Adinolfi et al., 2002; Gibson et al., 1996). The precursor form of frataxin contains N-terminal mitochondrial import sequence. Once translocated into the mitochondria, proteolitic processing occurs: mitochondrial processing peptidase (MPP) enzyme cleaves the precursor to give an intermediate form, followed by conversion of this product to mature form (Koutnikova et al., 1998; Gordon et al., 1999). In detail, the human frataxin is synthesized as a 210 amino acid precursor (23.1 KDa) and processing *in vitro* may originate an intermediate form of 169 amino acid size (18.8 KDa), but only the mature frataxin form of 130 amino acid size (14.3 KDa) has functional significance *in vivo* (Condò et al., 2007; Schmucker et al., 2008). Mature frataxin is a compact, globular protein composed of N-terminal α-helix, 7 β sheet strands, a second α helix and a C-terminal coil (Condò et al., 2007).

Although the function of frataxin is still under investigation, it seems to be involved as activator of iron-sulfur (Fe-S) cluster biogenesis in mitochondria (Schmucker et al., 2011). Fe-S clusters are fundamental prosthetic groups for a large number of proteins (Stehling et al., 2009). In mitochondria, Fe-S clusters are contained in factors that participate in Fe-S biogenesis (YAH1), in subunits of respiratory complexes I, II and III, in Krebs cycle enzyme aconitase (ACO2), in enzymes involved in amino acid and cofactor synthesis (Codazzi et al., 2016) (Figure 1.10)**.**

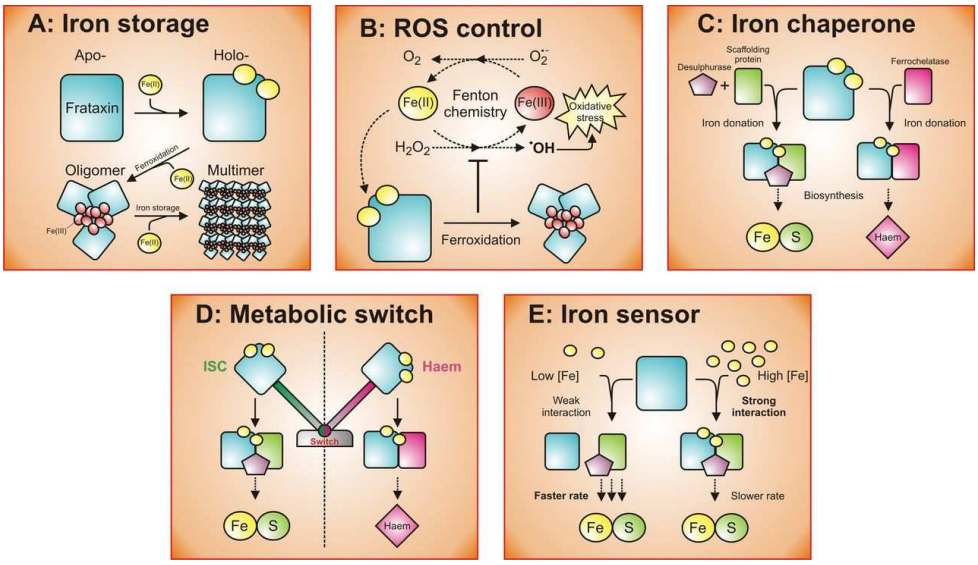


Figure 1.10. Schematic diagram showing the proposed functions for frataxin in mitochondrial iron metabolism. (**a**) It was originally proposed that frataxin might function as an iron-storage protein. The iron-storage hypothesis is thought to help rationalize the observation that in the presence of excess labile iron, the yeast frataxin orthologue (Yfh1) is capable of self-assembling into oligomers and higher-order multimers that possess ferroxidase activity. These multimeric structures appear to be capable of storing iron in a mineralized ferric form. (**b**) It has also been proposed that Yfh1's oligomerization-dependent ferroxidase activity may contribute to protection from iron-mediated oxidative stress resulting from toxic reactive oxygen species (ROS) formed via Fenton chemistry. (**c**) Some evidence suggests that frataxin may function as an iron chaperone or 'donor' in iron-dependent biosynthetic reactions such as ISC and haem biosynthesis. (**d**) An alternative, but related, hypothesis suggests that, rather than being an iron chaperone, frataxin may function as a metabolic 'switch' that results in the diversion of iron from one metabolic pathway (e.g. ISC biosynthesis) to another (e.g. haem biosynthesis). (**e**) A very recent suggestion is that the bacterial frataxin orthologue (CyaY) may function as a negative regulator that inhibits the rate of ISC biosynthesis if the availability of iron is high and the availability of downstream ISC apo-acceptors is low. Adapted from Lane and Richardson, 2010.

In the cytosol, defective Fe-S cluster synthesis leads to excessive iron uptake and iron overload in mitochondria (Martelli et al., 2015). Moreover, frataxin deficient cells display a higher sensitivity to oxidative stress (Condò et al., 2006; Schmucker and Puccio, 2010) (Figure 1.11).

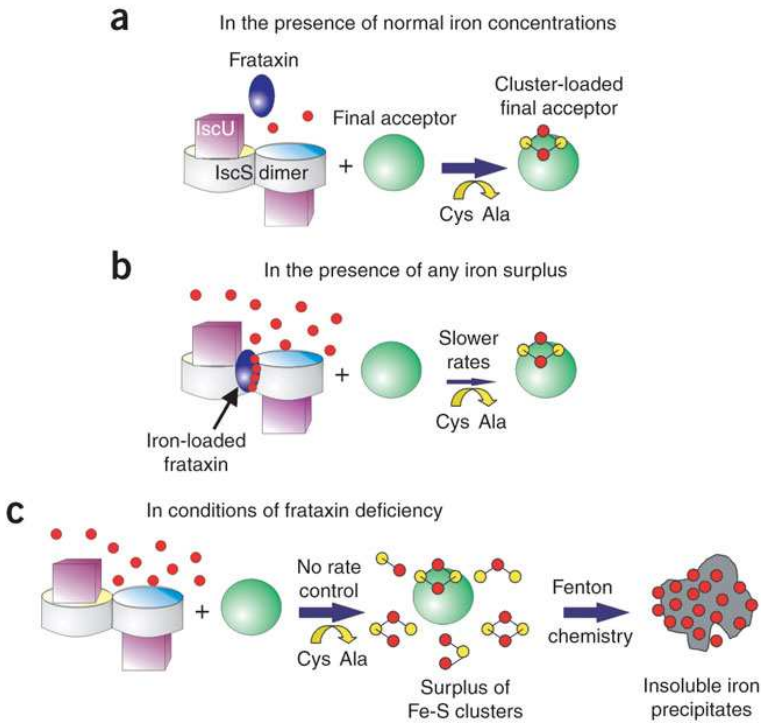


Figure 1.11. Schematic model of the molecular mechanism of frataxin in the cell. (a) At normal iron concentrations, the Fe-S clusters are assembled by the IscS–IscU complex and passed on to their final acceptors. (**b**) Any excess of iron as compared to the number of final acceptors will be rebalanced by slowing down the reaction to match the concentration of final acceptors and avoid unnecessary overproduction of Fe-S clusters. (**c**) When frataxin is absent or produced in insufficient quantities, as in FRDA, there is no regulation. Fe-S clusters will be produced irrespectively of whether they can be transferred to an acceptor. Any iron excess will result in a surplus of Fe-S clusters, which, being highly unstable, will fall apart, generating Fenton reactions. Fe^{3+} will precipitate and form insoluble aggregates. Adapted from Adinolfi et al., 2009.

1.3.3 *SCN1A* and Dravet syndrome

Dravet syndrome (DS), is a rare form of childhood-onset epileptic encephalopathy. It was originally known as Severe Myoclonic Epilepsy in Infancy (SMEI) (Dravet, 1978; Dravet et al., 2005) and is characterized by the prolonged febrile hemiclonic or generalized tonic, clonic and tonic-clonic seizures accompanied by fever during the first year of life (Scheffer et al., 2001; Ohmori et al., 2003; Mulley et al., 2005). DS patients also show a delay in psychomotor development, dysphasia, ataxia and other neuropsychological deficits from the second year of life (Harkin et al., 2007). Almost all seizures types are remarkably resistant to anti-epileptic medications (Ceulemans, 2011). Cognitive dysfunction stabilizes (but in general does not improve) in the second half of the first decade of life, and seizures tend to decline into adolescence and adulthood (Dravet, 2011). The incidence rate of DS is nearly 1 in 30,000 live births.

DS is caused by de novo heterozygous mutations in the sodium channel α1 subunit (SCN1A) gene in about 95% of the patients (Claes et al., 2001; Meisler et al., 2010). The SCN1A gene is located on the chromosome 2q24, composed of 26 exons spanning 6030 bp and encodes the large α-subunit of the voltage-gated sodium ion channel, type 1 (NaV 1.1) (Escayg et al., 2001) (Figure 1.12). Additional alternate exons harboring the 5'-untranslated region of the gene have been reported, but the exact combination of these with the coding exons is not fully known (Long et al., 2008).

In rodents, the expression of the Scn1a gene becomes evident post partum and it increases till the adulthood, mainly in the caudal region and the spinal cord (Copley, 2004; Gong et al., 1999). Within the CNS, Scn1a shows higher expression in dendrites, cell bodies (Westenbroek et al., 1989) and also at the parvalbumin positive inter-neuronal axon initial segments (Ogiwara et al., 2007). The SCN1A-coded α-subunit is a 260 kDa protein that harbors four homologous domains, each of them spanning six transmembrane segments (Catterall et al., 2010).The NaV 1.1 channel is heteromeric complex consisting of the α-subunit, which forms the larger central pore of the channel, and two smaller auxiliary β-

subunits (Meisler et al., 2010). The α-subunit regulates the sodium ion selectivity and can on its own function as a channel (Catterall et al., 2010; Escayg and Goldin, 2010; Gordon et al., 1987). β-subunits regulate the gating and kinetics of the channel and also help in the interaction with the cytoskeleton and other proteins for the trafficking of the channel protein to the cell membrane (Moran et al., 2003; Aman et al., 2009).

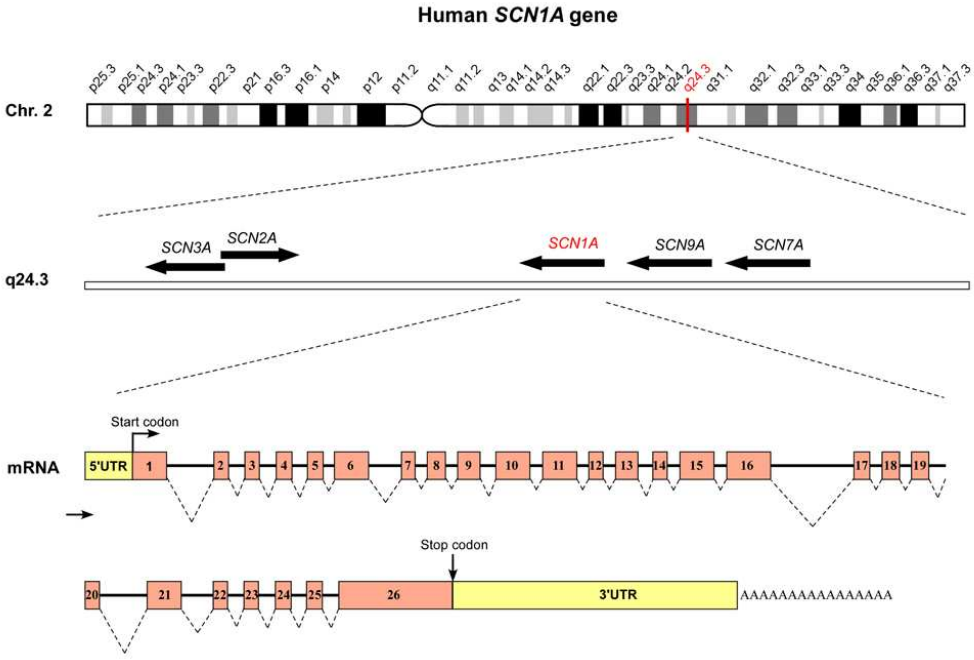


Figure 1.12. SCN1a locus on chromosome 2q24. Exons are represented in red, 5'UTR and 3'UTR are highlighted in yellow.

Approximately 700 distinct sequence variations in the human SCN1A gene are known to be associated with the DS and all of them were found in heterozygous state, suggesting that their homozygous state could be embryonic lethal. These variations were found all along the coding region of the gene and also include large deletions and duplications (Depienne et al., 2009) (Figure 1.13). Therefore, it can be proposed that these disease-associated variations are loss-of-function mutations and the DS results from gene haploinsufficiency (Suls et al., 2006; Yamakawa, 2011; Bechi et al., 2012). Indeed, both homozygous and heterozygous *Scn1a* knockout mice developed epileptic seizures soon after birth (Yu et al.,

2006). More importantly, a knock-in mouse model having a common DS-associated human *SCN1A* mutation developed seizure phenotype both in homozygous and heterozygous states (Ogiwara et al., 2007). Thus, a significant reduction in the sodium channel activity is likely to underlie the seizures phenotype (Yamakawa, 2011). These animal models have shown that sodium channels are essential for the survival, as *Scn1a* null mutants exhibited premature death (Cheah et al., 2012).

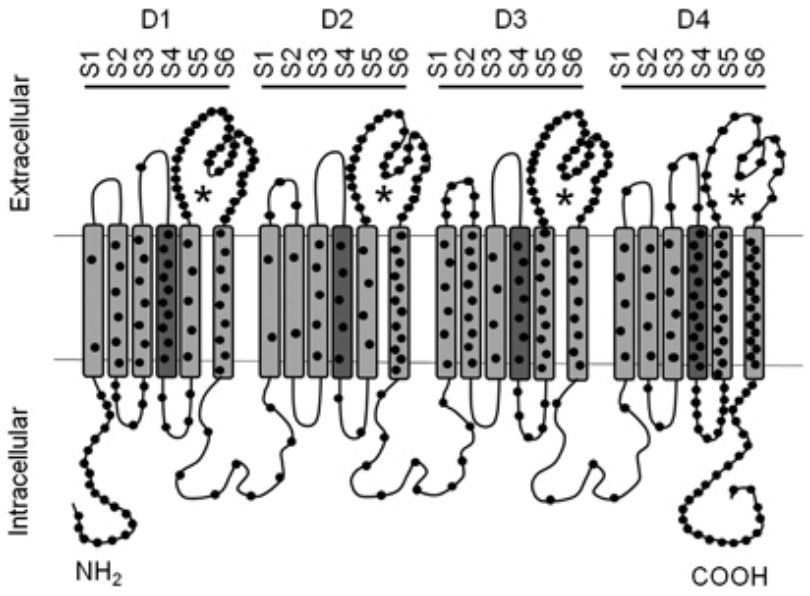


Figure 1.13. Scn1a channel schematic. It is reported the domain organization of the α-subunit of the voltage-gated sodium ion channel coded by the *SCN1A* gene and the positions of the missense mutations (shown as black circles). The α-subunit consists of four homologous domains (D1–D4), each having six trans-membrane segments (numbered S1–S6). The P-loop region of the channel, located between S5-S6, is identified with an asterisk. Adapted from Parihar and Ganesh, 2013

More in detail, patch clamp recordings in acutely dissociated hippocampal cells taken from postnatal day 14–16 (P14–16) *Scn1a*$^{+/-}$ animals showed that bipolar GABAergic neurons (but not glutamatergic pyramidal neurons) had a dramatic reduction in sodium current density (Yu et al., 2006). This loss in sodium current for GABAergic neurons limited their ability to increase firing frequency in response to injected current. Based on these results, it

was postulated that seizures in DS arise because selective defects in GABAergic interneurons produce a network that lacks sufficient inhibitory tone. This theory was named the "interneuron hypothesis."

Furthermore, mice harboring the mutation (*SCN1A*$^{R1407X/+}$) restricted to parvalbumin-positive interneurons displayed typical DS seizure pathogenesis (Ogiwara et al., 2007). $Na_V1.1$ was preferentially expressed in the axon initial segments of parvalbumin-positive interneurons, suggesting that this cell type might be preferentially affected by *SCN1A* haploinsufficiency. Indeed, trains of action potentials from parvalbumin-positive interneurons of the mice engineered with the mutation showed profound spike amplitude decrement as the spike train progressed. The results from this model suggested that hyperexcitability in DS might not result from dysfunction of GABAergic interneurons in general but, rather, from dysfunction of the parvalbumin-positive population.

Further evidence in favour of the interneuron hypothesis can be drawn from recent studies demonstrating that altering the balance of *Scn1a* expression in inhibitory versus excitatory neurons is sufficient to produce seizures. Forebrain GABAergic neuron-specific *Scn1a*$^{+/-}$ mice (using the *Dlx1/2* promoter to drive Cre expression) have a robust seizure phenotype, suggesting that reduction of $Na_V1.1$ expression in this population of inhibitory neurons is sufficient to induce hyperexcitability (Cheah et al., 2012). It was also shown that heterozygous *Scn1a* deletion in all inhibitory neurons (using a *VGAT*-Cre mouse line) produced a seizure phenotype that was more severe than that which was observed in the global *Scn1a* heterozygotes or in the excitatory neuron *Scn1a* heterozygotes (generated using the *EMX*-Cre mouse line) (Ogiwara et al., 2013).

However, recently, alternative theories to explain seizures in DS were reported: the employment of human patient-derived induced pluripotent stem cell (iPSC) neurons argues that intrinsic hyperexcitability of both GABAergic and glutamatergic neurons might underlie seizure activity in DS. Actually, both GABAergic and glutamatergic forebrain neurons from DS patients were hyperexcitable compared to nonepileptic controls, with increased sodium current density, increased rates of action potential firing in response to depolarizing current

injection, and epileptic-like spontaneous activity (Liu et al., 2013; Jiao et al., 2013). *SCN1A* haploinsufficiency may result in a compensatory increase in sodium current, presumably through the expression of other voltage-gated sodium channels (Liu et al., 2013; Auerbach et al., 2013).

2. MATERIALS AND METHODS

Animal handling

Wild-type, CD1 strain mice used in this study were purchased from Envigo-Italy and housed at the SISSA mouse facility. Animals handling and subsequent procedures were in accordance with European [European Communities Council Directive of November 24, 1986 (86/609/EEC)] and Italian laws (D.L. 04.03.2014, n°26) and were approved by SISSA Board for Animal Welfare. Embryos were staged by timed breeding and vaginal plug inspection. Neonates were staged as "P0" on their birthday.

Cell cultures

Embryo harvesting. Embryos (E10.5, E12.5 and E16.5) were harvested from pregnant dams killed by cervical dislocation and put in sterile ice-cold PBS supplemented with 0.6% glucose. Cerebral cortices (E12.5 and E16.5), mesencephalons (E10.5) and rhombocervical tracts (E10.5) were then dissected and collected in the same solution.

Primary cells. E12.5 cerebral cortices as well as E10.5 mesencephalons and rhombo-cervical tracts were mechanically dissociated to single cells by gentle pipetting. Neural precursor cells were subsequently counted in a Burker chamber and plated in 24-multiwell plates (Falcon), at the density of 1,000 cells/ml, in proliferative medium [DMEM-F12 (Gibco), 1X Glutamax (Gibco), 1X N2 (Invitrogen), 1 mg/ml BSA, 0.6% glucose, 2 mg/ml heparin (Stem Cell Technologies), 20 ng/ml bFGF (Invitrogen), 20 ng/ml EGF (Invitrogen), 1X Pen- Strept (Gibco), 10 pg/ml Fungizone (Gibco)]. Neural precursors were acutely infected by recombinant lentiviruses and kept in culture up to 96 h. Multiplicities of infection (moi's) are reported in the corresponding figures.

Cortical tissue from E16.5 mice was chopped to small pieces for 5 minutes, in the smallest volume of ice-cold 1X PBS-0,6% glucose-1mg/ml DNaseI. The minced tissue was then resuspended and digested in 0.25mg/ml trypsin-1mg/ml DNAseI for 5 minutes at 37°C.

Digestion was stopped by adding ≥1.5 volumes of DMEM/F12/10%FBS. Cortical tissue was spinned down and transferred to differentiative medium. The suspension was pipetted 5-8 times with a P1000 Gilson pipette and undissociated tissue was left to sediment for 1-2 minutes. The supernatant was harvested and the living cells counted. 1x10^6 cells/well were plated on poly-L-Lysine coated 12 multiwell plates, in 600 µl of differentiative medium [Neurobasal-A (Gibco), 1X Glutamax (Gibco), 1X B27 supplement (Invitrogen), 25µM L-glutamate, 25µM β-Mercaptoethanol (Gibco), 2% FBS, 1X Pen/Strept (Gibco), 10 pg/ml Fungizone (Gibco)]. Dissociated neural cells were infected 24 hours later and kept in culture up to 7 days. Multiplicities of infection (moi's) are reported in the corresponding figures. When required, doxycycline was added to the culture medium, at 2 mg/ml. Medium was half-replaced with fresh one every 3.5 days.

HEK293T and NIH/3T3 cells. Cells were cultured in DMEM-Glutamax™ (Gibco)-10% FBS, at 125,000 and 25,000 cells/cm^2, respectively, according to standard protocols. Lentiviral transductions were performed at moi's reported in the corresponding figures. When appropriate, αAgo1 and αGFP morpholinos (GeneTools) were delivered to NIH/3T3 cells at 10 µM, by 6 µM EndoPorter™ carrier (GeneTools), according to manufacturer's instructions. When appropriate, αAK158887-1.1 or control Antisense LNA GapmeRs (Exiqon) were delivered to cells at 50 nM, by Lipofectamine 3000 reagent (TermoFisher), according to manufacturer's instructions.

Murine embryonic fibroblasts (MEFs). CD1wt mouse embryonic fibroblasts (MEFs) were isolated from E14.5 embryos. The head, vertebral column, dorsal root ganglia and all internal organs were removed and discarded. The remaining tissue was manually dissociated and incubated in 0.05% trypsin (Gibco) for 10-15 minutes to create single cell suspension. Cells were then plated onto 10-cm tissue culture dish in mEFs medium (DMEM-Glutamax™ (Gibco), supplemented with 10% FBS and 1x penicillin/streptomycin. Cells were harvested, splitted and cryopreserved at passage 2. MEFS were used as feeders for FRDA induced pluripotent stem cells (iPSCs). To inhibit their proliferating capability, they were treated with 10 µg/ml of Mitomycin C (Sigma), for 3 hours prior to use.

FRDA lymphoblasts. Cell lines GM15849, GM15850 and GM15851 were purchased from Coriell Institute and were cultured in RPMI1640 medium (Sigma), supplemented with 15% FBS, 2mM L-glutamine and 1x penicillin/streptomycin, at 200,000 cells/ml. Cells were spininoculated with lentiviral particles for 90 minutes at 2500 rpm.

FRDA fibroblasts. Cell line GM04078 was purchased from Coriell Institute and was cultured in MEM-Glutamax^{TM} (Gibco) supplemented with 15% FBS and 1% non-essential amino acid (NEAA) at 14,000 cells/cm^2. Lentiviral transductions were performed at moi's reported in the corresponding figures.

Building the NMHV constructs

The codon- and restriction enzyme-optimized cds of NMHV (Nuclear-localization-signal, multimerized-MS2 peptide, Hemagglutinin-antigen, Virion-peptide-16) apo-transactivator is the following:

ACCATGGTTCCAAAAAAGAAGAGAAAGGTGCCAAAAAAGAAGAGAAAGGTAGCTTCTAACTTTACTC
AGTTCGTTCTCGTGGAAAATGGCGGAACTGGCGACGTGACTGTCGCCCCAAGCAACTTCGCTAACGG
GGTCGCTGAATGGATCAGCTCTAACTCGCGTTCACAGGCTTACAAAGTAACCTGTAGCGTTCGTCAGA
GCTCTGCGCAGAATCGCAAATACACCATCAAAGTCGAGGTGCCTAAAGTGGCAACCCAGACTGTTGG
TGGAGAGGAGCTTCCTGTAGCCGGCTGGCGTTCGTACTTAAATATGGAACTAACCATTCCAATTTTCG
CTACGAATTCCGACTGCGAGCTTATTGTTAAGGCAATGCAAGGTCTCCTAAAAGATGGAAACCCGATT
CCCTCAGCAATCGCAGCAAACTCCGGCATCTACTATCCGTATGATGTGCCGGATTATGCGACCGGTGA
CGCCCTTGACGATTTTGACTTAGACATGCTCCCAGCCGATGCCCTTGACGACTTTGACCTTGATATGCT
GCCTGCTGACGCTCTTGACGATTTTGACCTTGACATGCTCCCAGGCTAA (here, Kozak/start, NLS(2x), MS2_coat potein, HA tag, AgeI restriction site, VP16 transactivating peptide (3x), and stop modules are highlighted by alternate styles, normal and underlined).

NMHV cds was synthesized, cloned into pUC57, grown in Xl1-blue cells and sequence-verified for us by GenScript. The cds was trasferred as BamHI/SalI fragment into BamHI-SalI cut pCCLsin.PPT.hPGK.EGFP.Wpre (Follenzi and Naldini, 2002). The resulting plasmid, LV_NMHV, was subsequently grown in ElectroMAX^{TM} Stbl 4^{TM} (Invitrogen) cells and sequence-verified. LV_NMHV was used as an expression plasmid for FMR1, NAP22 and NRGN

experiments in HEK293T cells. The same construct was utilized in producing the corresponding recombinant lentivirus, for Emx2 and Foxg1 assays in neural precursors.

Please note that pCCLsin.PPT.hPGK. EGFP.Wpre was used as the negative control for LV_NMHV and is referred to as "EGFP", unless otherwise indicated.

The NMHE expressing lentivector was obtained from LV_NMHV, replacing its AgeI/SalI fragment (encoding for the VP16 peptide) by the 141bp AgeI/SalI fragment ACCGGTTACCTGAGCACCCAGTCCGCCCTGAGCAAAGACCCCAACGAGAAGCGCGATCACATGGTCC TGCTGGAGTTCGTGACCGCCGCCGGGATCACTCTCGGCATGGACGAGCTGTACAAGTAAAGCGGCC GCGTCGAC (encoding for the carboxyterminal EGFP peptide YLSTQSALSKDPNEKRDHMVLLEFVTAAGITLGMDELYK).

Building ncRNA constructs

The sequence of the RNA cofactor fragment MF6 was as follows ("MS2 coat protein-binding stem-and-loop moieties" are underlined):

MF6_AGATCTCGGGAAACATGAGGATCACCCATGTCGCCCGCTCCACCCAAACAACCCCCTAAACAT GAGGATCACCCATGTCGAGGGCACCACCCAAACAAACAATGAAACATGAGGATCACCCATGTCGCAT TCTCCAACCAACCAACCGGGGAAACATGAGGATCACCCATGTCGCCCCCTACACCCAAACAACCGCG CAAACATGAGGATCACCCATGTCGCGCGCATCACCCAAACAAACCAGGAAACATGAGGATCACCCAT GTCGCCTGGGATCCACCGATATC

MF6 was cloned as BglII/EcoRV fragment into BamHI-EcoRV cut pcDNA3DPvuII, thus obtaining MF6-∅.

FMR1-, NAP22- and NRGN-specific, wild-type ncRNA baits were amplified from genomic DNA by the oligos reported in Supplementary Table S1. NAP22.60L-derivative, mutant baits (for sequences, see Supplementary Table S7) were chemically synthesized as dsDNAs, flanked by sticky, BamHI/SalI compatible adaptors. All baits were then cloned as BamHI/XhoI or BamHI/SalI fragments into the BamHI/XhoI cut MF6-∅ plasmid, thus obtaining the corresponding MF6-bait constructs.

Sequences of the RNA cofactor fragments MF1 and MF2 were as follows (here "MS2 coat protein-binding stem-and-loop moieties" are underlined):

MF1_GATCGATATCCGGGAAACATGAGGATCACCCATGTCGCCCGCAGCGGATCCCCCGTCGACTTT TTTGGTACC;

MF2_GATCGATATCCGGGAAACATGAGGATCACCCATGTCGCCCGCAGCGGATCGATATCCGGGAA ACATGAGGATCACCCATGTCGCCCGCAGCGGATCCCCCGTCGACTTTTTTGGTACC.

MF1 was cloned as BamHI-compatible/KpnI fragment into BamHI-KpnI cut pCCLsin.PPT.hPGK.EGFP.Wpre vector (Follenzi and Naldini, 2002), thus obtaining LV_MF1-∅. LV_MF2-∅ was obtained by cloning an additional MF1 finger (a BamHI-compatible/KpnI fragment) into BamHI/KpnI cut LV_MF1-∅.

The Emx2 and FoxG1 ncRNA baits were generally amplified from genomic DNA, by the oligos reported in Supplementary Table S2. The Emx2 30bp bait was obtained by annealing the two oligos reported in the same Table. Baits were cloned as BglII/XhoI fragments into BamHI/SalI cut LV_MF1/2-∅ plasmids, thus obtaining the corresponding LV_MF1-bait and LV_MF2-bait constructs.

Off-target gene selection

ncRNA bait sequences were blasted against human and murine genomes by Blast software (accessible at http://blast.ncbi.nlm.nih.gov and run online with the following parameters: blastn, "for somewhat similar sequences"; expect threshold: 40; word size: 7; max matches in a query range : 0; match/mismatch scores, 2, -3; gap costs: existence 2, extension 2; filter low complexity regions: no; filter species-specific repeats: no). Homologous modules found by Blast were then prioritized and selected, based on their length (between 50 and 110 bp), gap density (<20%) and identity (>70%). Selected modules were subsequently mapped to the transcriptome, using the UCSC Genome browser (accessible at http://genome.ucsc.edu; assemblies mm10 and hg19) and the Ensemble-GENCODE track (accessible at http://www.ensembl.org). Lastly, they were filtered on the basis of their distance from TSS's of potential off-target genes (from -0.5kb to +0.5kb). The results are summarized in Supplementary Tables S5 and S6.

Building accessory expression plasmids

Plasmids driving constitutive expression of mCherry and EGFP referred to in Supplementary Figures S1 and S5, Pgkp1-mCherry and CMVp-EGFP, were obtained by replacing EGFP cds by mCherry cds in pCCLsin.PPT.hPGK.EGFP.Wpre and by cloning EGFP cds into pcDNA3DPvuII, respectively.

HEK293T cell cotransfection

Cells were generally cotransfected by LipoD reagent, according to Manufacturer's instructions. Where not otherwise specified, aliquots of 10^6 cells were cotransfected by 0.75 μg of a ncRNA cofactor-expressing plasmid, 1.25 μg of an apofactor (or a control)-expressing plasmid and 0.25 μg of pcDNA3DPvuII-EGFP (see above), as internal control.

In specific cases (as highlighted in Legends to Figures), cells were cotransfected by Lipofectamine 3000 reagent, according to Manufacturer's instructions. Here two rounds of cotransfection were performed, at a 12-hours interval. In each round, where not otherwise specified, aliquots of 10^6 cells were cotransfected by 0.95 μg of ncRNA cofactor-expressing plasmid and 1.60 μg of apofactor (or control)-expressing plasmid.

Selection of candidate saRNAs

cDNAs encoding for pri-miRNAs targeting the *Foxg1*, *FRATAXIN* and Scn1a loci were designed using “BLOCK-iT™ RNAi Designer" (Invitrogen). This is a proprietary, freely online accessible program, conceived for selection of pri-miRNA-155-based, artificial miRNAs to be employed for gene knock-down. We repurposed it for designing potential small miRNA-like activators of target genes.

The 4kb genomic region extending from -3.8kb to +0.2kb with respect to the 5' *Foxg1*-mRNA TSS (Fig. 4.7A) was scanned in 0.5kb frames, in both sense and antisense orientation. Candidate miRNAs with a score ≥4.5/5 were shortlisted.

Selected non-coding regions of the *FXN* locus (named R0, R1 and R6) were scanned in 0.5kb frames, in both sense and antisense orientation. Candidate miRNAs with a score ≥4.5/5 were shortlisted.

The transcription unit of the *Scn1a* locus and its 2kb surroundings were scanned, in both sense and antisense orientation. Candidate miRNAs with a score ≥4.5/5 were shortlisted. Candidate miRNAs were further filtered for absence of potential off-targets within the murine genome and transcriptome, by Blat (UCSC) and Blastn (NCBI) softwares, respectively. A summary of these candidate miRNAs and their key parameters is provided in Supplementary Tables S8, S9 and S10.

pri-miRNA Lentiviral vector construction

cDNAs encoding for pri-miRNAs targeting the *Foxg1* and *FRATAXIN* loci were prepared as follows: pri-miRNA-cDNAs were cloned into BfuAI-digested pLVmiR.23 (Diodato et al., 2013), so obtaining "LTR-pPgk1-eGFP-pri-miR-Wpre-LTR" constitutive expressors. The TetON-controlled "LTR-TREt-eGFP-pri-miR-Wpre-LTR" pri-miRNA expressors were obtained by transferring the AgeI/KpnI inserts originating from the corresponding constitutive expressors into AgeI/KpnI cut LV:TREt-IRES2-EGFP (Falcone et al., 2015). Finally, "LTR-pPgk1-rtTA^{M2}-Wpre-LTR" was described in ref (Spigoni et al., 2010). For each construct, inserts and their surroundings were checked by double strand sequencing.

Recombinant lentivirus production

Recombinant third generation self-inactivating (SIN) lentiviruses were produced and titrated as previously described (Spigoni et al., 2010).

RNA profiling

Total RNA was extracted from cells using TRIzol Reagent (Invitrogen) according to manufacturer's instructions. Agarose gel electrophoresis and spectrophotometric measurements (NanoDrop ND-1000) were employed to estimate its concentration, quality and purity. RNA preparations were treated by TurboDNAseI kit (Gibco) 1 h at 37°C. At least 0.5 µg of total RNA from each sample was retrotranscribed by SuperScriptIII^{TM} (Invitrogen) in the presence of random hexamers, according to the manufacturer's instructions. 1/100 of the resulting cDNA was used as substrate of any subsequent qPCR reaction. Next, negative

control PCRs were run on RT− cDNA preparations. In general, PCR reactions were performed by the SsoAdvanced SYBR Green Supermix™ platform (Biorad), according to manufacturer's instructions. For each transcript under examination and each sample, cDNA was PCR-analyzed in technical triplicate, against absolute standards, and average results calculated. Averages were normalized against *Gapdh* and further normalized against controls. Experiments were performed at least in biological triplicate and analyzed by Student's t-test.

Western Blotting

Western analysis was performed according to standard methods. Total cell lysates in CHAPS buffer were quantified by BCA protein assay kit (Fisher Scientific # 10678484) and denatured at 95°C for 5 min, prior to loading. At least 15 µg of proteins were loaded per each lane and were run on a 12% acrylamide - 0.1% SDS gel (NAP22 and FoxG1/FOXG1), or 15% acrylamide - 0.1% SDS gel (FXN), or 8% acrylamide - 0.1% SDS gel (Scn1a). NAP22 was detected by a primary rabbit anti-BASP1 polyclonal antibody (Sigma #SAB2107478), used at 1:2,500, and a secondary HRP-conjugated anti-rabbit antibody (LifeTech # 32260), used at 1:2000. As previously reported (Carpenter et al., 2004), under these conditions NAP22 gives rise to a 50kDa dimer band. FOXG1/Foxg1 was detected by a primary rabbit anti- Foxg1 polyclonal antibody (Brancaccio et al., 2010), used at 1:2000, and a secondary HRP-conjugated anti-rabbit antibody (LifeTech #32260), used at 1:2000; Frataxin was detected by a primary mouse anti-FXN (Abcam ab110328), used 1:200, and a secondary HRP-conjugated anti-rabbit antibody (LifeTech #31430); Scn1a was detected by a primary rabbit anti-Scn1a (abcam24820) used 1:100, and a secondary HRP-conjugated anti-rabbit antibody (LifeTech #32260). bACT was detected by a peroxydase C-conjugated mouse monoclonal antibody (Sigma # A3854), used 1:10,000. Target proteins and bACT were sequentially revealed by an ECL kit (GE Healthcare # GERPN2109). Images were acquired by an Alliance LD2-77.WL apparatus (Uvitec, Cambridge) and analyzed by Adobe Photoshop CS2 software™ and Microsoft Excel 11 software™.

ChIP-qPCR

The chromatin immunoprecipitation quantitative polymerase chain reaction assays (ChIP-qPCRs) were performed on chromatin extracted from HEK293T cells (case *NAP22*) or neural cell cultures (case *Emx2*). Cells were transfected with constitutive expression plasmids (case *NAP22*) or acutely infected with bio-active and control lentiviruses (case *Emx2*), similar to transactivation assays. Then, they were kept in culture for 72 and 96 hours, respectively. ChIP analysis was performed according to the MAGnify™ Chromatin Immunoprecipitation System protocol (Invitrogen), with minor modifications.

For each ChIP assay, chromatin from 10^6 cells was fixed by 1% formaldehyde, for 10 min at RT. After cell lysis, fixed chromatin was sonicated by a Soniprep 150 apparatus (on ice; 5 sec ON, 55 sec OFF; oscillation amplitude 5 microns; 4 cycles) into ~600bp fragments. Sonicated chromatin was immunoprecipitated for 2 hours at 4°C, by 1.5μg of an α-HA rat antibody (clone 3F10, Roche), 2.5μg of an α-RNApolII mouse antibody (clone 4H8, Abcam), 2.5 μg of an α -Ago1 (mouse clone 6D8.2, Millipore #04-083), 3.0 μg of an α -Ago2 (rabbit polyclonal, Abcam #32381) or 2.5μg of murine IgG (Invitrogen), in a final volume of 100μl. Immunoprecipitated DNA was purified according to the Manufacturer's instructions. Lastly, 1/30 of each immunoprecipitated (IP) DNA sample (case α-HA-IP) or 1/60 of it (case α-RNApolI-IP and IgG-IP controls) were amplified by qPCR. For each sample, qPCRs were performed in technical triplicate. Averages were normalized against input chromatin and further normalized against control-treated samples. Experiments were performed at least in biological triplicate and analyzed by Student's t-test.

siRNA-RNAiMAX transfection.

Sequences of siRNAs targeting the *Foxg1* locus and their anti-GFP control are provided in Supplementary Table S8. For transfection, E16.5 mouse post-mitotic neurons were seeded in 12-well plates at about 3x10^5 cells/well in 600 μl Neurobasal A-based differentiative medium. At the same time of seeding, 15pmol of each siRNA was complexed with 2μl of Lipofectamine RNAiMAX reagent (Invitrogen) and transfected to the cells to a final 25nM concentration, according to the manufacturer's protocol. 24 h after transfection,

medium was replaced and siRNAs were re-transfected as described above. RNA was extracted 48 h after the second transfection and analyzed by qRTPCR.

siRNA-RVG-9dR transfection.

The sequence of RVG-9dR peptide (synthesized by LifeTein) is reported in Supplementary Table S8. For RVG-9dR-mediated transfection, the different siRNA duplexes (100 pmol each) were incubated with RVG-9R peptide at a 1:10 molar ratio in 15 µl, for 15 min at room temperature. RNA-polypeptide binding was assessed on not-denaturing agarose gel by electrophoretic mobility shift assay. Next, the complexes were added to acutely dissociated E12.5 or E16.5 neural cells, plated in 24-well plates, at 1,5x10^5 cells/300 ml, or in 12-well plates, at 3x10^5 cells/600 ml, respectively. 24 h later, the transfection was repeated as described above. Cells were cultured for further 48h and, finally, RNA was extracted and examined by qRTPCR.

Adeno-associated virus cloning and production.

As for AAV production, genomic plasmids were obtained by transferring "Pgk1p-EGFP-pri-miRNA" modules from the corresponding lentiviral expressors into a scAAV2-type backbone [AAVscCB6(p1023)Q], upstream of a rabbit-polyA signal. Recombinant AAVs were packaged as previously described (Zhang et al., 2011b).

***In vivo* RNAa assays**

P0 pups were anaesthetized on ice for 40-60s. $3*10^{10}$ AAVs particles, mixed with 0.02% fast-green dye, were injected through the skull into the lateral ventricle, by free hands, using a sharp pulled micropipette (hole external diameter about 40 µm) with the help of light fibers. Animals were left to recover in a warm clean cage. Next they were transferred to their mother. 21 days later they were finally sacrificed. Brains were dissected from the skull, neocortices were homogenized and resuspended in TRIzol reagent (Ambion). Alternatively, for immunofluorescence, brains were fixed in fresh 4% PFA overnight at 4°C.

Next, they were cryoprotected overnight in 30% sucrose-1X PBS at 4°C and finally frozen on dry ice in Killik (BioSigma).

Immunofluorescence

HEK293T cells, naive or lipofected with LV_NMHV or LV_NMHV/pcDNA3DPvuII-MF6-NAP22, were grown on poly-L-lysine coated glass coverslips in 12 multiwell plates, fixed with 4% paraformaldehyde (PFA) for 20 min at 4°C and then washed 3 times in 1X PBS. Lentivirus-transduced, floating neural precursor aggregates were gently trypsinized to single cells and left to attach one hour at 37°C to poly-L-lysine (200µg/µl) coated SuperFrost Plus microscope slides (Menzel-Glaser). Here they were fixed by 4% PFA for 20 min at 4°C and washed 3 times in 1X PBS.

In all cases, immunofluorescence was performed as previously described (Diodato et al., 2013). The following primary antibodies were used: anti-HA, rat clone 3F10 (Roche #12158167001), 1:500; anti-beta-actin, mouse clone AC-15 (Sigma #A3854, 1:1000); anti H3K9me3, rabbit polyclonal (Invitrogen #P7N49-1008), 1:200; anti-Tubb3, mouse clone Tuj1 (Covance #MMS-435P), 1:1000; anti-GFP (chicken polyclonal, Abcam ab13970), 1:400; anti-Foxg1 (rabbit polyclonal, (Brancaccio et al., 2010), 1:200; anti-Frataxin (mouse monoclonal, Abcam ab110328) 1:200. Secondary antibodies were conjugates of Alexa Fluor 488, and Alexa Fluor 594 (Invitrogen), used at 1:600.

Tubb3 immunofluorescences were photographed on a Nikon Eclipse TS100 fluorescence microscope equipped with a DS-2MBWC digital microscope camera with a 20X objective. Immunoprofiled brain sections were photographed on a Nikon TI-E microscope, equipped with 20X or 40X objectives and a Hamamatsu C4742-95 camera. HA, beta-actin, H3K9me3 and Frataxin immunofluorescences were photographed on a Nikon Eclipse TI microscope, equipped with a 40X objective and a Nikon C2 confocal system. For each sample, Z-stacks of 6, 0.5mm-spaced optical sections, flattened and averaged, were shown. All images were processed using Adobe 9.0.2 Photoshop 2 CS2 software and ImageJ Cell Counter plug-in.

Statistical analysis

As for *in vitro* assays, each "biological replicate" included cells pooled from at least two independent wells/petri dishes. As for *in vivo* tests, each "biological replicate" corresponded to a single brain. Numbers of biological replicates analyzed in each experiment (*n*) are shown under the corresponding graphs. Each biological replicate was scored at least in technical triplicate.

Data were normalized as reported in figure legends and averaged. Variability was graphically shown by standard error of mean bars.

Statistical significance of results was evaluated by Student's t-test (unpaired, one-tail) or ANCOVA. In case of multiple comparisons, to make each dataset suitable for drawing reliable conclusions from its comprehensive evaluation, statistical results were further filtered by the Benjamini and Hochberg algorithm (Benjamini, Y., Hochberg, Y., 1995). In such cases, the false discovery rate (FDR) was placed at <1/m, where m is the multiplicity of the comparison-set. Finally, statistical significance was graphically represented as follows: =, not significant; *, $p<0.05$; **, $p<0.01$; ***, $p<0.001$; ****, $p<0.0001$; *****, $p<0.00001$.

3. AIM OF THE WORK

In this thesis I intend to provide proofs of principles that ad hoc RNA-programmable transactivators and small activator RNAs (saRNAs, as effectors of RNA activation, RNAa) might be exploited for clean treatment of gene haploisufficiencies, by stimulating transcription of the spared gene allele. Both of these effectors elicit moderate transcriptional gains that leave gene expression levels within the physiological range. Moreover, artificial transactivators and saRNAs stimulate target genes *only where* these target genes are normally expressed, avoiding detrimental ectopic gene activation.

4. RESULTS

4.1 Upregulating endogenous genes by an RNA-programmable artificial transactivator

Artificial transactivation of specific endogenous genes ad libitum is a desirable goal for a number of basic and applied research purposes. To address these issues, we have conceived a novel, small and non-CRISPR-based device. This consists of a fully synthetic, ribonucleoproteic transcription factor, including a polypeptidic trans-activating domain as well as a non-coding RNA "bait" domain. The former stimulates transcription. The latter specifically drives the whole ribonucleoprotein to the target gene of interest (GOI). The two elements are kept together by two ancillary domains, a polypeptidic MS2 RNA-interacting domain (LeCuyer et al., 1995a), covalently joined to the former and forming with it the polypeptidic "apo-factor", and its corresponding hairpin RNA interactor (Carey et al., 1983; Romaniuk et al., 1987), covalently joined to the latter and forming with it the RNA "co-factor".

4.1.1 Upregulation of endogenous genes by artificial, non-CRISPR, RNA-programmable transactivators

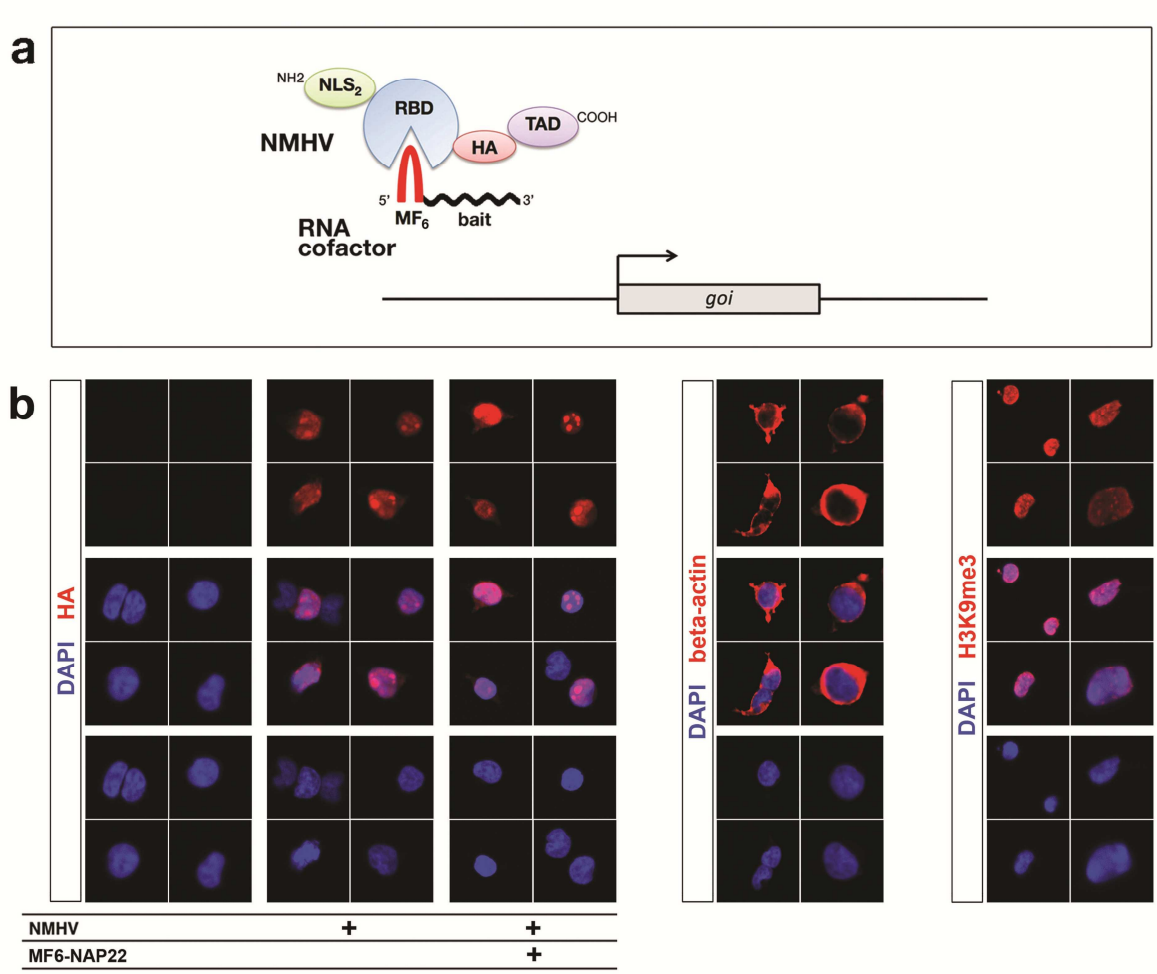
To overactivate our GOIs by a programmable device, we first assembled a chimeric cDNA encoding for a novel polypeptidic apo-transactivator, NMHV (Figure 4.1a). This included an RNA binding domain (RBD) as well as a transactivating domain (TAD). The former corresponds to the V75E;A81G mutant version of the bacteriophage MS2 coat protein, with a low tendency to aggregate as well as an ability to bind its mRNA with high affinity (LeCuyer et al., 1995b). The latter consisted of three tandemly arranged F-type domains from the VP16 protein of the herpes simplex virus (Urlinger et al., 2000). To target the apo-transactivator to the cell nucleus, RBD was preceded by two copies of the SV40-T protein

nuclear localization signal (NLS) (Kalderon et al., 1984). To allow immunodetection of the resulting polypeptide, a monomeric A influenza virus haemoagglutinin tag (HA) (Perdue et al., 1996) was interposed between RBD and TAD.

Then, for each GOI we built the DNA copy of a dedicated non coding RNA cofactor (Figure 4.1a). This included a hexameric, MS2 coat protein-binding stem-and-loop moiety (Carey et al., 1983; Romaniuk et al., 1987) (MF6) and a mid-sized (around 120 bases long), gene-specific RNA bait, complementary to a region near the GOIs transcriptional start-site (TSS) and co-oriented with its mRNA.

As a proof of principle, we decided to test our device in HEK293T cells, on three genes, *FMR1*, *NAP22* and *NRGN*, robustly expressed by these cells (http://webserver.mbi.ufl.edu/~shaw/293.html). We built the cDNAs encoding for the NMHV apo-transactivator and the MF6-containing cofactors specific for these genes (Figure 4.1c and Supplementary Table S1). We cloned them into RNA polymerase II (RNApolII) expression vectors, downstream of the constitutive *Pgk1* and CMV promoters, respectively. Next, we assessed the capability of the NMHV polypeptide to enter cell nuclei (Figure 4.1b) and we set up a DNA delivery protocol, suitable to cotransfect a large fraction of HEK293T cells in the presence of limited signs of toxicity (Supplementary Figure S1).

Later, we co-delivered NMHV, MF6-FMR1, MF6-NAP22 and MF6-NRGN plasmids (as well as their controls) to HEK293T cells, in different combinations. After three days, the transfected cells were profiled for the three GOIs by qRTPCR (Figure 4.1c-f). Each NMHV/ncRNA cofactor pair consistently stimulated the corresponding GOI. Upregulation was 47±18% for *FMR1* ($p<0.030$), 83±16% for *NAP22* ($p<0.004$) and 25±4% for *NRGN* ($p<0.014$) (Figure 4.1d-f). Conversely, overexpression of the three ncRNA cofactors in the absence of NMHV did not elicit any significant effect (Figure 4.1d-f) and the replacement of the VP16 domain by an EGFP moiety abolished gene upregulation (Supplementary Figure S2). Interestingly, NMHV and MF6-NAP22 delivery to HEK293T cells also led to a robust upregulation of NAP22 protein (5.77±2.03 fold, $p<0.039$, n=3,3; see Figure 4.1g,h).


a
NH2
NLS2
RBD
TAD
COOH
NMHV
HA
5'
3'
MF6
bait
RNA
cofactor
goi
b
DAPI HA
DAPI beta-actin
DAPI H3K9me3
NMHV + +
MF6-NAP22 +
c
2kb
DNA RNA
FMR1-qRTPCR-amplicon
FMR1.1-bait
FMR1
FMR1-AS1_variant 4
FMR1-AS1_variant 5
FMR1-AS1_variant 1
ENST00000334557
ENST00000218200
ENST00000440235
chr.X:146,989,501-147,033,500
NAP22-qRTPCR-amplicon
NAP22-bait
NAP22
LOC285696
NM_001271606
NM_006317
chr.5:17,214,001-17,280,000
NRGN-qRTPCR-amplicon
NRGN-bait
NRGN
ENST00000531241
ENST00000284292
ENST00000412681
chr.11:124,608,001-124,618,000

continued…

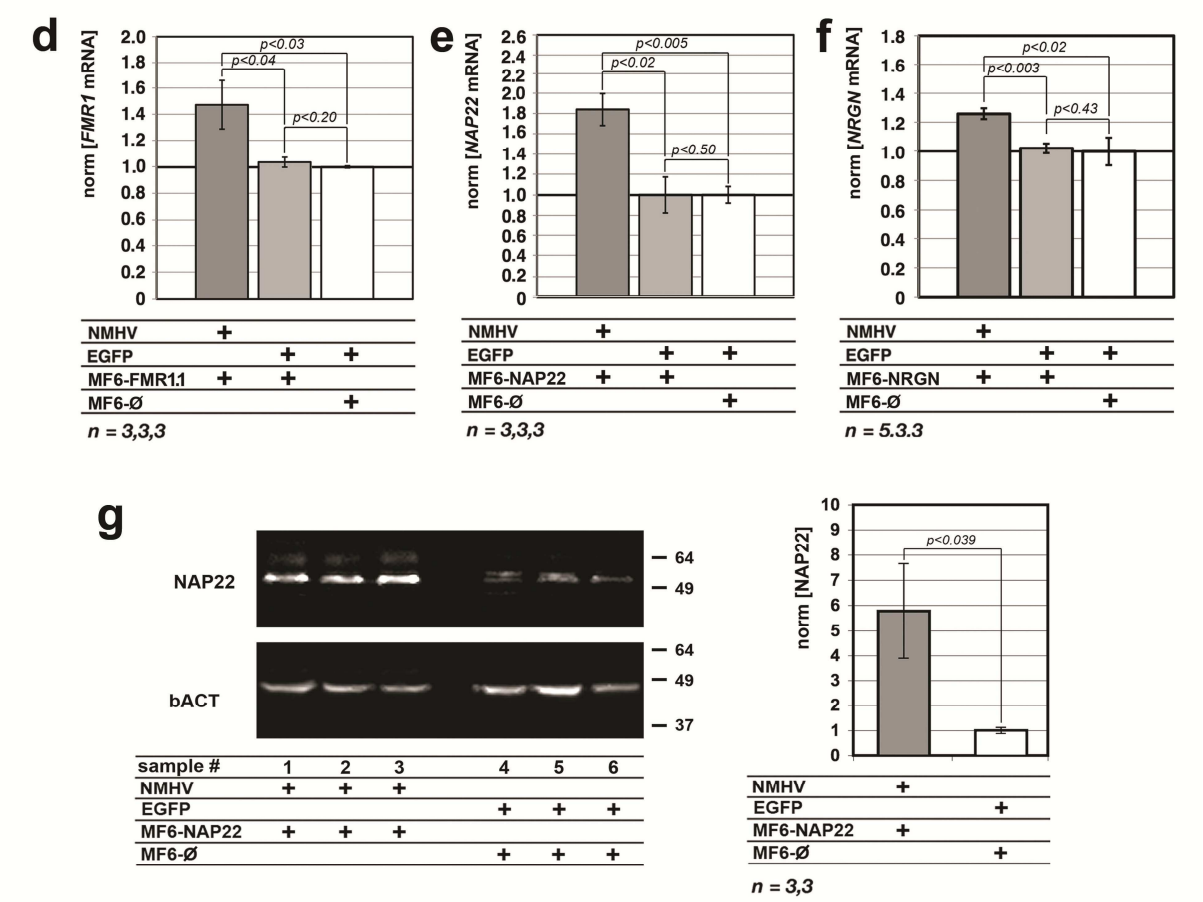


Figure 4.1. Design of the ribo-transactivator and its proof-of-principle validation. (a) Structure of the NMHV apo-activator and its RNA cofactor. NMHV includes: NLS2, nuclear localization signal 2x; RBD, MS2 RNA-binding domain; HA, hemoagglutinin epitope; and TAD, VP16-related transactivator domain, 3x. The RNA cofactor includes: MF6, MS2-high affinity, stem-and-loop finger, 6x; and "bait", short, target gene specific, RNA tag. *GOI* is the gene of interest. **(b)** Subcellular distribution of NMHV in HEK293T cells, in the presence or in the absence of its MF6-NAP22 RNA cofactor, as revealed by anti-HA immunofluorescence. Beta-actin and H3K9me3 distributions, cytoplasmic and nuclear, respectively, are also shown, as references. **(c)** Schematics of human *FMR1*, *NAP22* and *NRGN* loci, with natural transcripts, artificial baits and diagnostic amplicons used in this study. Nucleotide numbering refers to UCSC-hg19. Color code: blu, DNA; green, sense-oriented RNA; red, antisense-oriented RNA. **(d-f)** Upregulation of *FMR1, NAP22* and *NRGN* mRNAs in HEK293T cells cotransfected with NMHV- and MF6-bait-encoding plasmids, as evaluated 72 hours post-transfection. Pgkp1-

EGFP ("EGFP") and MF6-ø plasmids were used as controls. Results were normalized against *GAPDH* and further normalized against the EGFP/MF6-ø combination. **(g,h)** Upregulation of NAP22 protein by NMHV/MF6-NAP22. (**g**) Western blotting of NAP22 in HEK293T cells, four days after transfection by NMHV/MF6-NAP22 or EGFP/MF6-ø, via the "Lipofectamine 3000 protocol". (**h**) Quantification of NAP22 protein detectable in (g). Results were normalized against bACT and further normalized against the EGFP/MF6-ø combination. Numbers of biological replicates, *n*, are displayed under the graphs. Bars represent s.e.m.'s.

Remarkably, gene transactivation was specific. In fact, each NMHV/ncRNA pair, while stimulating the corresponding GOI, did not affect the other two genes (Supplementary Figure S3). Moreover, selected genes sharing extensive homologies with the three GOIs in the surroundings of their TSS's (Supplementary Table S5) were not affected (Supplementary Figure S3). Transactivation did not spread along the chromosome far from the intended bait target (Supplementary Figure S4a). Conversely, it was restricted to transcription units having their TSSs located in the 5' and 3' surroundings of such target (Figure 4.1c-e and Supplementary Figure S4b). Interestingly, the outcome of the manipulation depended on bait orientation. While sense-oriented RNA baits consistently supported NMHV-dependent GOI transactivation (Figure 4.1c-f and Supplementary Figure S4b), the antisense-oriented ones often failed to achieve this effect (Supplementary Figure S4c).

To corroborate these findings and explore mechanisms mediating transactivation, we monitored the level of *NAP22*-pre-mRNA in HEK293T cells cotransfected with NMHV and, alternatively, MF6-NAP22 or its negative control. [Here, to ease the detection of consequences of our manipulations, we employed a further optimized transfection protocol (Supplementary Figure S5)]. We found that, upon delivery of NMHV and MF6-NAP22, the qRTPCR signal corresponding to distinct regions of *NAP22*-pre-mRNA was differentially affected. This signal was unchanged across the splice donor site, while it was upregulated by +41$\pm$4% ($p<0.032$, n=4,4) closer to the splice acceptor site (Figure 4.2a,b).

Moreover, we evaluated the enrichment of *NAP22* chromatin for select transcription effectors. We employed two antibodies, recognizing the HA epitope and the RNApoIII

carboxyterminal domain (CTD). As for anti-HA ChIP, MF6-NAP22 expression enriched the region immediately downstream of the bait target (Figure 4.2a) by 5.5±2.0 fold, compared to MF6-∅ ($p<0.039$, n=3,3) (Figure 4.2c). With the same antibody, no enrichment was observed for chromatin of *SLC4A2* (Figure 4.2c), a potential off-target of MF6-NAP22 (Supplementary Table S5). Concerning anti-RNApolII-ChIP, no change of the IP fraction was detected in the region between the NAP22-bait target and the *NAP22* splice donor. However, a moderate statistically significant enrichment was observed at three more distal sites, by the 5' and 3' ends of the intron (+29±7%, $p<0.005$, n= 4,4; +32±2%, $p<0.023$, n=3,3; and +16±8%, $p<0.051$, n=3,4; respectively; see Figure 4.2a,d and Supplementary Figure S6).

All this suggests that, in the presence of the MF6-NAP22 cofactor, NMHV specifically binds to the surroundings of *NAP22*-TSS. In turn, this seems to promote the progression of RNApolII from the region immediately downstream of the TSS towards the 3' end of the gene and results in increased transcription.

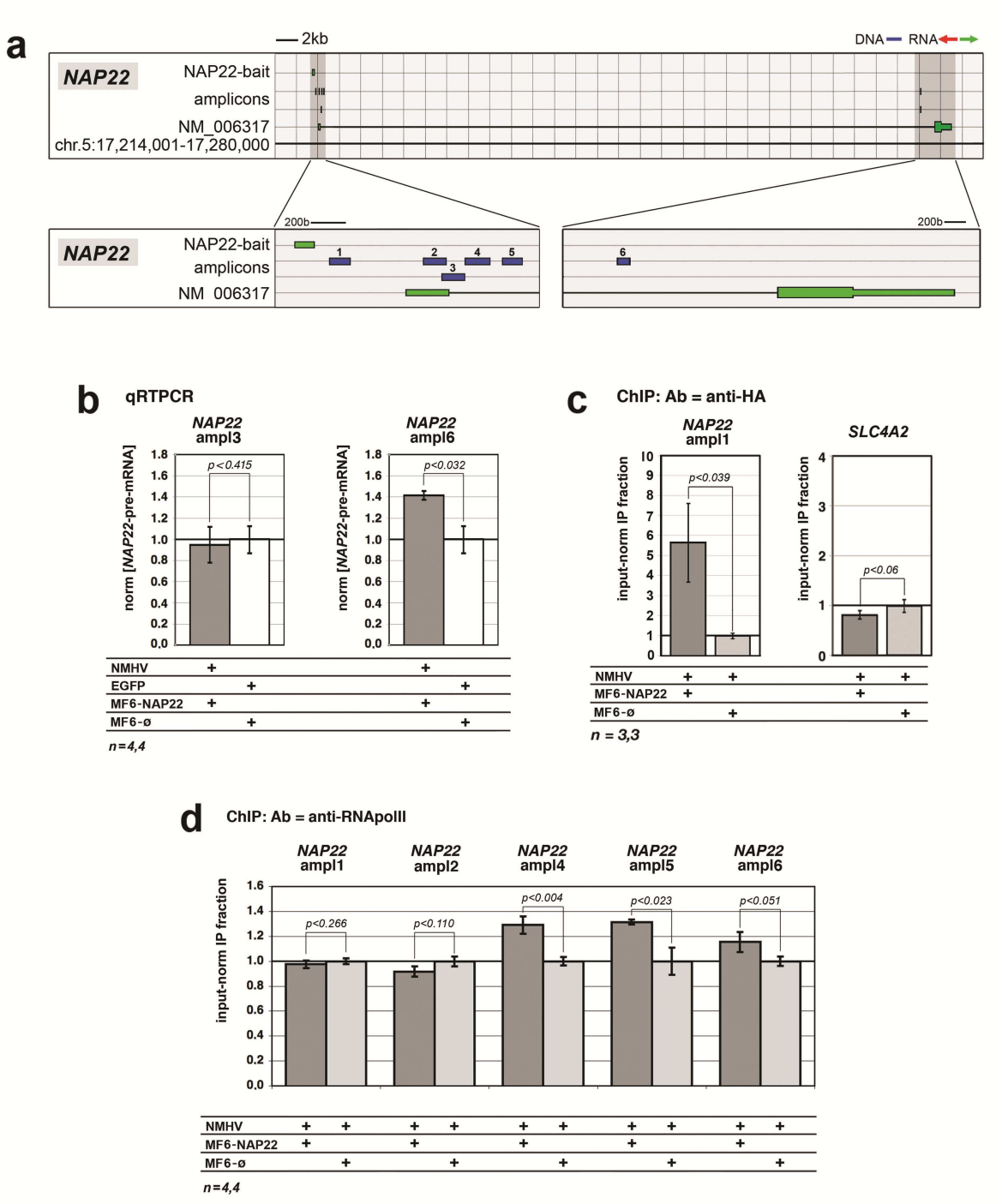


Figure 4.2. Mechanisms underlying *NAP22* transactivation in HEK293T cells. (**a**) Schematics of the *NAP22* locus with NAP22-bait and diagnostic amplicons employed for the analysis. (**b**) Modulation of *NAP22*-pre-mRNA in NMHV/MF6-NAP22-expressing cells, evaluated by intronic qRTPCR. Results were normalized against *GAPDH* and further normalized against the EGFP/MF6-ø combination. **(c)** Recruitment of NMHV at *NAP22* promoter in NMHV/MF6-NAP22-expressing cells, evaluated by anti-HA-ChIP/qPCR. The potential *NAP22*-offtarget

SLC4A2 was used as a specificity control. (**d**) RNApolII binding at different sites of the *NAP22* locus in NMHV/MF6-NAP22-expressing cells, evaluated by anti-RNApolII-ChIP/qPCR. In (**c,d**) results were normalized against input chromatin and further normalized against the NMHV/MF6-ø control. Noticeably, in (**b,d**) cells were transfected by the "Lipofectamine 3000 protocol". In (**b-d**) cell culture timing was as described for Figure 4.1. Numbers of biological replicates, *n*, are displayed under the graphs. Bars represent s.e.m.'s.

4.1.2 Specific upregulation of brain patterning genes in pallial precursors by dedicated RNA-programmable transactivators and its biological consequences.

Encouraged by these results, we decided to test the portability of this strategy to a gene mastering cortico-cerebral histogenesis, in an established in vitro model of this process. We stimulated the embryonic patterning gene *Emx2* in high-density, primary cultures of murine, cortico-cerebral precursors. Due to poor transfectability of these cells, we moved to lentiviral vectors. As the hexameric MF6 moiety resulted unstable in our lentiviral backbone (Follenzi and Naldini, 2002), we replaced it by its monomeric MF1 version. To MF1 we added an *Emx2*-specific bait, obtaining the MF1-Emx2 cofactor. We co-delivered lentiviruses encoding for NMHV, MF1-Emx2 and their controls to *Emx2*-expressing (Mallamaci et al., 1998), murine embryonic day 12.5 (E12.5) pallial precursors, in different combinations. Each virus was administered at a multiplicity of infection (moi) of 10, which is sufficient to transduce the almost totality of neural precursors, regardless of their rostro-caudal identity (see Figure S4 of (Brancaccio et al., 2010) and Supplementary Figure S7 of this thesis). Four days later, infected cells were profiled for *Emx2*-mRNA by qRTPCR (Figure 4.3a). Compared to controls, co-expression of NMHV and MF1-Emx2 upregulated *Emx2* by 16% ($p<0.002$, $n=9,7$). Neither NMHV nor MF1-Emx2 alone elicited any significant effect (Figure 4.3b). Moreover, compared to uninfected cells, co-infection of precursors with both control viruses was ineffective (+2.4%, with $p<0.36$ and $n=5,6$, Supplementary Figure S8).

It has been reported that upregulation of *Emx2* in pallial precursors slows down their neuronal differentiation (Diodato et al., 2013; Heins et al., 2001; Muzio et al., 2005). To

assess biological relevance of the small *Emx2* upregulation elicited by NMHV and MF1-Emx2, we evaluated the frequencies of cells expressing Tubb3 (an early neuronal postmitotic marker) within engineered neural cultures (Figure 4.3c,d and Supplementary Figure S9). Compared to controls, NMHV and MF1-Emx2 halved the frequency of $Tubb3^{+}$ cells ($p<10^{-6}$, with n=10,10), meaning that gene upregulation obtained by our strategy, albeit small, can yield robust biological effects.

We suspected that the limited *Emx2* upregulation elicited could be due to suboptimal interaction between the apo-transactivator and its ncRNA cofactor. Therefore, we tried to improve performances of our device, addressing this issue in two different ways. First, it has been reported that RNAs containing increasing numbers of MS2-binding stem-and-loop fingers interact with the MS2 coat protein in a progressively stronger way (Lykke-Andersen et al., 2000). Therefore, we replaced the monomeric-finger MF1-Emx2 cofactor by its dimeric-finger MF2-Emx2 derivative and assessed the performance of such derivative, paired with NMHV. Interestingly, this device increased *Emx2*-mRNA by about 40% (p<0.005, n=5,4), while MF2-Emx2 alone did not elicit any significant effect (Figure 4.3e). Second, we hypothesized that non-optimal apo-transactivator/RNA cofactor ratios might jeopardize the outcome of the system, because of defective holo-transactivator formation and possible dominant-negative effects. So we modulated the LV_NMHV/LV_MF2-Emx2 moi's ratio, while keeping the total moi fixed. When this ratio equalled 3:1, *Emx2*-mRNA was increased by 55% (p<0.002, n=3,3) (Figure 4.3f).

To assess if MF2-Emx2/NMHV-dependent stimulation was restricted to *Emx2*, we monitored the expression levels of six other genes (*Pax6*, *Hes6*, *Sip1*, *Couptf1*, *Nf1a* and *Lhx2*), randomly chosen among those active in pallial precursors (Mallamaci, 2011), that were potentially accessible to exogenous transactive complexes. None were affected, when neural cells were challenged by the best *Emx2*-transactivating strategy described above (Supplementary Figure S10a). Four additional genes (*Arid1a, CachD1, Ptpn12* and *Dvl3*), sharing extensive homologies with *Emx2* in the surroundings of their TSS's (Supplementary Table S6), were neither affected (Supplementary Figure S10a). Notably, the replacement of

the original ncRNA bait with its reverse complementary counterpart abolished *Emx2* transactivation (Supplementary Figure S11a).

To corroborate these findings, we performed a ChIP analysis. We immunoprecipitated chromatin of neural precursors infected with LV_NMHV and, alternatively, LV_MF1-Emx2 or its negative control, by an anti-HA antibody. Then, we quantified the genomic region downstream of the *Emx2*-bait by qPCR (Figure 4.3a). LV_MF1-Emx2 expression enriched this region by 3.0±0.2, compared to LV_MF1-∅ ($p<0.0005$, n=3,3). No enrichment was conversely observed for the chromatin of three potential LV_MF1-Emx2 off-targets, *Ptpn12*, *CachD1* and *Dvl3* (Figure 4.3g and Supplementary Table S6). This suggests that NMHV physically and specifically interacts with the *Emx2* locus in living cells, depending on the *Emx2*-bait, and possibly stimulates *Emx2* transcription.

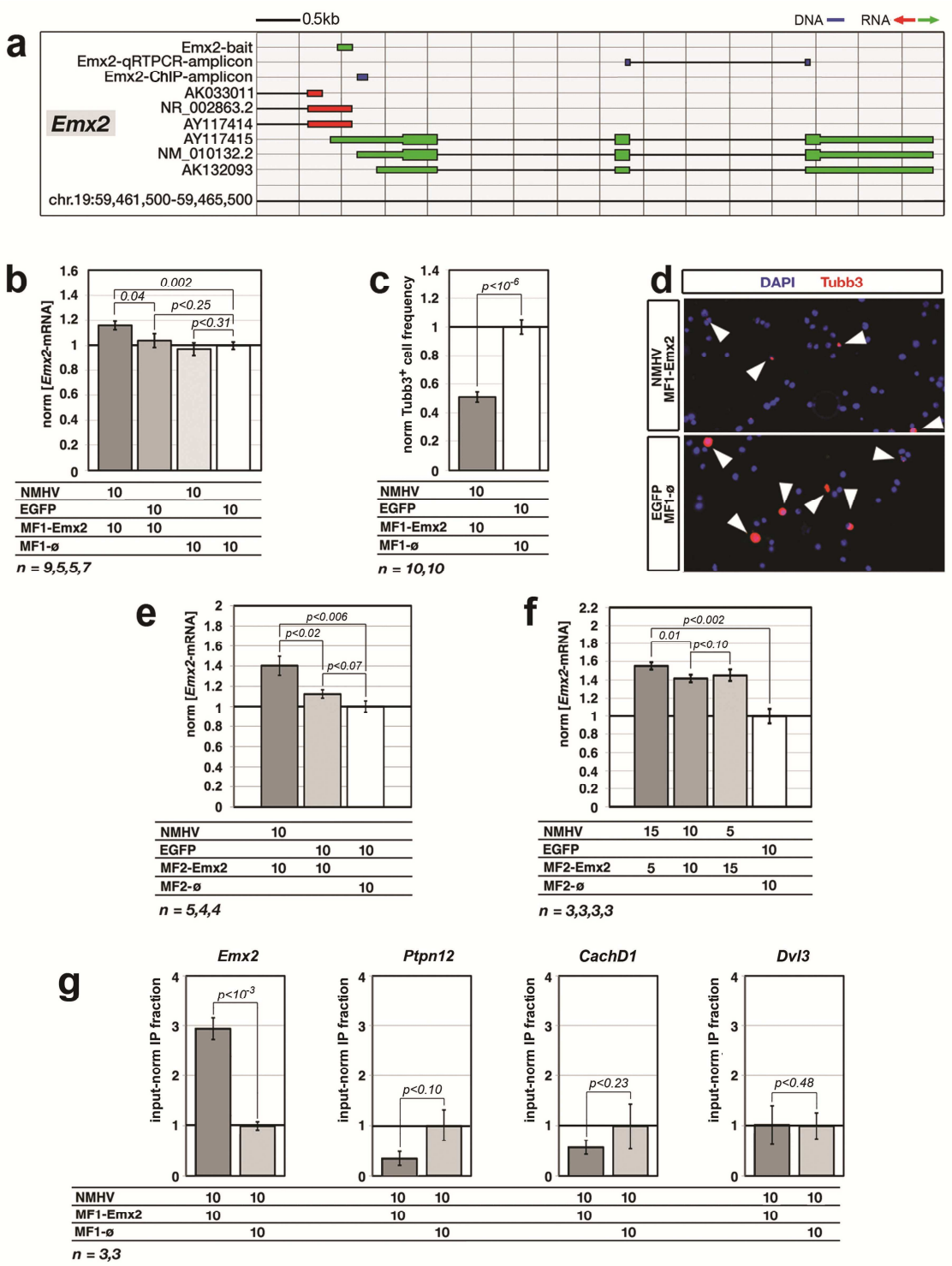


Figure 4.3. NMHV-mediated transactivation of *Emx2* in murine, embryonic cortico-cerebral precursors and its molecular and biological correlates. (a) Schematics of the murine *Emx2* locus, with natural transcripts, artificial baits and diagnostic amplicons used in this study.

Nucleotide numbering refers to UCSC-mm10. Color code: blu, DNA; green, sense-oriented RNA; red, antisense-oriented RNA. **(b)** *Emx2*-mRNA upregulation in precursors infected by NMHV- and MF1-Emx2-encoding lentivectors. EGFP and MF1-ø viruses were used as controls. Results were normalized against *Gapdh* and further normalized against the EGFP/MF1-ø combination. **(c)** Reduced frequency of cells immunopositive for the neuron-specific Tubb3 marker, in cultures of NMHV/MF1-Emx2-overexpressing precursors. Results were normalized against EGFP/MF1-ø controls. **(d)** Examples of aTubb3 immunofluorescences referred to in **(c)**. **(e)** Enhancing *Emx2* transactivation by improving the RNA cofactor structure. The assay was run similar to Figure 2a, replacing the monomeric-finger "MF1-bait" cofactor by its dimeric-finger "MF2-bait" derivative. **(f)** Enhancing *Emx2* transactivation by increasing the m.o.i. ratio of NMHV- and MF2-Emx2-encoding lentiviruses. The best results were obtained by an NMHV/MF2-Emx2 ratio of 3:1. **(g)** *Emx2* promoter enrichment in chromatin of NMHV/MF1-Emx2-overexpressing precursors, immunoprecipitated by an anti-HA antibody. Results were normalized against input chromatin and further normalized against the NMHV/MF1-ø control. Promoters of potential *Emx2*-offtargets *Ptpn12, CachD1 and Dvl3* were used as specificity controls. In all cases **(b-g)**, cortico-cerebral cells were dissociated from E12.5 embryos, acutely infected, cultured for 96 hours and finally analyzed. Throughout the figure, lentiviral multiplicities of infection (moi's) and numbers of biological replicates, *n*, are displayed under the graphs. Bars represent s.e.m.'s.

To generalize these results, we built a ncRNA cofactor specific for another key gene involved in brain patterning, *Foxg1* (Figure 4.4a). Coexpression of NMHV and MF1-Foxg1 cofactor in murine pallial precursors upregulated *Foxg1* by 23% ($p<0.002$, $n=3,3$) (Figure 4.4b). This led to a pronounced decrease of newborn, $Tubb3^{+}$ neurons generated by the engineered culture (about -70%, with $p<0.0004$ and $n=3,3$) (Figure 4.4c-d). Transactivation was restricted to the intended transcription unit. Neither the structurally unrelated *Emx2* nor the *Foxg1*-cis-associated AK158887 and 3110039M20Rik-001 units were affected (Supplementary Figures S10b and S11b).

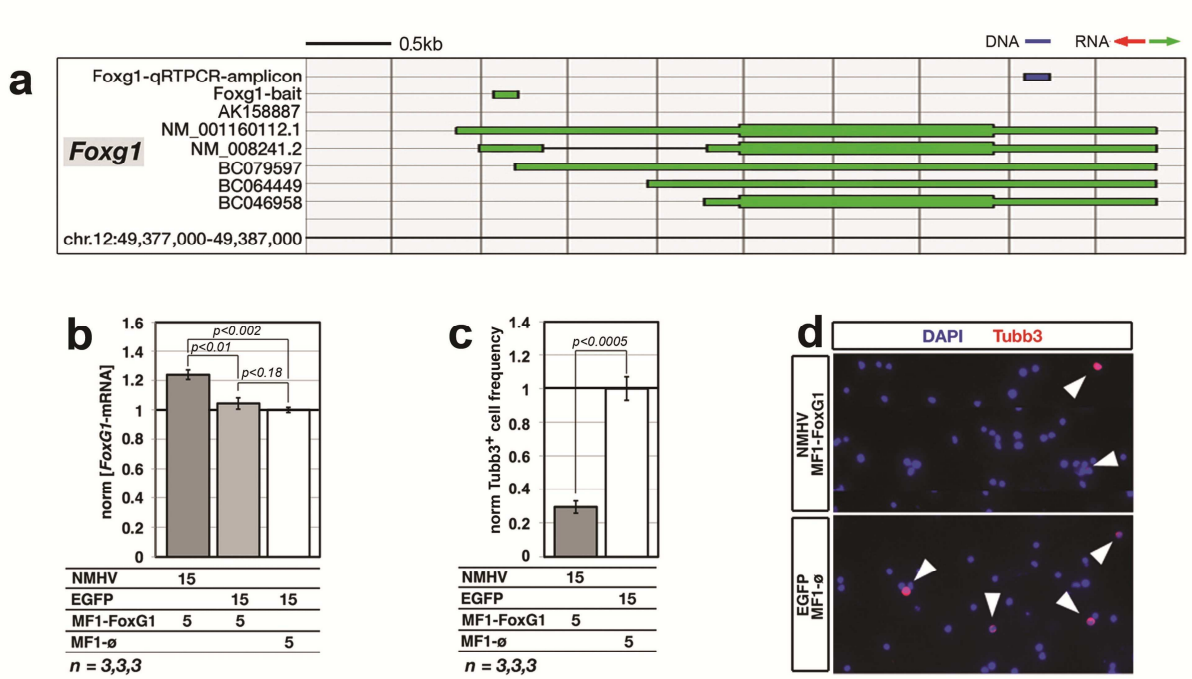


Figure 4.4. NMHV-mediated transactivation of *Foxg1* in murine, embryonic cortico-cerebral precursors and its biological correlate. (a) Schematics of the murine *Foxg1* locus, with natural transcripts, artificial baits and diagnostic amplicons used in this study. Nucleotide numbering refers to UCSC-mm10. Color code: blu, DNA; green, sense-oriented RNA. (b) *Foxg1*-mRNA upregulation in precursors infected by NMHV- and MF1-Foxg1-encoding lentivectors. EGFP and MF1-ø viruses were used as controls. Results were normalized against *Gapdh* and further normalized against the EGFP/MF1-ø combination. (c) Reduced frequency of cells immunopositive for the neuron-specific Tubb3 marker, in cultures of NMHV/MF1-Foxg1-overexpressing precursors. (d) Examples of aTubb3 immuno-fluorescences referred to in (c). In all cases (b-d) time-frame of the experiments as well as representation of moi's and statistical parameters are as in Figure 4.3.

Lastly, to better define the prospective scope of application of our device, we considered its effectiveness in correlation to the baseline expression level of the GOI. The question arose since our ncRNA cofactors did not harbor long polypurine/polypyrimidine tracts required for RNA:DNA triple helix formation (Morgan and Wells, 1968). For this reason, the interaction of these cofactors with chromatin could require a transcriptionally active conformation, prone to alternative mechanisms of ncRNA tethering (such as ncRNA:DNA heteroduplexing or ncRNA docking to nascent RNAs). To preliminarily address this issue, we delivered our best performing *Emx2*- and *Foxg1*-promoting protocols to neural precursors taken from two regions of the embryonic neural tube which do not express these two genes, rhombo-spinal tract (Mallamaci et al., 1998) and mesencephalon (Dou et al., 1999), respectively. As expected, GOI-mRNA levels remained extremely low as compared to cortico-cerebral precursors. No gene upregulation was elicited at all (Figure 4.5a-c).

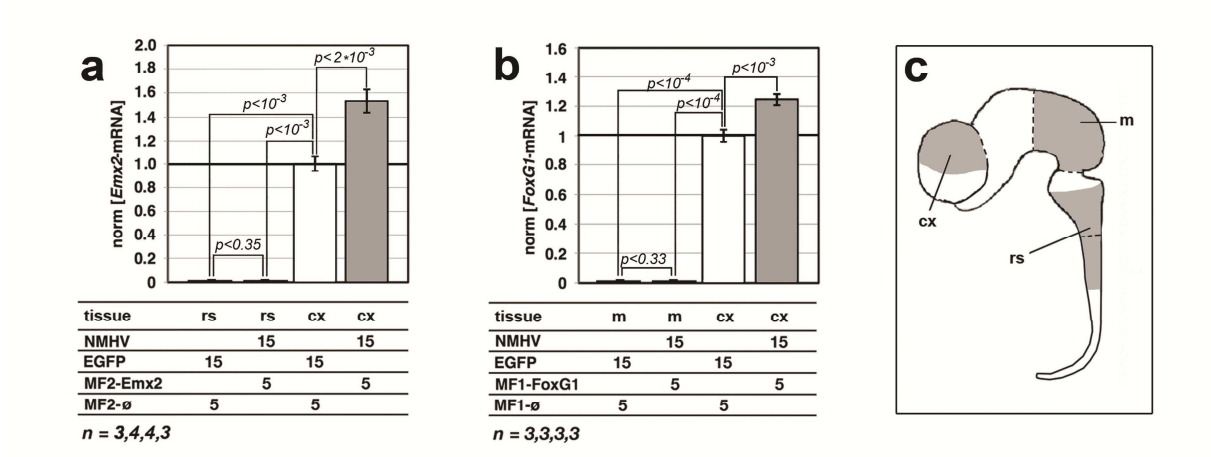


Figure 4.5. Lack of responsivity to *Emx2*- and *FoxG1*-specific ribo-transactivators by neural precursors of non-cortico-cerebral origin. (a) Unchanged *Emx2*-mRNA levels in E10.5 rhombo-spinal precursors, infected by NMHV- and MF2-Emx2-encoding lentiviruses or EGFP- and MF2-ø controls. **(b)** Unchanged *FoxG1*-mRNA levels in E10.5 mesencephalic precursors, infected by NMHV- and MF1-FoxG1-encoding lentiviruses or EGFP and MF1-ø controls. In both (**a**) and (**b**), transactivation of the two genes in E12.5 cortico-cerebral precursors is shown, as a positive control. Moreover, in both cases, results were normalized against *Gapdh* and further normalized against E12.5 cortico-cerebral precursors treated by EGFP/MF2-ø and EGFP/MF1-ø combinations, respectively. Time-frame of the experiments as well as representation of moi's and statistical parameters are as in Figure 4.3. **(c)** Idealized

representation of the murine E10.5 neural tube. cx, cerebral cortex; m, mesencephalon; rs, rhombo-spinal tract.

4.1.3 Shortening the baits and assessing mismatch tolerance of our device.

To further optimize our device, we shortened the RNA bait in charge of recognizing the GOI. This would minimize off-target risks and it would make chemical synthesis of baits for therapeutic applications easier. We replaced the NAP22 and FMR1.1 baits, sense-oriented and approximately 120b long, with their respective 5' and 3' halves (.60L and .60R, respectively, see Supplementary Table S1), and assayed the corresponding MF6-containing cofactors with the NMHV apofactor, in HEK293T cells. All four baits were able to support transactivation of the intended target genes (Figure 4.6a,b).

To confirm this result, additional tests were run on the *Emx2*-activating device, in cortico-cerebral precursors. Here, reducing the ncRNA bait from 179 to 60 bases (Supplementary Table S1) did not jeopardize device activity, which was slightly increased (Figure 4.6c). Further halving of bait length reduced such activity to hemi-maximal values (Figure 4.6c), suggesting that 60 base-long baits could be a satisfactory tool for gene stimulation.

Finally, to further confirm the specificity of our device, we mutagenized the most effective ".60-type" bait referred to above, NAP22.60L, and assessed the performances of the resulting MF6 chimaeras. Replacement of 30% of the original bases by mutant ones, distributed in 1 to 4 equispaced mismatch modules, fully suppressed *NAP22* transactivation (Figure 4.6d and Supplementary Table S7). Conversely, replacement of 15% of these bases resulted into a more articulated pattern. Transactivation was still observed when the baits included fully homologous modules of ≥18 bases. It was completely abolished as the length of these modules fell below 14 (Figure 4.6e and Supplementary Table S7).

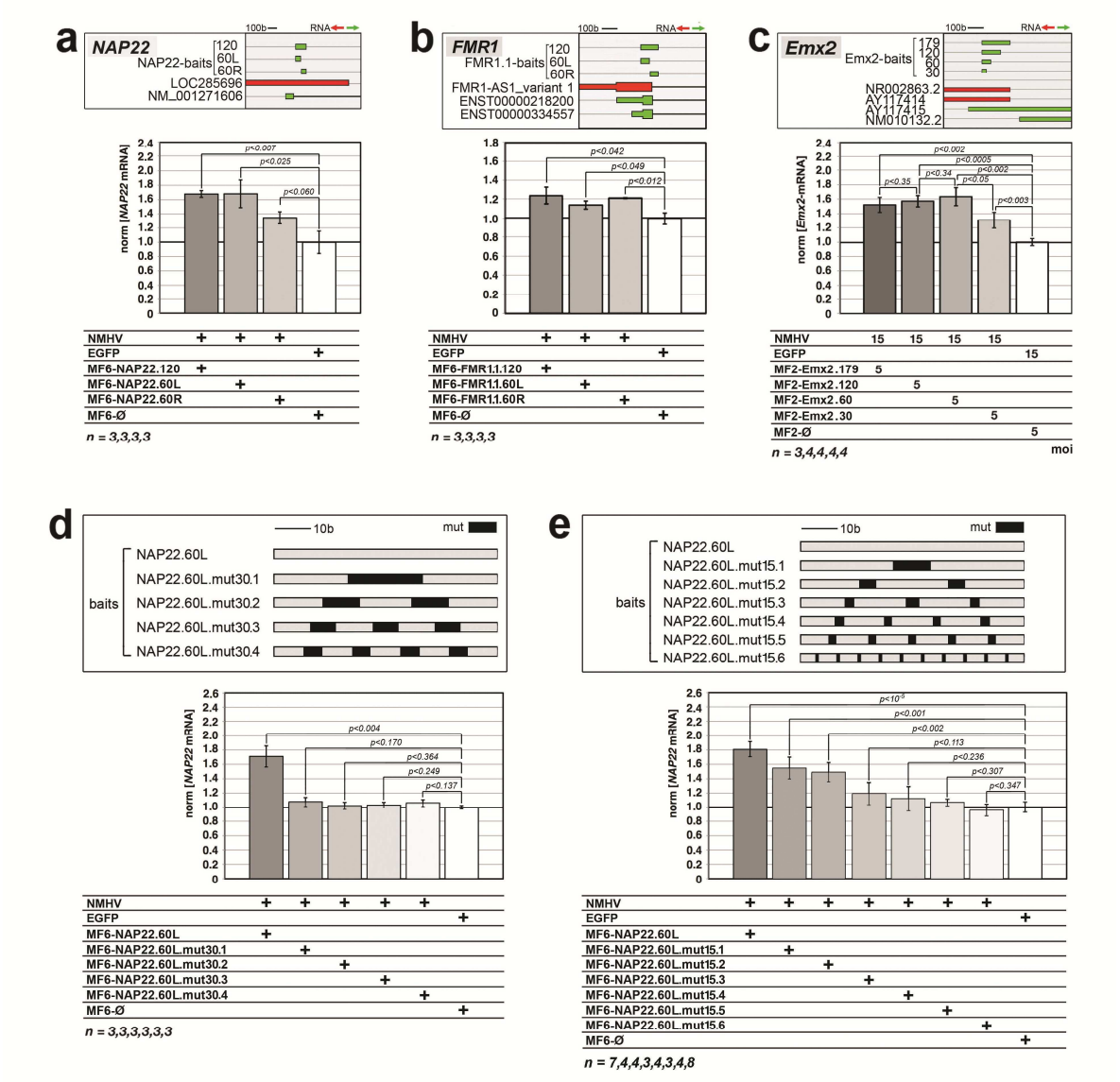


Figure 4.6. Consequences of RNA-bait shortening and mutagenesis. (a-c) Comparison of NMHV-dependent gene activation driven by select "primary" baits, NAP22 (a), FMR1.1 (b) and Emx2-S (c), and "secondary" baits obtained by heminested shortening of the former ones. (d,e) Full or partial suppression of NMHV-dependent *NAP22* transactivation driven by the NAP22.60L bait, upon replacement of 30% (d) or 15% (e) of its original bases by mutant ones. Mutant bases were distributed in up to 4 (d) and up to 10 (e) equispaced mismatching modules, as shown in top panels (sequences of mutant baits are reported in Supplementary Table S7). Results were normalized against *GAPDH* (a,b,d,e) and *Gapdh* (c) and further normalized against EGFP/MF6-ø (a,b,d,e) and EGFP/MF2-ø (c) control samples. Time-frame of the experiments as well as representation of moi's and statistical parameters were as in Figures 4.1 (a,b,d,e) and 4.3 (c).

4.2 RNA activation (RNAa) of haploinsufficient *Foxg1* gene in murine neocortex

Radical repair of haploisufficient gene deficits via genome engineering is hardly feasible. The same applies to therapeutic stimulation of the spared allele by artificial transactivators. Small activating RNAs (saRNAs) offer an alternative, appealing approach.

As a proof-of-principle, here we tested this approach on the Rett syndrome-linked, haploinsufficient, *Foxg1* brain patterning gene**.** We selected a set of artificial small activating RNAs (saRNAs) upregulating it in neocortical precursors and their derivatives. Expression of these effectors achieved a robust biological outcome. saRNA-driven activation (RNAa) was limited to neural cells which normally express *Foxg1* and did not hide endogenous gene tuning. saRNAs recognized target chromatin through a ncRNA stemming from it. Gene upregulation required Ago1 and was associated to RNApolII enrichment throughout the *Foxg1* locus. Finally, saRNA delivery to murine neonatal brain replicated *Foxg1*-RNAa *in vivo*.

4.2.1 Selecting miRNA-like saRNAs upregulating *Foxg1*-mRNA

In order to identify potential genomic targets appropriate for *Foxg1*-RNAa, we inspected the 5' surroundings of NCBI-RefSeq *Foxg1*-mRNA transcriptional start sites (TSSs) for sequences specifically amenable to miRNA targeting via the pri-miRNA-155-based Block-It platform (Diodato et al., 2013). We selected eight high-score candidates (Figure 4.7A and Supplementary Table S8) and we cloned the cDNAs, encoding for the corresponding precursors, into the lentiviral constitutive expressor pLVmiR.23 (Diodato et al., 2013) (Figure 4.7B,(*a*)). We acutely delivered the resulting lentiviruses to murine E12.5 neocortical precursors, we kept these cells as floating neurospheres in pro-proliferative medium for four days and we eventually scored them for *Foxg1*-mRNA levels by qRTPCR (Figure 4.7C). We found that 8 out of 8 miRNAs, 4 antisense-oriented (miR-αFoxg1.0650, miR-αFoxg1.1653, miR-αFoxg1.2764 and miR-αFoxg1.3700) and 4 sense-oriented (miR-αFoxg1.0755, miR-

αFoxg1.1694, miR-αFoxg1.2273 and miR-αFoxg1.3795), upregulated *Foxg1*, at different extents. The expression gain ranged from 1.28±0.24-folds (miR-αFoxg1.2764) to 2.88±0.34-folds (miR-αFoxg1.0650) (Figure 4.7E). Similar results were achieved upon delivery of miR-αFoxg1.0650 and miR-αFoxg1.1694 to HEK293T and NIH3T3 cells, which led to an increase of FOXG1/Foxg1 proteins of similar magnitude (Figure S12).

Next, we wondered if *Foxg1*-RNAa may be also achieved in differentiating derivatives of neocortical precursors. We transferred pri-miRNA-cDNAs of the four best-performing miRNAs (Figure 4.7E) into LV_TREt-IRES2EGFP (Raciti et al., 2013), inbetween the doxycyclin-controlled TREt promoter and an IRES2EGFP reporter gene (Figure 4.7B, (*b2*)). We employed the resulting lentiviruses - paired to a constitutive rtTA^{2S}-M2 transactivator expressor, LV_Pgk1p-rtTA^{2S}-M2 (Raciti et al., 2013) (Figure 4.7B, (*b1*)), to drive delayed, TetON-controlled miRNA expression. Unexpectedly, we found that only one miRNA (miR-αFoxg1.1694) upregulated *Foxg1*, by 1.56±0.11-folds (Figure 4.7F). The remaining ones were uneffective (Figure 4.7F).

Finally, to corroborate the significance of these results, we tested if the small expression gain elicited by our saRNAs led to an appreciable biological readout. For this purpose, we stimulated *Foxg1* by miR-αFoxg1.0650 and .1694 in proliferating murine neocortical precursors (Figure 4.8 A,B) and we evaluated the impact of this manipulation on generation of postmitotic, Tubb3^{+} neurons. *Foxg1* - in fact - inhibits the exit of neuronogenic precursors from cell cycle (Brancaccio et al., 2010; Martynoga et al., 2005) and even a small increase of its expression level is known to exert a deep impact on neuronogenic differentiation rates (Fimiani et al., 2015). Interestingly, both miRNAs halved the neuronal output of the culture, in a highly reproducible fashion (Figure 4.8 C,D).

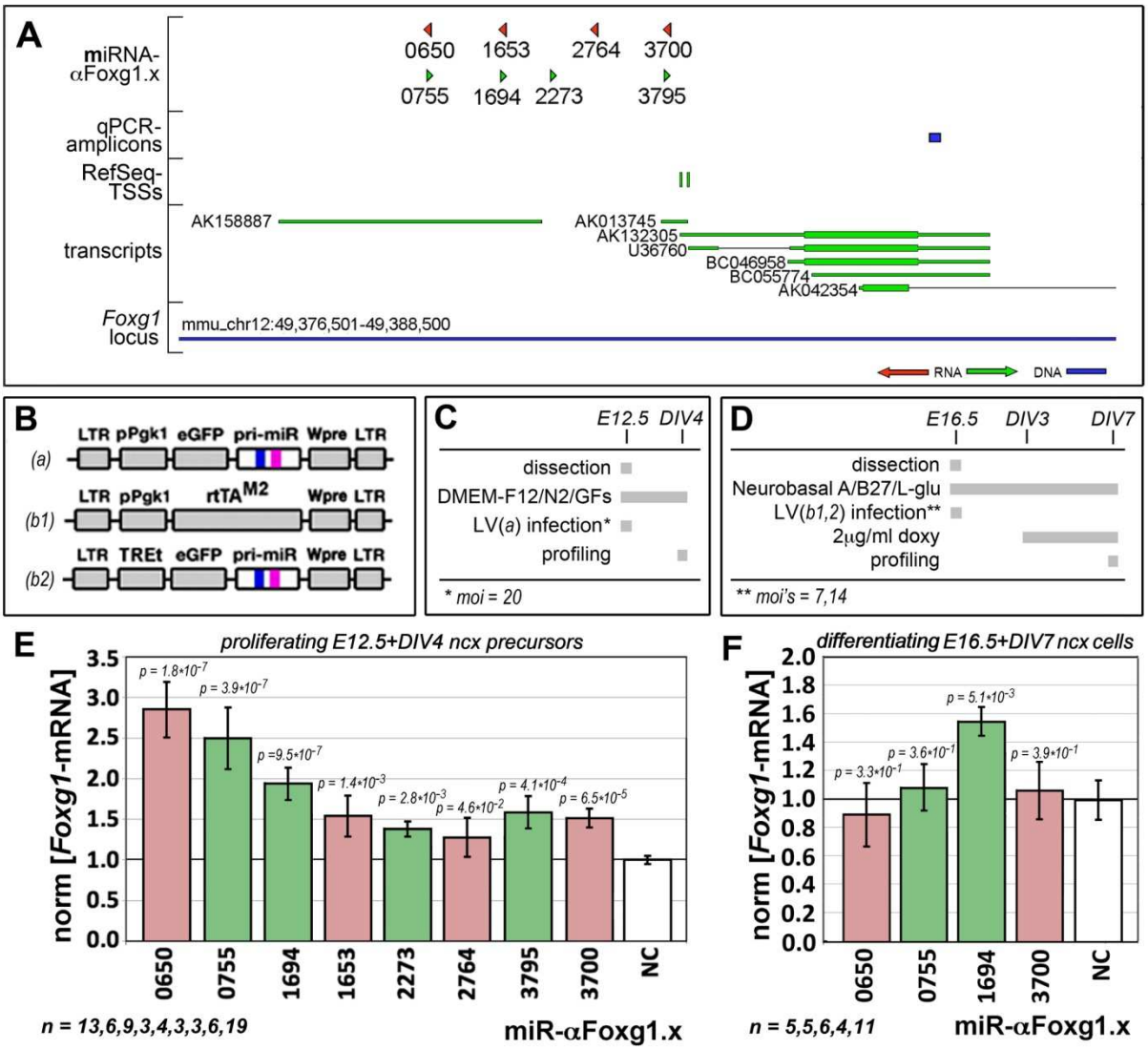


Figure 4.7. Screening for miRNA-like, small RNAs activating Foxg1-mRNA (Foxg1-saRNAs) in murine neocortical precursors and derivatives. (A) Schematics of the Foxg1 locus including saRNA positions and orientations as well as the diagnostic qRTPCR amplicon. **(B-D)** Lentiviral reagents and protocols employed for this screening. **(E,F)** Foxg1-mRNA levels in proliferating neocortical precursors and their differentiating derivatives, manipulated as in (C) and (D), respectively. Values double normalized, against Gapdh and control (NC). E, embryonic day. DIV, days in vitro. Bars represent sem's. n = number of biological replicates. p values calculated by t-Student assay (one-tail, unpaired).

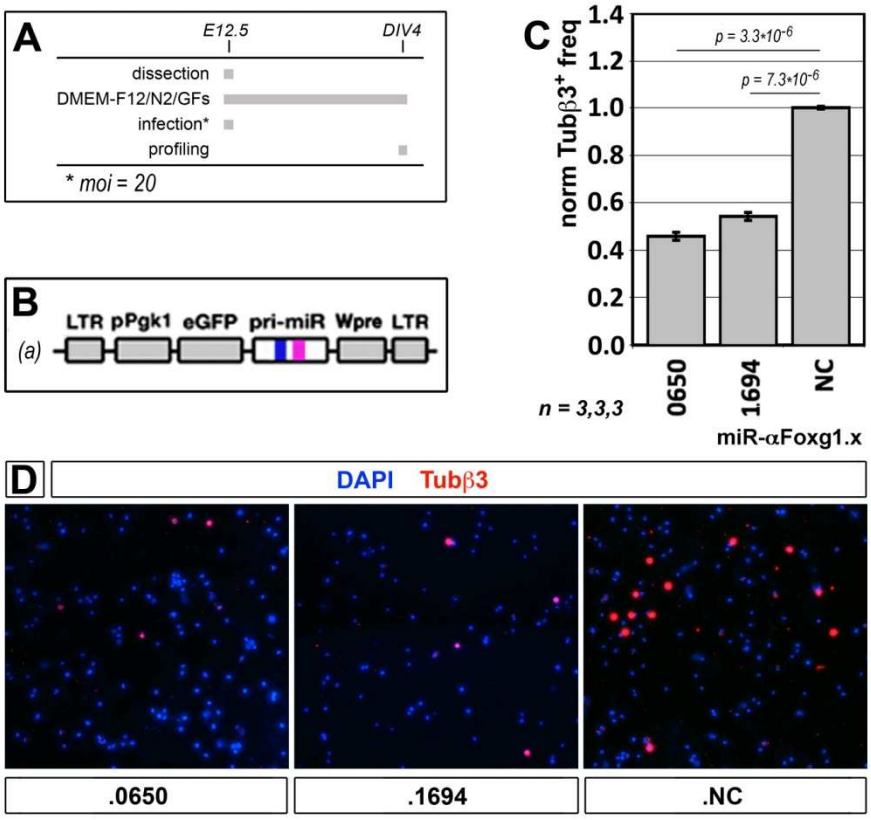


Figure 4.8. Histogenetic outcome of *Foxg1*-RNAa. (A,B) Protocols and lentiviral reagent employed for this assay. (C) Quantification of cells immunopositive for the neuron-specific Tubb3 marker, in cultures of neocortical precursors expressing *Foxg1*-saRNAs. (D) Examples of Tubb3^{+} immuno-fluorescences referred to in (C). E, embryonic day. DIV, days *in vitro*. Bars represent sem's. *n* = number of biological replicates. *p* values calculated by t-Student assay (one-tail, unpaired). Absolute average frequency of Tubb3^{+} cells in NC samples was (27.25±0.16)%.

4.2.2 Compliance of RNAa with endogenous tuning of *Foxg1*-mRNA.

Therapeutic exploitation of RNAa for correction of haploinsufficiencies would be easier if the *activity* of saRNAs would be confined to cells normally expressing the gene in order. To assess the fulfilment of this requirement, we delivered miR-αFoxg1.0650 and .1694 to proliferating neural precursors originating from the murine E10.5 meso-rhombo-cervical neural domain, which does not express *Foxg1* (Hatini et al., 1994). We employed neural precursors dissected out of the E12.5 neocortex as histogenetically-equivalent positive controls (Figure 4.9 A). Interestingly, *Foxg1* levels, albeit weakly upregulated by miR-αFoxg1.0650 and .1694, remained about 3 orders of magnitude lower in meso-rhombo-cervical derivatives, compared to neocortical controls (Figure 4.9 B,C). This suggests that risks of ectopic gene activation upon RNAa can be negligible.

Neuronal genes often undergo fine, electrical activity-related tuning which may be crucial to proper implementation of their function (Okuno, 2011). An acceptable therapy of neuropathogenic haploinsufficiencies relying on stimulation of the spared gene allele must take into account such physiological gene modulation. Exposure of neocortical neurons to high extracellular [K^+] was followed by a prompt arousal of *Foxg1*-mRNA levels (Figure 4.9 D,E), a likely *in vitro* correlate of activity-dependent *Foxg1* stimulation. We reasoned that this phenomenon might provide a valuable opportunity for probing compliance of RNAa with "endogenous" gene tuning. Remarkably, the delivery of miR-αFoxg1.1694 to K^+-challenged neocortical neurons elicited a delicate upward shift of the *Foxg1* activation curve under high extracellular [K^+]. However, ANCOVA analysis of data provided no evidences of interaction between K^+ stimulation and RNAa (Figure 4.9E), suggesting that RNAa does not hide activity-driven *Foxg1* tuning.

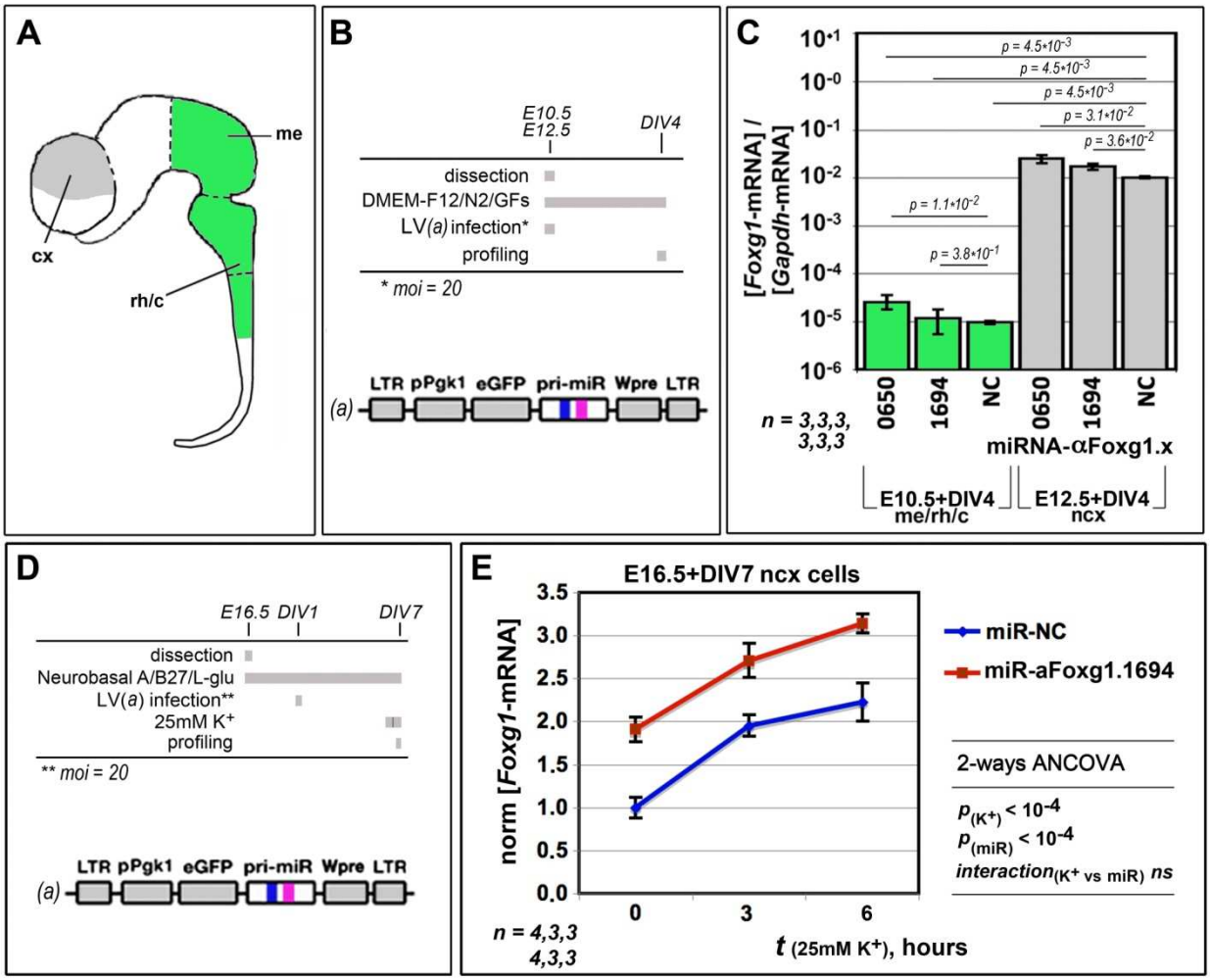


Figure 4.9. Compliance of *Foxg1*-RNAa with endogenous gene regulation. (A) Idealized representation of the murine early neural tube, including cortical (cx), mesencephalic (me) and rhombo-cervical (rh/c) domains. (**B**) Protocols and lentiviral reagent employed for the assay referred to in (C). (**C**) Impact of miR-αFoxg1.0650 and .1694 on *Foxg1*-mRNA levels in proliferating precursors from me/rh/c and cx domains. (**D**) Protocols and lentiviral reagent employed for the assay referred to in (E). (**E**) *Foxg1*-mRNA modulation by miR-αFoxg1.1694 in differentiating neocortical derivatives upon their timed terminal exposure to 25mM K^+. E, embryonic day. DIV, days *in vitro*. Bars represent sem's. *n* = number of biological replicates. *p* values calculated by t-Student assay (one-tail, unpaired) (C) and ANCOVA (two-ways, unpaired)(E). *ns*, not significant.

4.2.3 Molecular mechanisms underlying *Foxg1*-RNAa

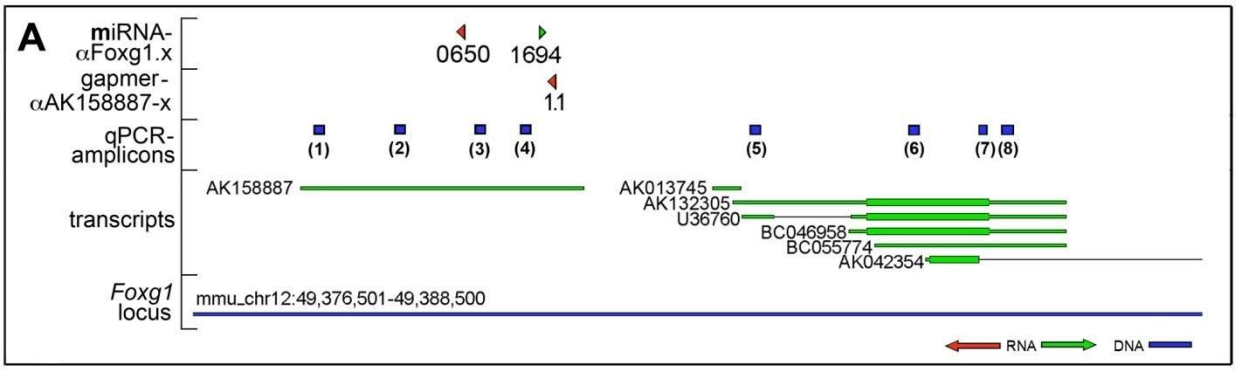
RNAa is supposed to be a heterogeneous process and at least two classes of molecular mechanisms likely underlie it. RNAa may take place via downregulation of ncRNAs which limit transcription of the associated gene of interest. Alternatively, saRNAs may drive molecular machinery promoting transcription to target chromatin (Morris et al., 2008; Schwartz et al., 2008). To cast light on this issue, we monitored expression levels of *Foxg1*-associated AK158887 ncRNA (Figure 4.10A), following the delivery of antisense-oriented, miR-αFoxg1.0650 and miR-αFoxg1.1653. No down-regulation of AK158887 was found, suggesting that, at least in these cases, the latter mechanism may apply (Fig. S13).

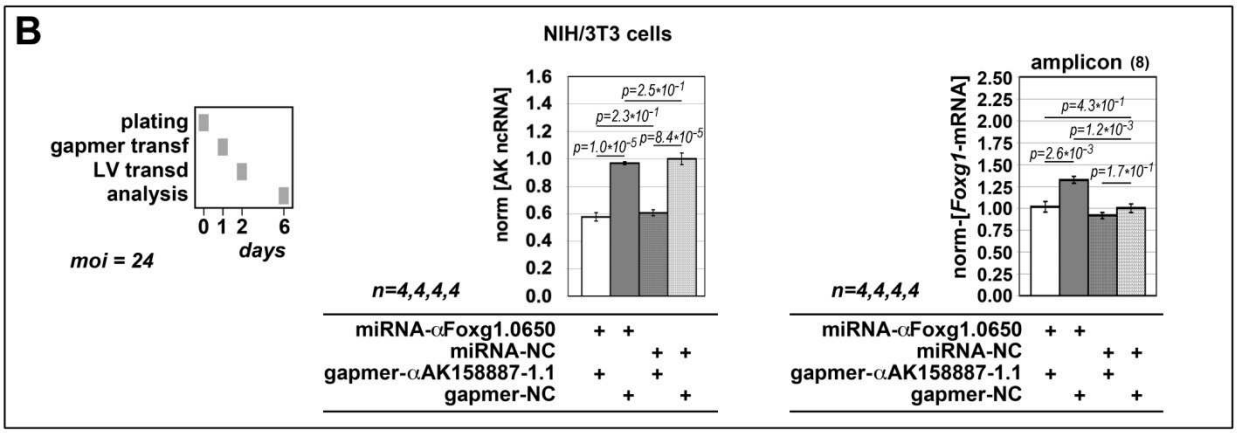
As for recognition of target chromatin, saRNAs might straightly bind to unwound chromosomal DNA. Alternatively, they might pair to nascent RNA molecules stemming from it. To distinguish between these possibilities, we downregulated the putative miR-αFoxg1.0650 target AK158887 RNA, by gapmer-αAK158887-1.1 in easily transfectable NIH/3T3 cells (Figure 4.10 A,B). Interestingly, such manipulation fully abolished miR-aFoxg1.0650-dependent *Foxg1* transactivation (Figure 4.10 B), while not affecting *Foxg1* levels in miRNA-NC-treated samples. All this suggests that miR-αFoxg1.0650 recognizes its chromatin target via RNA/RNA pairing.

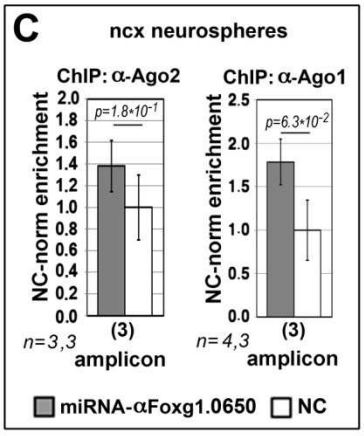
Both Ago1 and Ago2 are detectable in the nucleus and able to bind miRNAs (Huang et al., 2012). Ago2 was also specifically implicated in a number of RNAa cases, possibly as a bridge between the saRNA and the supramolecular transactivating complex (Matsui et al., 2013). To assess the involvement of Ago2 in *Foxg1*-RNAa, we evaluated its recruitment to miR-aFoxg1.0650 and .1694 target sequences, upon saRNA delivery to neocortical precursors, by ChIP. Enrichment for Ago1 was monitored as a specificity control. Unexpectedly, both saRNAs increased the recruitment of Ago1, but not of Ago2 (Figure 4.10 C,D), pointing to a selective involvement of the former in *Foxg1*-RNAa. To corroborate this inference, we antagonized Ago1 translation by a dedicated morpholino in NIH/3T3 cells (Figure 4.10E). Remarkably, this treatment suppressed miR-αFoxg1.1694-dependent *Foxg1*

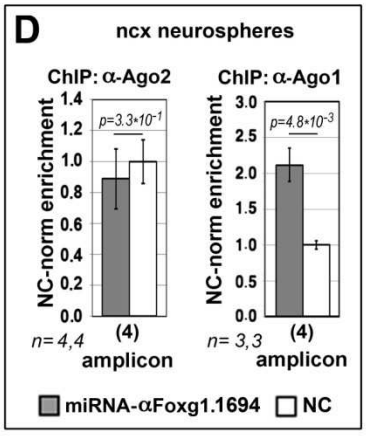
transactivation (Figure 4.10E), while not affecting *Foxg1* levels in miRNA-NC-treated samples. All this confirms the pivotal role of Ago1 in *Foxg1*-RNAa.

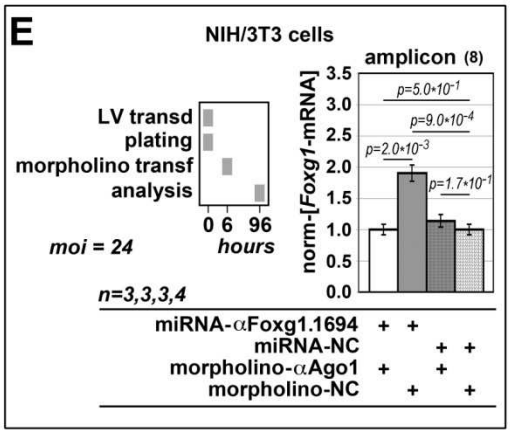
To further explore mechanisms leading to RNAa, we monitored enrichment of the *Foxg1* locus for RNApolII upon saRNA delivery to neural precursors. We found that both miR-αFoxg1.0650 and .1694 robustly increased RNApolII recruitment all over the locus (Figure 4.10A,F,G), reasonably leading to augmented transcription rates. Intriguingly, the absolute RNApolII enrichment profile did not display any sudden decrease downstrem of *Foxg1*-TSS in control conditions (Figure 4.10A and S13). Moreover, no abrupt increase of RNApolII recruitment took place in the same position upon saRNA delivery (Figure 4.10A,F,G). Altogether these data suggest that RNApolII pausing at *Foxg1*-TSS does not normally occur and saRNAs stimulate *Foxg1* transcription promoting RNApolII recruitment to TSS.

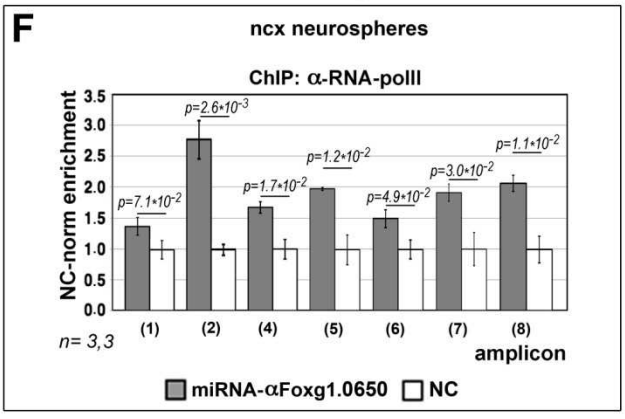

A
miRNA-αFoxg1.x
0650
1694
gapmer-αAK158887-x
1.1
qPCR-amplicons
(1)
(2)
(3)
(4)
(5)
(6)
(7)(8)
transcripts
AK158887
AK013745
AK132305
U36760
BC046958
BC055774
AK042354
Foxg1 locus
mmu_chr12:49,376,501-49,388,500
RNA
DNA


B
NIH/3T3 cells
plating
gapmer transf
LV transd
analysis
0 1 2 6
days
moi = 24
norm [AK ncRNA]
p=2.5•10-1
p=2.3•10-1
p=1.0•10-5
p=8.4•10-5
n=4,4,4,4
amplicon (8)
norm-[Foxg1-mRNA]
p=4.3•10-1
p=1.2•10-3
p=2.6•10-3
p=1.7•10-1
n=4,4,4,4
miRNA-αFoxg1.0650
miRNA-NC
gapmer-αAK158887-1.1
gapmer-NC


C
ncx neurospheres
ChIP: α-Ago2
ChIP: α-Ago1
NC-norm enrichment
p=1.8•10-1
p=6.3•10-2
n=3,3
n=4,3
(3)
amplicon
miRNA-αFoxg1.0650
NC


D
ncx neurospheres
ChIP: α-Ago2
ChIP: α-Ago1
NC-norm enrichment
p=3.3•10-1
p=4.8•10-3
n=4,4
n=3,3
(4)
amplicon
miRNA-αFoxg1.1694
NC


E
NIH/3T3 cells
LV transd
plating
morpholino transf
analysis
0 6 96
hours
moi = 24
amplicon (8)
norm-[Foxg1-mRNA]
p=5.0•10-1
p=9.0•10-4
p=2.0•10-3
p=1.7•10-1
n=3,3,3,4
miRNA-αFoxg1.1694
miRNA-NC
morpholino-αAgo1
morpholino-NC


F
ncx neurospheres
ChIP: α-RNA-polII
NC-norm enrichment
p=7.1•10-2
p=2.6•10-3
p=1.7•10-2
p=1.2•10-2
p=4.9•10-2
p=3.0•10-2
p=1.1•10-2
n=3,3
(1)
(2)
(4)
(5)
(6)
(7)
(8)
amplicon
miRNA-αFoxg1.0650
NC

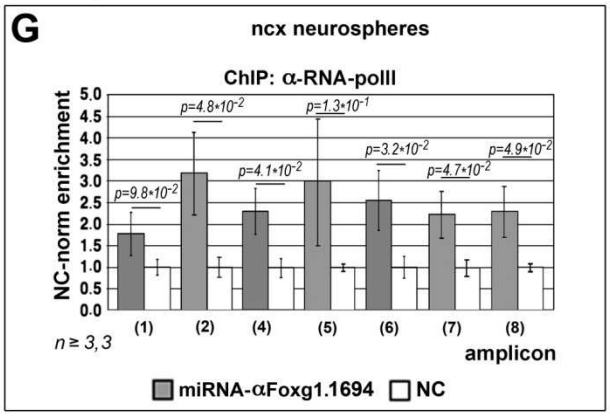

G
ncx neurospheres
ChIP: α-RNA-polII
NC-norm enrichment
p=9.8•10-2
p=4.8•10-2
p=1.3•10-1
p=4.1•10-2
p=3.2•10-2
p=4.7•10-2
p=4.9•10-2
n≥3,3
(1)
(2)
(4)
(5)
(6)
(7)
(8)
amplicon
miRNA-αFoxg1.1694
NC

Figure 4.10. Molecular mechanisms underlying Foxg1-RNAa. (A) Schematics of the Foxg1 locus including miRNA and gapmer positions and orientations, as well as diagnostic qPCR amplicons. (B) AK158887-ncRNA and Foxg1-mRNA levels in NIH/3T3 cells upon combined delivery of miR-αFoxg1.0650 and gapmer-αAK158887-1.1. Values double normalized, against Gapdh and control (NC). (C,D) qPCR quantification of Foxg1 chromatin enrichment, upon immunoprecipitation (ChIP) by antibodies against Argonaute 2 (α-Ago2) and Argonaute 1 (α-Ago1). Evaluation performed in neocortical precursors challenged by miR-αFoxg1.0650 (C) and miR-aFoxg1.1694 (D), according to the protocol shown in Figure 1B,C. Values double normalized against input chromatin and control (NC). (E) Foxg1-mRNA levels in NIH/3T3 cells upon combined delivery of miR-αFoxg1.1694 and morpholino-αAgo1. Values double normalized, against Gapdh and control (NC). (F,G) qPCR quantification of Foxg1 chromatin enrichment, upon ChIP by antibodies against RNA polymerase II (α-RNA-polII). Evaluation performed in neocortical precursors challenged by miR-αFoxg1.0650 (F) and miR-αFoxg1.1694 (G), according to the protocol shown in Figure 4.7B,C. Values double normalized against input chromatin and control (NC). Bars represent sem's. n = number of biological replicates. p values calculated by t-Student assay (one-tail, unpaired).

4.2.4 In vivo Foxg1-RNAa.

Although highly flexible and powerful for analytical purposes, lentiviral vectors employed throughout this study would pose obvious concerns for *in vivo* exploitation, due to their insertional mutagenesis activity. In principle, we could circumvent this issue replacing lentivirus-encoded saRNAs by their synthetic siRNA-like analogues. To preliminarily explore this possibility, we delivered siRNA-αFoxg1.1694 (analogue of miR-αFoxg1.1694) or the siRNA-aGFP control to murine neocortical differentiating derivatives, by Lipofectamine-RNAimax transfectant. Interestingly, siRNA-αFoxg1.1694 specifically upregulated *Foxg1*-mRNA, by 1.48±0.04-folds (Figure S15A,B). Encouraged by this result, we repeated this *in vitro* assay, replacing the commercial transfectant by the Chimeric Rabies Virus Glycoprotein Fragment (RVG-R9). This polypeptide may be easily loaded with nucleic acids, it crosses the blood-brain-barrier (BBB) and targets the vast majority of CNS cells via specific interaction with the a7 chain of the nicotinic receptor (Kumar et al., 2007). As such, it is a promising tool for therapeutic brain targeting. Interestingly, RVG-R9-mediated siRNA-αFoxg1.1694 transfection replicated *Foxg1*-mRNA upregulation obtained by RNAimax (Figure S15C,D). Given the documented expression of a7 in proliferating neocortical precursors (Atluri et al.,

2001), we tested if the RVG-R9/siRNA-αFoxg1.1694 complex might upregulate *Foxg1* even in neurospheres originating from E12.5 cortical tissue. Unfortunately, the huge upregulation detected (about 9-folds) was not specific, since it was also achieved by the RVG-R9/siRNA-aGFP control complex (Figure S15E,F). Even worse, such upregulation was associated to massive differentiation of proliferating precursors to postmitotic neurons (Figure S15G). Therefore, *in vivo* employment of RVG-R9 might lead to a detrimental precocious exhaustion of neuronogenic niches. Because of that, we considered an alternative delivery tool for our saRNAs.

We chose to administer miR-αFoxg1.1694 to the living brain through AAV9-pseudotyped, self-complementary AAV2-derivative, adeno-associated viral vectors, under the control of a constitutive promoter (Figure 4.11A). We injected $3*10^{10}$ infecting particles into the right lateral ventricle of P0 mouse pups by free hands. We sacrificed these animals three weeks later (P21) and scored their right neocortices for *Foxg1*-mRNA content as well as for the frequency at which $Foxg1^+$ cells were AAV-transduced (Figure 4.11B,C). Remarkably, *Foxg1* was upregulated by 1.68±0.25 folds (Figure 4.11D), even though the transduction frequency of $Foxg1^+$ cells was only 0.17±0.01 (Figure 4.11E,F).

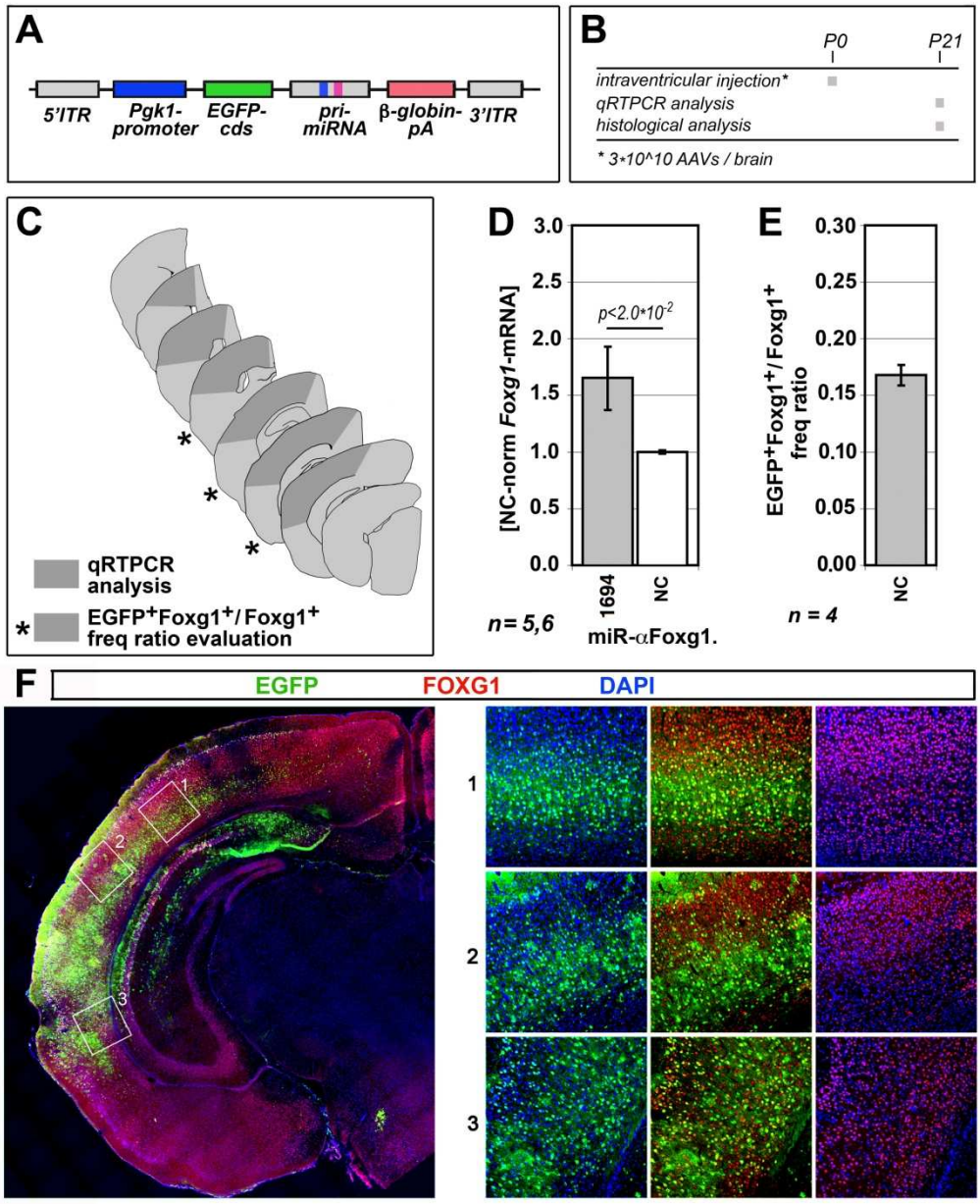


Figure 4.11. *Foxg1*-RNAa in murine neocortex. (A) Schematics of AAV9-pseudotyped, self-complementary AAV2-derivative, adeno-associated viral vector, driving constitutive expression of *Foxg1*-activating miRNAs. (B) Protocol employed for the assays referred to in (C-F). (C) Location of neocortical sectors subject of the analyses shown in (D-F). (D) Quantification of *Foxg1*-mRNA levels in neocortex of juvenile mice previously injected by scAAVs encoding for miR-aFoxg1.1694. (E) Evaluation of frequency of Foxg1^{+} cells transduced by EGFP-encoding control virus (NC). (F) Examples of aFoxg1/aEGFP-immunoprofiled sections referred to in (C,E). P, post-natal day. Bars represent sem's. *n* = number of biological replicates (i.e. brains). *p* values calculated by t-Student assay (one-tail, unpaired).

4.3 Portability of RNA activation (RNAa) to other haploinsufficient genes

4.3.1 Selecting miRNA-like saRNAs upregulating *FRATAXIN-mRNA*

In order to identify potential genomic targets appropriate for *FXN*-RNAa, we inspected the 5' surroundings of NCBI-RefSeq *FXN*-mRNA transcriptional start sites (TSSs) for sequences specifically amenable to miRNA targeting via the pri-miRNA-155-based Block-It platform (Diodato et al., 2013). We selected four high-score candidates and we cloned the cDNAs, encoding for the corresponding precursors, into the lentiviral constitutive expressor pLVmiR.23 (Diodato et al., 2013).

Pri-miRNAs were directed against non-coding regions of the *FXN* locus. miR-αFXN.304 and miR-αFXN.546 were directed against the antisense non-coding RNA *FAST1,* which stems from a *FXN-TSS-centered* region of about 800 bp (De Biase et al., 2009), including the head of *FXN-mRNA* (Figure 4.12A)*. FAST1* expression is increased in human patients with *FXN-GAA* triplet expansions, possibly for defective CTCF recruitment to a promoter-proximal insulator. *FAST1* upregulation has been suggested to promote heterochromatization and silencing of the *FXN* locus (De Biase et al., 2009). Therefore we expected that *FAST1* destabilization could upregulate *FXN.* The other two miRNAs, miR-αFXN.387 and miR-αFXN.1456, were conversely directed against two conserved cis-active modules, R1 and R6, which lie at 5.3kb and 15.3 kb upstream of *FXN-I* exon and promote *FXN* transcription (Puspasari et al., 2011) (Figure 4.12A, Supplementary table S9).

As proof of principle, we transfected HEK293T cells with 4 miRNA and we found that all of them (miR-αFXN.304, miR-αFXN.546, miR-αFXN.387 and miR-αFXN.1456) upregulated *FXN* mRNA, at different extents. The expression gain ranged from 1.24-folds (miR-αFXN.387) to 1.54 folds (miR-αFXN.546) (Figure 4.12B).

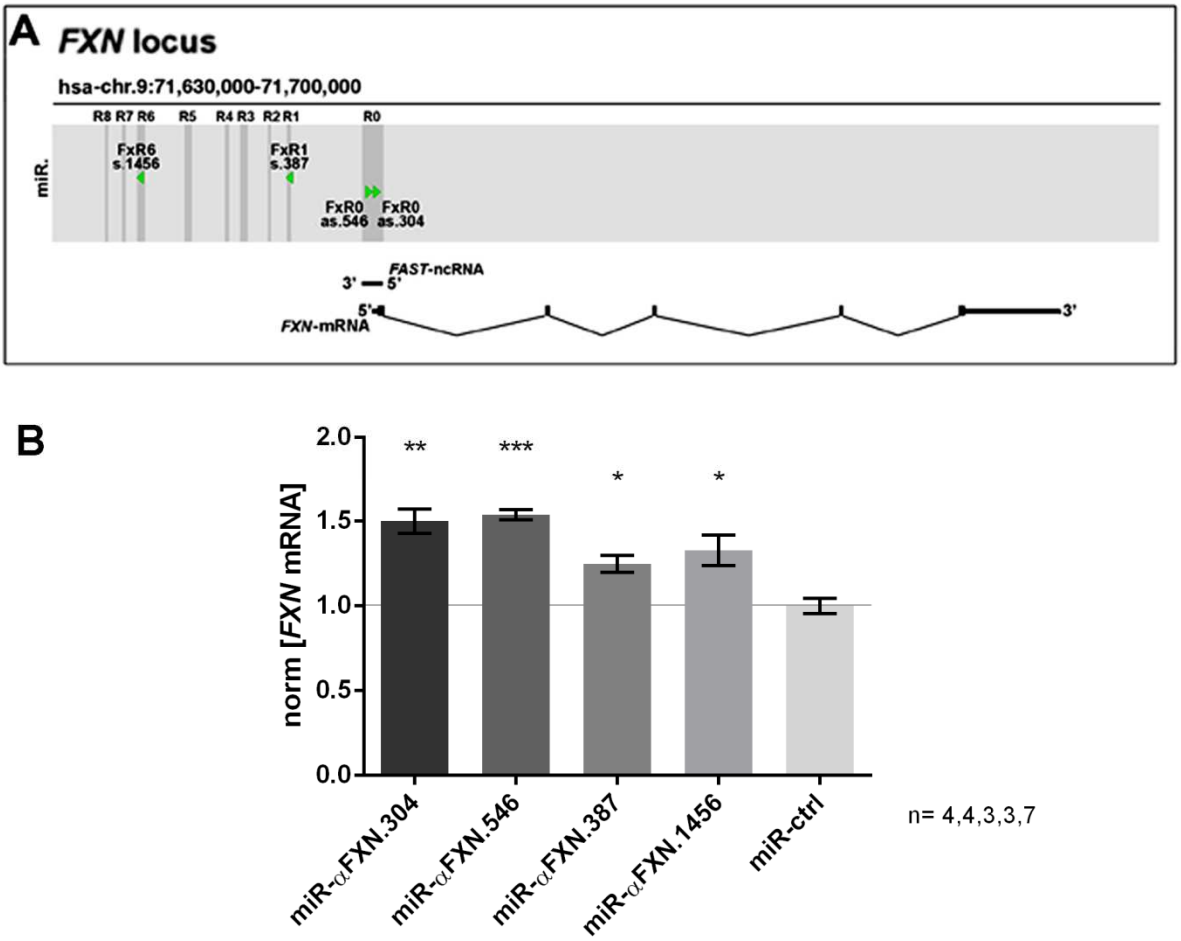


Figure 4.12. RNAa at the *FXN* locus in HEK293T cells. (A) Mapping artificial miRNAs triggering RNAa at the *FXN* locus. R0 is the *FAST1*-ncRNA/*FXN*-mRNA overlapping region described in (De Biase et al., 2009)*;* R1-R8 are the cis-active modeules described in (Puspasari et al., 2011)*.* **(B)** Expression levels of *FXN* upon lentiviral-mediated delivery of saRNAs to HEK293T cells. Values double normalized, against *GAPDH* and control (miR-ctrl). Bars represent sem's. *n* = number of biological replicates . *p* values calculated by t-Student assay (one-tail, unpaired) are * p<0,05; ** p<0.01; *** p< 0,001.

Taking advantages of the possibility to exploit cells derived from patients affected from Friedreich's ataxia (FRDA), we delivered our bioactive saRNAs on cells that harbor the pathological mutation. We selected a lymphoblastoid cell trans-heterozigous for GAA expansions (GM16798, from Coriell Institute), which harbors 750-GAA and 1000-GAA. Cells were challenged with lentiviruses encoding for miR-αFXN.304 and miR-αFXN.546. Despite

the poor transducibility of lymphoblasts (40% of efficacy), *FXN* mRNA was upregulated by 59% ($p < 0,0016$) and 32% ($p< 0,0029$), respectively (Figure 4.13).

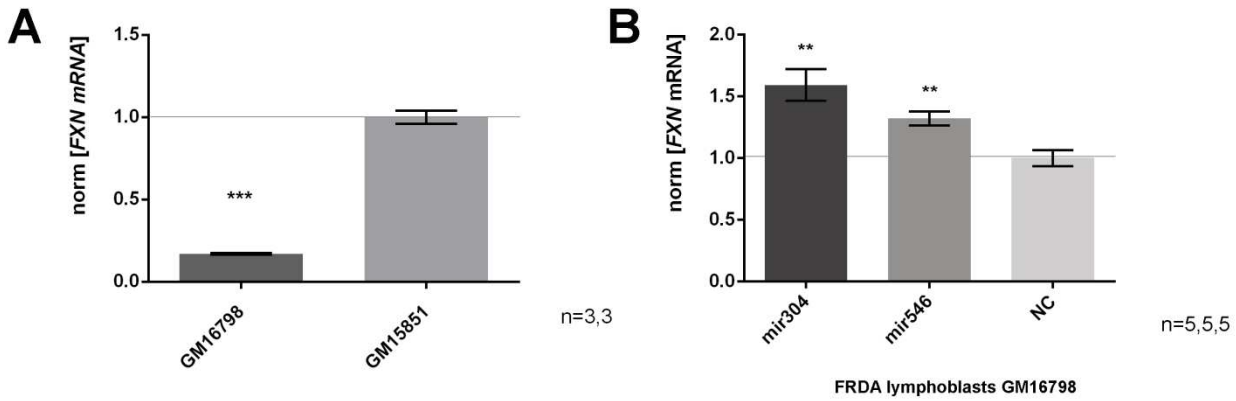
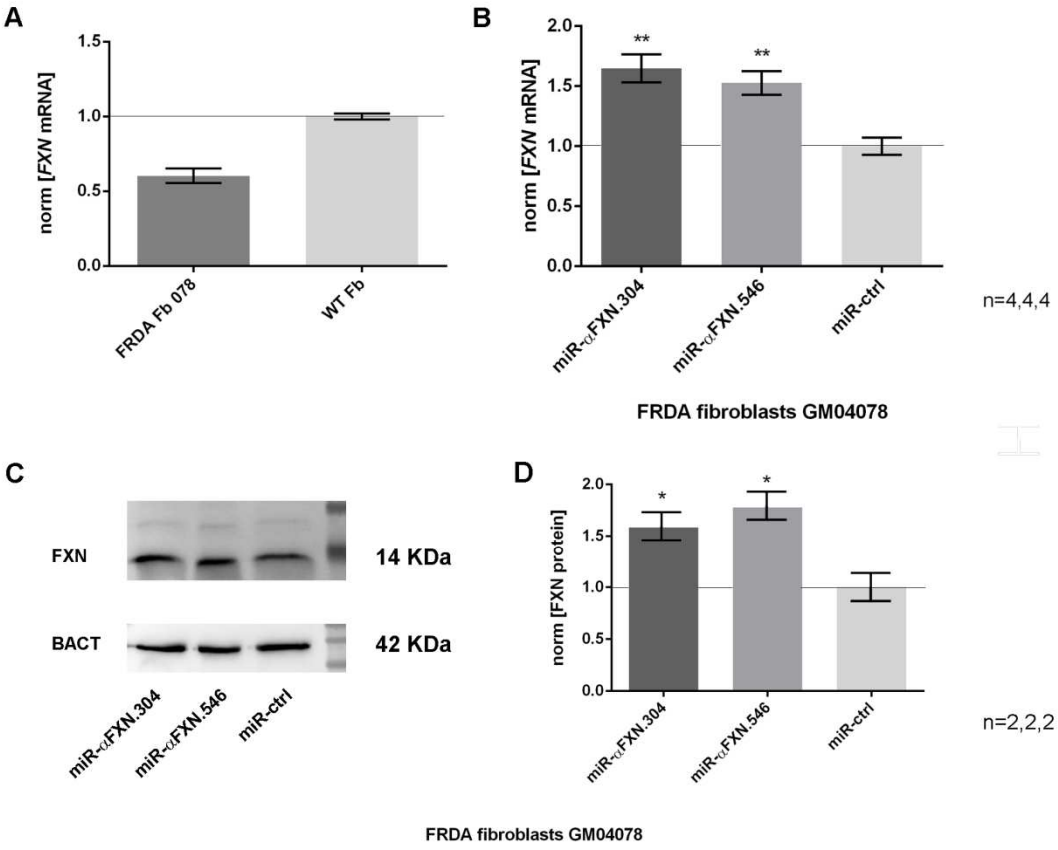


Figure 4.13. RNAa at the *FXN* locus in FRDA lymphoblastoid cell line. (A) Expression levels of *FXN* in GM16798 FRDA lymphoblasts, compared to GM15851 wild type lymphoblasts. Values normalized against *GAPDH.* **(B)** Expression levels of *FXN* upon lentiviral-mediated delivery of miR-αFXN.304 and miR-αFXN.546 to lymphoblasts GM16798, with a multiplicity of infection (moi) of 16, for 96 hours. Values double normalized, against *GAPDH* and control (miR-ctrl). Bars represent sem's. *n* = number of biological replicates . *p* values calculated by t-Student assay (one-tail, unpaired) are * $p<0,05$; ** $p<0.01$; *** $p< 0,001$.

Encouraged by these results, we selected a primary FRDA fibroblast culture, trans-heterozygous for GAA expansion (GM04078), for further experiments. This line harbors triplet expansion on both alleles (541-GAA and 420-GAA). Adherent fibroblasts are, moreover, easier to manipulate with lentiviral vectors, compared to lymphoblasts. Firstly, we we compared *FXN* mRNA levels in GM04078 cells versus non-affected fibroblasts. As expected, *FXN* dosage of FRDA fibroblasts was almost halved compared their healty couterparts (Figure 4.14A). Remarkably, delivery of lentiviral vectors encoding for miR-αFXN.304 and miR-αFXN.546 upregulated FXN mRNA by 65% and 53%, respectively (Figure 4.14B). Interestingly, FXN protein level was also upregulated by 58% and 77% (Figure 4.14 C,D,E).


A
norm [FXN mRNA]
1.5
1.0
0.5
0.0
FRDA Fb 078
WT Fb
B
norm [FXN mRNA]
2.0
1.5
1.0
0.5
0.0
**
**
miR-αFXN.304
miR-αFXN.546
miR-ctrl
n=4,4,4
FRDA fibroblasts GM04078
C
FXN
14 KDa
BACT
42 KDa
miR-αFXN.304
miR-αFXN.546
miR-ctrl
D
norm [FXN protein]
2.0
1.5
1.0
0.5
0.0
*
*
miR-αFXN.304
miR-αFXN.546
miR-ctrl
n=2,2,2
FRDA fibroblasts GM04078

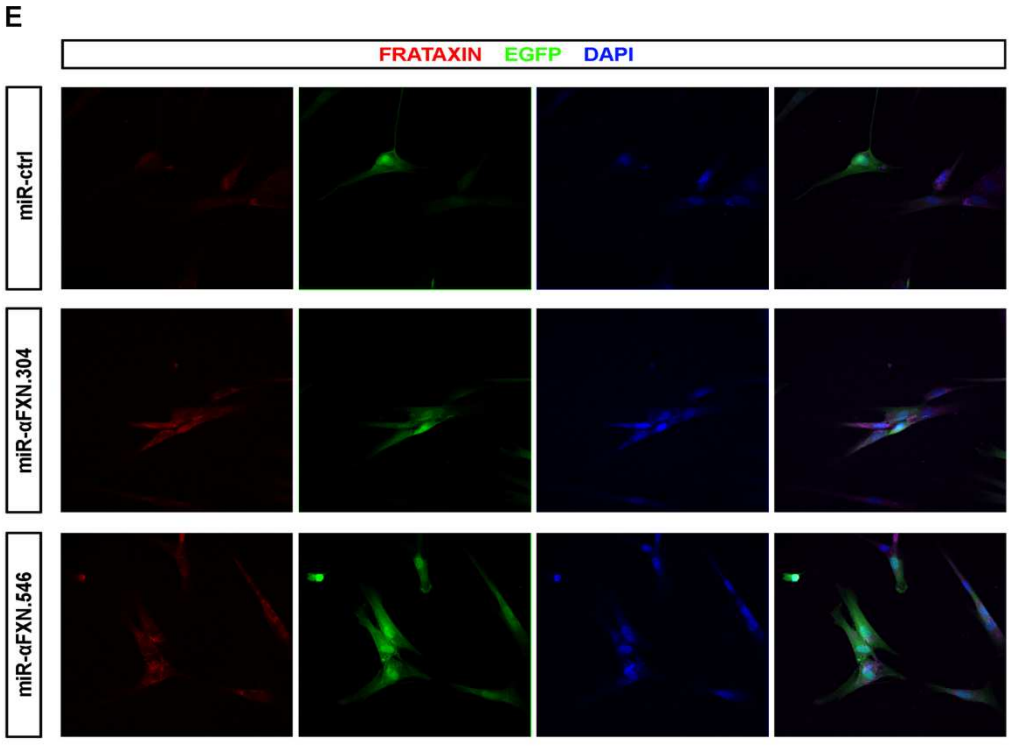

E
FRATAXIN
EGFP
DAPI
miR-ctrl
miR-αFXN.304
miR-αFXN.546

Figure 4.14. RNAa at the *FXN* locus in FRDA fibroblasts. (A) Expression levels of *FXN* in GM04078 FRDA fibroblasts, compared to wild type fibroblasts. Values normalized against *GAPDH.* **(B)** Expression levels of *FXN* upon lentiviral-mediated delivery of miR-αFXN.304 and miR-αFXN.546 to GM04078 FRDA fibroblasts, with a multiplicity of infection (moi) of 15, for 96 hours. Values double normalized, against *GAPDH* and control (miR-ctrl). **(C)** Example of western blot evaluation of FXN protein upon saRNA delivery. **(D)** Western blot evaluation of FXN protein upon saRNA delivery. Values double normalized, against *βACTIN* and controls (miR-ctrl). **(E)** Immunofluorescence evaluation of FXN protein upon saRNAs delivery. Bars represent sem's. *n* = number of biological replicates. *p* values calculated by t-Student assay (one-tail, unpaired) are * p<0,05; ** p<0.01; *** p< 0,001.

4.3.2 Combination of *FXN*-saRNAs with HDAC inhibitors

It has been demonstrated that GAA repeat expansions can lead to heterochromatin-mediated frataxin gene silencing. These events include DNA methylation and hydroxymethylation, histone deacetylation and histone methylation (Sandi et al., 2014). Some reports described that treatment of FRDA lymphoblasts with HDAC inhibitors is able to increase *FXN* mRNA. In particular, the HDAC inhibitor BML-210 compound increased *FXN* mRNA more the 2 folds (Herman et al., 2006). We hypothesized to combine our "RNA-based" treatment with the "drug-based" treatment, in order to obtain a synergistic stimulation of *FXN* transcription. We treated FRDA lymphoblasts with 5μM of BML-210 and we observed a *FXN* mRNA increase of 50% (Figure 4.15A). Unfortunately, when we treated FRDA fibroblasts with 5 μM BML-210, no *FXN* mRNA upregulation was elicited at all (Figure 4.15B).

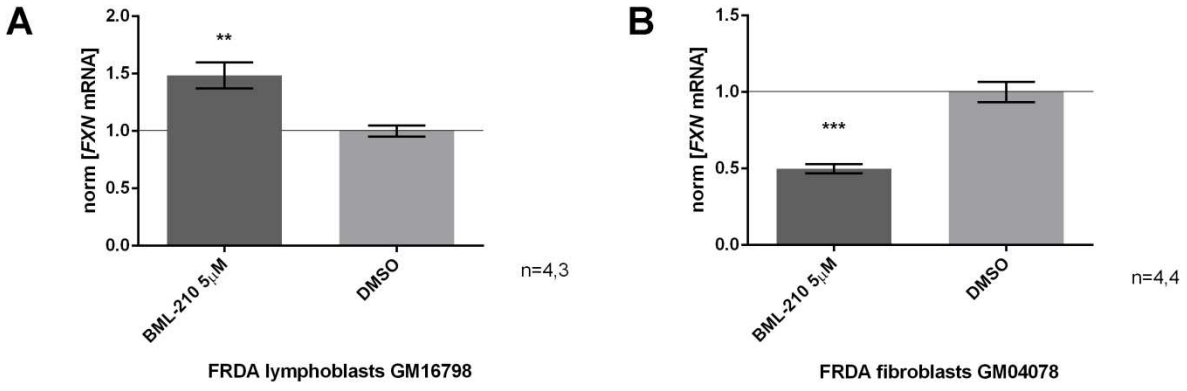


Figure 4.15. Effect of BML-210 HDAC inhibitor on FRDA lymphoblasts and fibroblasts. (A) Expression levels of *FXN* in GM16798 FRDA lymphoblasts treated with 5 μM of BML-210, compared to cells treated with DMSO. **(B)** Expression levels of *FXN* in GM04078 FRDA fibroblasts treated with 5 μM of BML-210, compared to cells treated with DMSO. Values double normalized, against *GAPDH* and control cells. Bars represent sem's. *n* = number of biological replicates. *p* values calculated by t-Student assay (one-tail, unpaired) are * p<0,05; ** p<0.01; *** p< 0,001.

Nicotinamide is a precursor of nicotinic acid and a form of vitamin B which was shown to be potentially useful for treating mitochondrial encephalopathies and neurodegenerative diseases (Bitterman et al., 2002). It is a noncompetitive end product inhibitor of the NAD^+-dependent histone deacetylase Sir2 family. In both *in vitro* and mammalian cell models, nicotinamide has been found to effectively inhibit the enzymatic activity of SIRT1 which plays a critical role in the formation of repressive heterochromatin by different mechanisms including deacetylation of histone tails (Dittenhafer-Reed et al., 2011), recruitment of deacetylated histone H1 (Vaquero et al., 2004) and regulation of histone methyltransferase (SUV39-H1) activity (Vaquero et al., 2007).

It has been demonstrated that nicotinamide could be beneficial to EBV-transformed FRDA lymphoblastoid cell lines. A 1.5 to 1.8-fold up-regulation of *FXN* mRNA levels was obtained in patient-derived cell lines, with relatively negligible effects on *FXN* expression in a normal control cell line (Chan et al., 2013; Libri et al., 2014). When we treated FRDA fibroblasts with 10mM of nicotinamide for 72 hours, we observed that *FXN* mRNA was increased by 73% (Figure 4.16A). Interestingly, even the administration of miR-αFXN.304 yielded an appreciable, albeit weak, *FXN* stimulation. However, codelivery of miR-αFXN.304 and nicotinamide did not improve *FXN* mRNA upregulation elicited by nicotinamide alone. This suggests that the two effectors might share a common pathway, eventually leading to *FXN* stimulation, or - worse - that the former might somehow limit the activity of the latter (Fig. 4.16B).

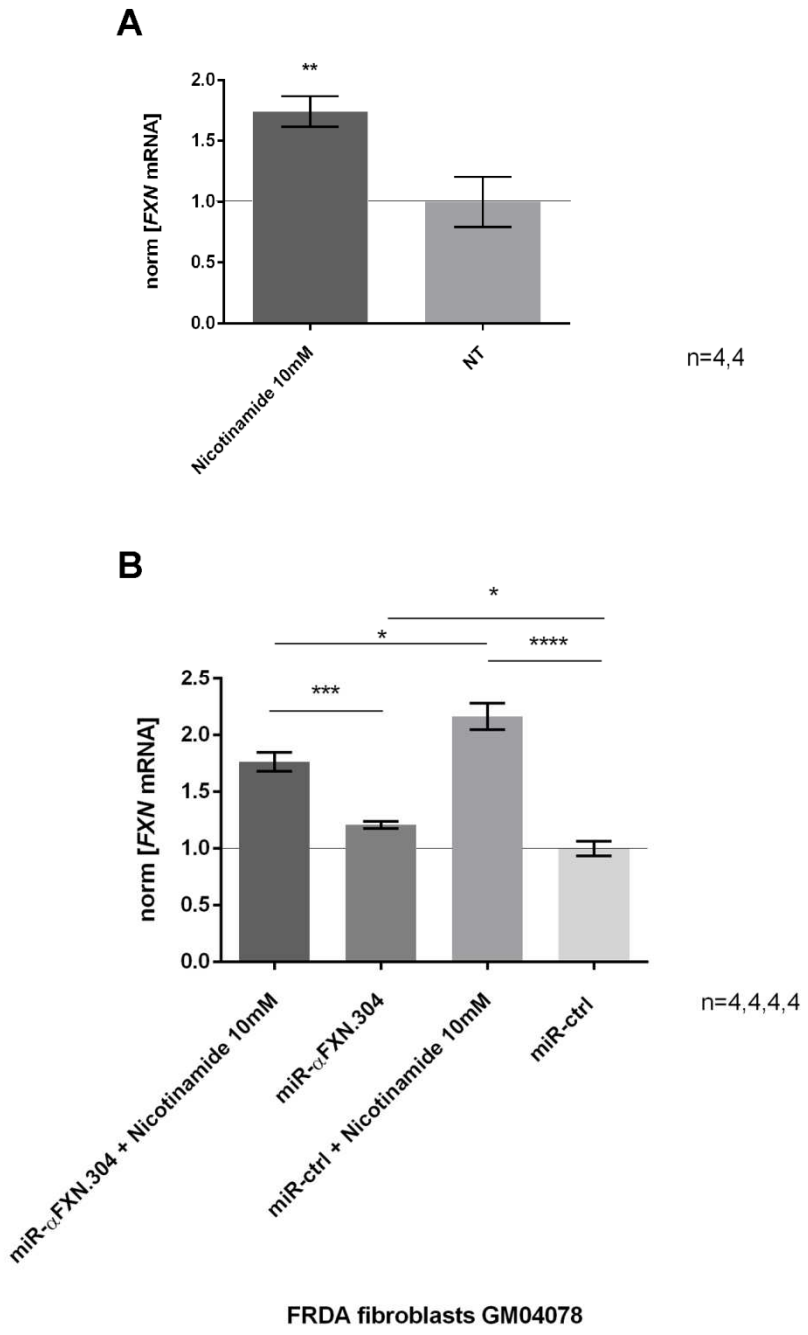


Figure 4.16. Effects of nicotinamide on FRDA fibroblasts. (A) Expression levels of *FXN* in GM04078 FRDA fibroblasts treated with 10mM of nicotinamide, compared to non-treated cells (NT). **(B)** Expression levels of *FXN* in GM04078 FRDA fibroblasts treated with miR-αFXN.304 and 10mM of nicotinamide, compared to control cells (miR-ctrl). Values double normalized, against *GAPDH* and control cells. Bars represent sem's. *n* = number of biological replicates. *p* values calculated by t-Student assay (one-tail, unpaired) are * p<0,05; ** p<0.01; *** p< 0,001; **** p<0.0001.

4.3.3 Molecular mechanisms underlying *FXN*-RNAa: a preliminary assessment

We preliminary investigated how saRNAs designed to target *FXN* locus could lead to *FXN* upregulation. As described above (section *4.2.3 Molecular mechanisms underlying Foxg1-RNAa*), RNAa may take place via downregulation of ncRNAs which limit transcription of the associated gene of interest. Alternatively, saRNAs may drive molecular machinery promoting transcription to target chromatin (Morris et al., 2008; Schwartz et al., 2008). To cast light on this issue, we monitored expression levels of *FXN*-associated *FAST-1* antisense ncRNA (Figure 4.17A) (De Biase et al., 2009). When compared to wild-type fibroblasts, FRDA fibroblasts displayed an increase of *FAST*-1 transcript of 76% (Figure 4.17B). Interestingly, when we delivered sense-oriented miR-αFXN.304 and miR-αFXN.546 to FRDA fibroblasts, *FAST-1* was downregulated by 59% and 53%, respectively (Figure 4.17C), suggesting that our saRNAs might act by destabilizing it.

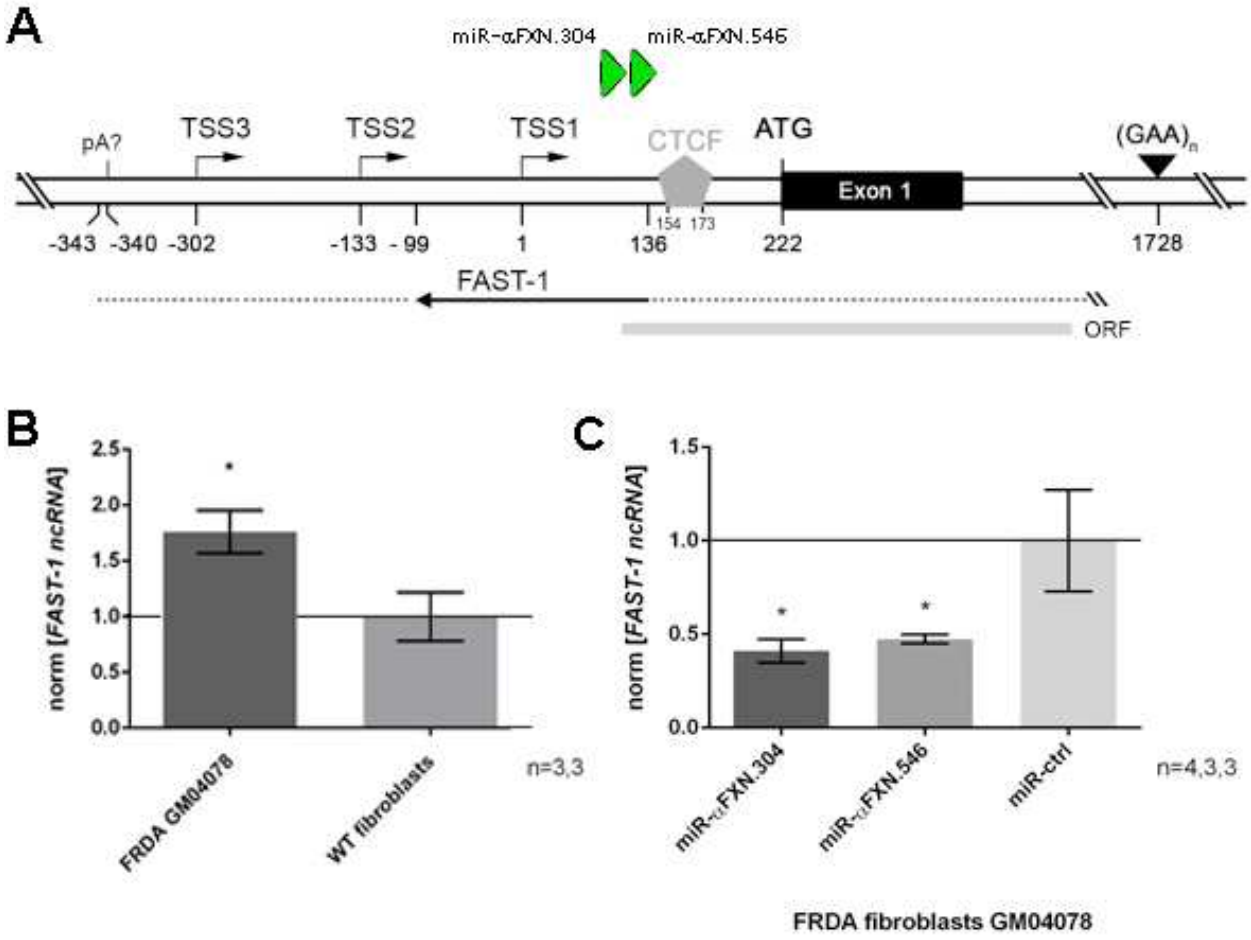


Figure 4.17. Effects of saRNAs on FXN-associated antisense *FAST-1* transcript. (A) Schematics of the *FXN* locus including saRNAs positions and orientations (green arrowheads), *FAST*-1 transcript and *FXN* TSS. Adapted from (De Biase et al., 2009). **(B)** Expression levels of antisense *FAST-1* ncRNA in GM04078 FRDA fibroblasts, compared to wild-type fibroblasts. **(C)** Expression levels of antisense *FAST-1* ncRNA upon lentiviral-mediated delivery of miR-αFXN.304 and miR-αFXN.546 to GM04078 FRDA fibroblasts, compared to control cells (miR-ctrl). Values double normalized, against *GAPDH* and control cells. Bars represent sem's. *n* = number of biological replicates. *p* values calculated by t-Student assay (one-tail, unpaired) are * p<0,05; ** p<0.01; *** p< 0,001.

4.3.4 Selecting miRNA-like saRNAs upregulating *Scn1a*-mRNA

In order to identify potential genomic targets appropriate for *Scn1a*-RNAa, we inspected the NCBI-RefSeq Scn1a-mRNA transcriptional start sites (TSSs) and their surroundings for non-coding evolutionary conserved elements (ncECRs), by ECR-Browser. Among these ncECRs, we selected targets potentially attackable by artificial miRNAs synthesized starting from a pri-miR155-based backbone, by Block-It (Invitrogen) (Diodato et al., 2013). We filtered candidate targets by Blast and Blat, to prevent off-targeting, and prioritized them based on their vicinity to TSS and Block-It ranking (Supplementary Table S10 and Figure 4.18A). Finally, we cloned the cDNAs encoding for the corresponding precursors into the lentiviral constitutive expressor pLVmiR.23 (Diodato et al., 2013).

We delivered 4 miRNAs (miR-aScn1a.001.1, miR-aScn1a.001.2, miR-aScn1a.201.1 and miR-aScn1a.201.2) to cortico-cerebral neurons originating from E16.5 embryos. One of them, miR-aScn1a.201.2, upregulated *Scn1a* mRNA by 20% (Figure 4.18B).

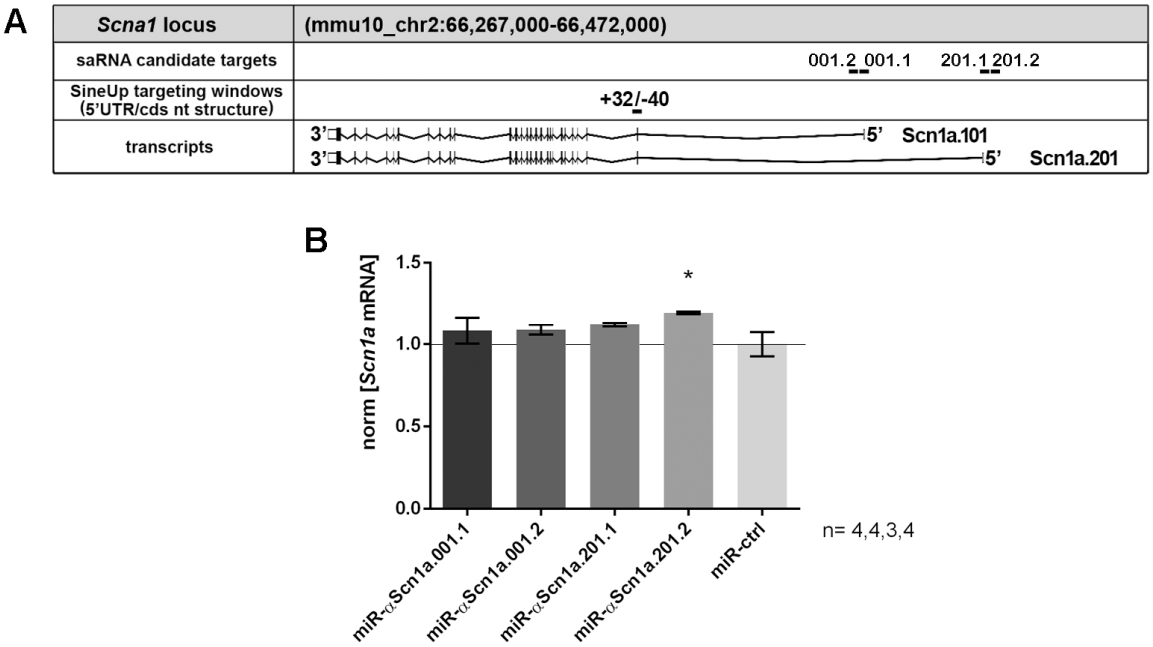


Figure 4.18. RNAa at the Scn1a locus in murine E16.5 post mitotic neurons. (A) Mapping targets of artificial miRNAs triggering RNAa and SINEUPs at the *Scn1a* locus. **(B)** *Scn1a*-mRNA modulation by Scn1a-saRNAs in differentiating neocortical derivatives, compared to control

cells (miR-ctrl). Values double normalized, against *Gapdh* and control cells. Bars represent sem's. *n* = number of biological replicates. *p* values calculated by t-Student assay (one-tail, unpaired) are * p<0,05; ** p<0.01; *** p< 0,001.

4.3.5 Combinatorial transcriptional/translational stimulation of *Scn1a* gene

The moderate Scn1a upregulation achieved by miR-aScn1a.201.2 is not sufficient for therapeutic purposes. Screening additional candidate saRNAs is obviously needed. As an alternative, not mutually exclusive approach, we hypothesized to combine *Scn1a* transcriptional activation with translational stimulation in order to improve the overall gene upregulation.

To do so, we took advance of SINEUPs, a novel scalable device able to upregulate protein levels. SINEUPs are non-coding RNA molecules that form partial double strand hybrids with protein-encoding mRNAs, stimulating their translation (Zucchelli et al., 2015; Gustincich et al., 2016) (Supplementary Figure S16). Targeting two distinct ATG sites of the Scn1a locus (Figure 4.18A) with Scn1.SU1 and Scn1.SU2, we upregulated SCN1a protein by 60% and 18%, respectively (Figure 4.19 A-D).

This is a promising result. Interestingly, the theoretical expression gain resulting from combined employment of miR-aScn1a.201.2 and Scn1.SU1, 1.20*1.60 = 1.92, is close to what needed for allowing *one Scn1a allele* to vicariate *two Scn1a alleles*. We look forward to verify this prediction experimentally.

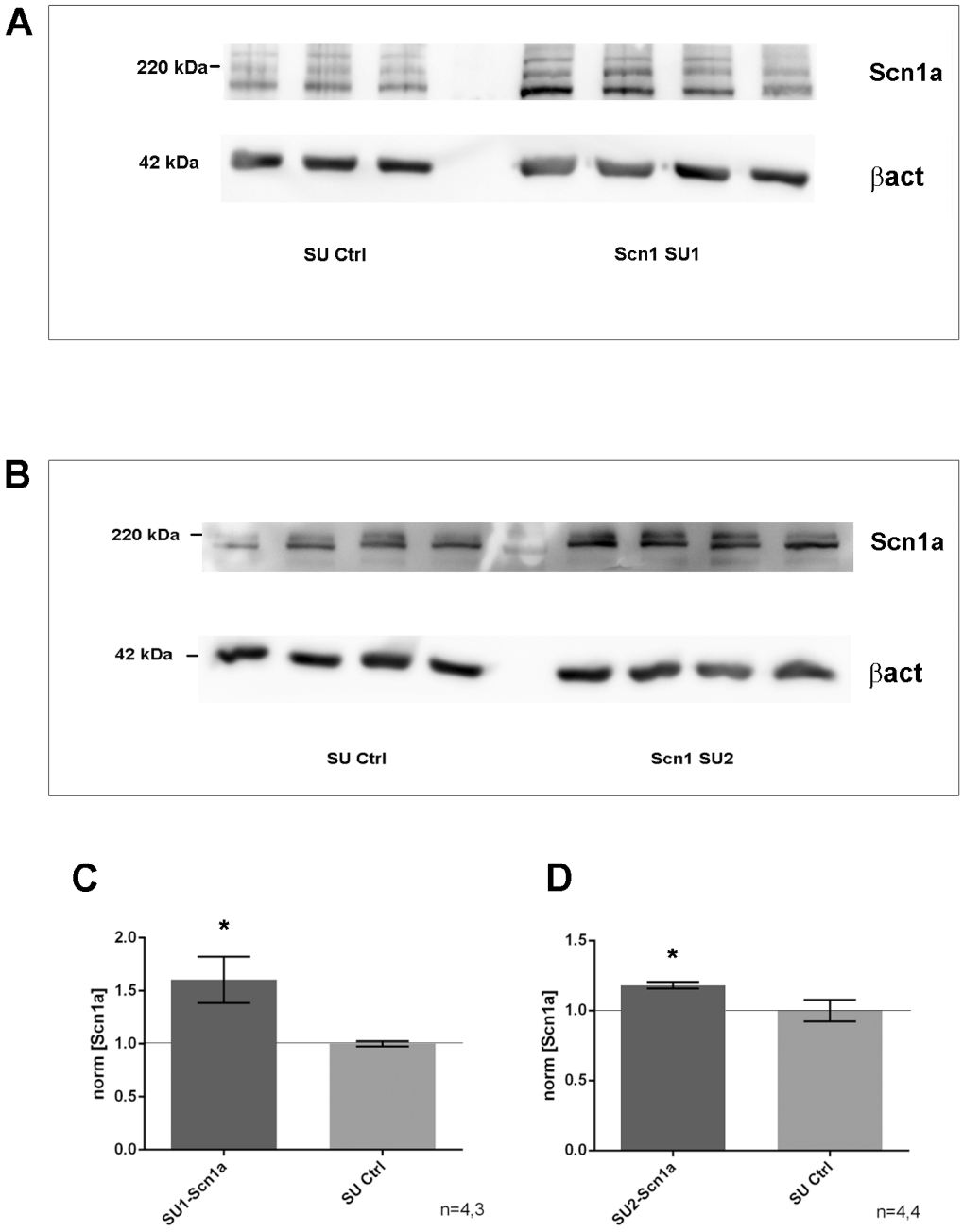


Figure 4.19. Scn1a SINEUPs activity in murine E16.5 post mitotic neurons. (A,B) Western blot evaluation of Scn1a protein levels upon SINEUPs (Scn1.SU1 and Scn1.SU2) delivery. **(C,D)** Graphical representation of SINEUP-mediated Scn1a transaltional transactivation, respresented in A and B. Values double normalized, against *βactin* and controls (SU-ctrl). Bars represent sem's. *n* = number of biological replicates. *p* values calculated by t-Student assay (one-tail, unpaired) are * p<0,05; ** p<0.01; *** p< 0,001.

5. DISCUSSION

In this thesis I reported the development of RNA-based platforms able to stimulate haploisufficient genes that are involved in different examples of neuropathies.

In particular, in the first part of the work I described a novel ribonucleoproteic transactivator able to upregulate endogenous genes ad libitum. This device was able to enter the nucleus and interact with the GOI chromatin through its RNA cofactor. By means of it, I specifically transactivated five independent genes, in cell lines as well as in primary cultures of murine pallial precursors. Such upregulation was small. However, it was sufficient to trigger an appreciable biological effect. Remarkably, activity of this device was restricted to cells where the GOI is normally transcribed. Finally, it was possible to improve this transactivator, by optimizing the interaction between polypeptidic and RNA components of it as well as reducing the size of the GOI-specific RNA bait.

The expression gains I observed primarily in HEK293T cells were +47±18% for *FMR1*, +83±16% for *NAP22* and +25±4% for *NRGN*. I am aware that random fluctuations of cell cultures upon experimental manipulation and trivial off-target effects could substantially contribute to them. However, the high bait-target homology needed for mRNA upregulation (Supplementary Figure S3, S10 and Figure 4.6), as well as the reproducibility of results (see MF6-NAP22.60L-dependent *NAP22* upregulation, shown in Figure 4.6a,d,e, and MF1-Emx2-dependent *Emx2* upregulation, shown in Figure 4.3b and Supplementary Figure S11a) suggest that these expression gains were largely due to specific gene stimulation.

Notably, the results referred to above were obtained upon cotransfection of about only one third of the total cell population (Figure 4.1 and Supplementary Figure S1). Likewise, the best upregulation elicited in neural precursors (+55±4%, for *Emx2*) was detected in a cell population infected at moi's of 15 and 5 (Figure 4.3f) and therefore cotransduced at only 75% (see Supplementary Figure S3 of ref (Brancaccio et al., 2010)). When the transfected

HEK293T cell fraction was doubled (thanks to an optimized protocol), *NAP22* and *NRGN* upregulation increased up to +143±17% and +38±12%, respectively (Supplementary Figure S5).

However, incomplete cell population transduction could not be the only cause of limited gene expression gain and additional issues likely contributed to it. Among them there is the poor stability of our apoenzyme/coenzyme complex. In fact, better performances were elicited, as the number of MF fingers included into the RNA cofactor increased (Figures 4.1d-f, 4.3b,e and 4.4b). In addition, substantial benefits could be achieved by appropriately modulating the apofactor/cofactor ratio (Figure 4.3f). Second, the limited power of our device could reflect suboptimal interaction between the transactivator and its target gene. In this respect, a stronger transactivation might be achieved by targeting the same gene with multiple baits. On the other hand, the possibility of implementing a multi-gene overexpression program by a polygenic bait should be explored.

Even if *Emx2* and *Foxg1* upregulation obtained in this study was <2-fold, it was sufficient to robustly change the behaviour of neural precursors (Figures 4.3c,d and 4.4c,d). This occurred in dorsal telencephalic (i.e. pallial) precursors, kept as high density floating cultures under growth factors. These conditions do not affect precursors' positional identity (Kelly et al., 2009; Onorati et al., 2010), stimulate their mitotic activity and largely recreate the complexity of cell-cell interactions characterizing proliferative layers of the developing brain (Brancaccio et al., 2010). The responsivity that neural cells showed to even subtle variations of gene expression levels was not surprising. In fact, similar findings were previously reported for *Emx2* and other genes involved in brain patterning (Diodato et al., 2013; Hamasaki et al., 2004; Sansom et al., 2009). The inhibition of neuronal differentiation triggered by *Emx2* and *Foxg1* upregulation might be exploited to enlarge the proliferating neural pool, namely a result of obvious therapeutic interest (Brancaccio et al., 2010).

Gene stimulation obtained by our device was specific, in at least three key aspects. First, it required the coexpression of both the NMHV apofactor and the GOI-cofactor. Removal of NMHV or replacement of the NMHV-VP16 moiety by an EGFP polypeptide

fragment abolished it (Figures 4.1d-f, 4.3b,e,f, 4.4b and Supplementary Figure S2). [Actually, two baits out of eight working ones, FMR1.2 and NAP22-AS, upregulated the corresponding genes to some extent, even in the absence of the apofactor. However, in these two cases, gene upregulation was far more pronounced upon further NMHV expression (Supplementary Figure S4b,c). Moreover, NMHV reversed gene-downregulation induced by two antisense baits, MF6-NRGN-AS and MF1-Emx2-AS (Supplementary Figures S4c and S11a, respectively)].

Second, GOI stimulation required high homology between the RNA bait and its intended target sequence. Potential off-target genes, suitable to be transcribed and/or provided with partial homology to our GOIs in the surroundings of their TSSs, were not affected (Supplementary Figures S3 and S10 and Supplementary Tables S5 and S6). The RNA bait could be shortened up to 60 bases, in the absence of adverse effects (Figure 4.6a-c). Mutagenizing the 60bp-long NAP22 bait by 30% fully abolished *NAP22* stimulation (Figure 4.6d and Supplementary Table S7). As the mutagenesis rate was lowered to 15%, transactivation was detectable only when the bait included fully matching modules longer than 17 bases (Figure 4.6e and Supplementary Table S7).

Third, the bait-dependent transactivating effect exerted by NMHV was tightly restricted to the surroundings of the bait target and depended on bait orientation. TSSs located >1kb far from the bait target were not affected (Supplementary Figures S4a and S11b). Conversely, transcription units having their 5' ends <0.5kb far from the bait target displayed a more articulated behaviour. Upon NMHV overexpression, they were generally stimulated by sense-oriented baits (Figures 4.1c-g, 4.3a,b,e,f, 4.4a,b and Supplementary Figure S4b), while variably responding to antisense ones (Supplementary Figures S4c and S11a).

To summarize, as length, orientation and distance from TSS of the RNA bait were properly tuned, our device appeared to work specifically and reliably. As many as six primary baits out of six tested, 115-179 bases long, sense-oriented and directed against TSS-proximal targets (Figures 4.1c-f, 4.3a,b,e,f and 4.4a,b, and Supplementary Figure S4b), supported an

appreciable and selective gene upregulation. Moreover, the same happened for six more baits, obtained from shortening of the primary ones (Figure 4.6a-c).

During the execution of this study, several groups reported the successful creation of a novel RNA-programmable transactivator type (Gilbert et al., 2013; Cheng et al., 2013; Perez-Pinera et al., 2013; Maeder et al., 2013; Kearns et al., 2014; Hu et al., 2014), originating from domestication of Type II, bacterial Clustered Regularly Interspaced Short Palindromic Repeat (CRISPR) adaptive immune system. Compared to CRISPR effectors, our NMHV apofactor shows three substantial differences. First, it is seven-fold smaller (Gasiunas and Siksnys, 2013), which may facilitate its artificial synthesis and delivery. Second, it is considerably less powerful than CRISPR effectors (Perez-Pinera et al., 2013). This may reflect the helicase activity intrinsic to CRISPR molecules (Mali et al., 2013b), absent in ours. Third, CRISPR-DNA interactions are not prevented by repressive epigenetic marks, such as H3K27me3 (Kearns et al., 2014) or 5meC (Hsu et al., 2013; Hu et al., 2014), and CRISPR-stimulated genes include silent transcription units (Hu et al., 2014; Maeder et al., 2013) (our data not shown). Conversely, our device only works with genes already expressed at sustained levels (Figure 4.5). These last two features obviously limit the general interest in our device. On the other side, they make it potentially suitable for specific applications, such as rescue of haploinsufficiencies.

In theory, the best performing RNA-baits used in this study, being co-oriented with the upregulated mRNAs (Figures 4.1c-f, 4.3a,b,e,f, 4.4a,b and Supplementary Figure S4b), might act as molecular decoys for possible antisense transcripts. However, except one case (Supplementary Figure S4b), gene upregulation elicited by our RNA cofactors generally required the presence of the bulky NMHV apofactor (Figures 4.1d-f, 4.3b,e,f, 4.4b and Supplementary Figure S2), which is at odds with the decoy hypothesis. Moreover, the majority of our working RNA cofactors, being co-oriented with their cognate mRNAs, cannot directly interact with them. This rules out any further possibility of post-transcriptional regulation. On the other side, ChIP data show that the NMHV polypeptide is recruited to chomatin in a RNA-cofactor-dependent way (Figures 4.2c and 4.3g). Moreover, the

enrichment of 3' regions of the GOI for RNApolII arises (Figure 4.2d). Finally, upregulation of mRNA is associated to increased levels of its pre-mRNA precursor (Figure 4.2b). Altogether, these data suggest that our device rather acts by promoting gene transcription.

We do not know how our transactivator recognizes its target and promotes transcription. Concerning gene recognition, should the RNA cofactor directly interact with its cognate DNA, this would hardly occur via a triple helix structure, as triple helix formation requires long homopurinic-homopyrimidinic traits, absent in our baits (Morgan and Wells, 1968). Conversely, the RNA cofactor could bind to the DNA template - previously unwound by the transcription machinery - via Watson&Crick base pairing, leading to D-loop formation. Alternatively, gene recognition could be indirect, i.e. the RNA cofactor might be docked to chromosomes via nascent antisense RNA molecules, still tethered to the sense-TSS surroundings. Actually, antisense transcripts spanning sense-TSSs were documented at the *NAP22*, *FMR1* and *Emx2* loci, the most responsive to NMHV/RNA-cofactor stimulation (Figures 4.1c-f and 4.3a,b,e,f). Similar transcripts could have escaped detection at the *NRGN* and *Foxg1* loci, less responsive to NMHV/RNA-cofactor, because of their lower abundance (Figures 4.1c-f and 4.4a,b). Interestingly, docking of ncRNA co-transactivators to nascent antisense RNAs would nicely account for preferential requirement of sense-oriented RNA baits to achieve gene transactivation (Supplementary Figures S4c and S11a).

Regardless of the mechanism of chromatin recognition, RNA-mediated tethering of NMHV to 5'TSS surroundings might promote transcription by a variety of VP16-dependent mechanisms (Blau et al., 1996; Kobayashi et al., 1995; Lin et al., 1991; Stringer et al., 1990; Xiao et al., 1994; Zhu et al., 1994). VP16 can promote both transcription initiation and pre-mRNA elongation (Blau et al., 1996). However an antibody recognizing RNApolII enriched the immunoprecipitate from NMHV/MF6-NAP22-treated cells for *NAP22* intronic regions, but not for *NAP22*-TSS surroundings (Figure 4.2d). This is puzzling. It could reflect the fact that the gain in RNApolII progression driven by NMHV/MF6-NAP22 matched or exceeded the gain in RNApolII recruitment at the TSS, resulting in no net increase of RNApolII bound to the TSS region. No doubt, all these mechanistic aspects deserve further in depth investigation.

In conclusion, here I described a novel programmable transactivator, including a polypeptidic effector and an RNA bait in charge of recognizing the intended target gene. We provided a basic characterization of its functional properties. I preliminarly addressed molecular mechanisms mediating its action. This device might be useful for some specific applications. However, it is presently a simple prototype, which still needs a substantial improvement of its transactivation power as well as a better characterization of its target specificity and mechanism of action.

****

In the second part of the work I describe how RNA activation (RNAa) might be a powerful tool to stimulate the haploisufficient gene *Foxg1* in murine neocortex. Active in telencephalic precursors and their postmitotic derivatives, the brain patterning gene *Foxg1* controls a variety of neurodevelopmental and physiological processes. Its allele dosage is crucial, since its duplication and deletion result in West and Rett-like syndromes, respectively. As a proof-of-principle of RNAa therapy of *Foxg1* haploinsufficiency, we selected 8 artificial saRNAs upregulating *Foxg1* in neocortical precursors, 1 of which worked in their postmitotic derivatives too (Figure 4.7). Expression of these saRNAs elicited an appreciable biological outcome (Figure 4.8). RNAa was restricted to neural cells expressing the target gene and did not interfere with its endogenous tuning (Figure 4.9). saRNAs recognized target chromatin through nascent ncRNAs and, possibly via Ago1, recruited RNApolII to it (Figure 4.10). Finally, delivery of one saRNA to mouse neonates, by intraventricular AAV injection, replicated *Foxg1*-RNAa *in vivo* (Figure 4.11).

Interestingly, only one out of the best four miRNAs activating *Foxg1* in proliferating neocortical precursors worked satisfactorily in their postmitotic derivatives (Figure 4.7A,E,F). This may be due to the different epigenetic state of chromatin, generally more accessible in the former ones (Meshorer and Misteli, 2006; Takizawa and Meshorer, 2008). It may

specifically reflect a different ncRNA landscape at the *Foxg1* locus. Despite the moderate amplitude of *Foxg1*-upregulation achieved by RNAa, such manipulation elicited a pronounced histogenetic effect (Figure 4.8). This was not a surprise. A high sensitivity of neuronogenic rates to even subtle changes of *Foxg1* levels was already reported (Fimiani et al., 2015). Moreover, similar phenomena were described for a number of other patterning genes, including *Emx2* and *Pax6* (Diodato et al., 2013; Hamasaki et al., 2004; Sansom et al., 2009).

We also found that saRNAs achieved a relevant molecular outcome only in primary cultures where the gene of interest was active (Figure 4.9A-C). This suggests that therapeutic saRNA delivery, driven by a ubiquitous promoter or achieved via straight administration of pre-made, synthetic molecules, should be followed by activation of the target gene limited to its standard expression domain. Moreover, within responsive neurons, saRNAs elicited a gentle and reproducible stimulation of the gene in order, which did not interfere with its fine endogenous tuning (Figure 4.9D,E). All these evidences strengthen the saRNA suitability for precise and affordable treatment of haploinsufficiences, with special emphasis on those of neurological interest.

Concerning mechanisms of RNAa, the employment of gapmers against ncRNAs stemming from the target locus is an elegant method for unveiling its molecular logic. Specifically, if the gapmer reproduces the saRNA effect, then gene activation should originate from destabilization of its ncRNA target, as described for *Bdnf* by (Modarresi et al., 2012). If the gapmer suppresses saRNA activity - as reported for *PR* and *COX2* by (Schwartz et al., 2008) and (Matsui et al., 2013) - then RNAa should rather rely on recruitment of transactivating effectors to the target locus, via ncRNA docks stemming from it. The latter scenario is what we observed for *Foxg1* upon delivery of miR-αFoxg1.0650 (Figure 4.10B). Other antisense saRNAs stimulating this gene might work in a similar way. Sense-oriented saRNAs might land on not yet mapped, *Foxg1*-associated antisense-ncRNAs, or act according to a different molecular logic.

Beyond target chromatin recognition by saRNAs, a crucial role in RNAa is played by Argonautes, which act as adaptors between the chromatin-bound saRNA and the effector complex stimulating transcription. In a number of cases, Ago2 was reported to be the key player. It binds the target gene through saRNA, it mediates the assembly of a supramolecular dock for RNApolII, and it is ultimately necessary for RNAa (Chu et al., 2010; Li et al., 2006; Matsui et al., 2010, 2013; Portnoy et al., 2016). Even Ago1 binds to TSS surroundings. Moreover, it interacts with RNApolII and is involved in transcription regulation (Huang et al., 2012). However, initial reports implicated it in transcriptional gene silencing (TGS) rather than RNAa (Chu et al., 2010; Li et al., 2006). Unexpectedly, we found that suppressing Ago1 by morpholino abolished *Foxg1*-RNAa (Figure 4.10E). This phenomenon is consistent with saRNA-dependent Ago1 recruitment we found at the *Foxg1* promoter (Figure 4.10D). It actually echoes the recent report of Ago1-dependent RNAa at the *IL2* locus (Li et al., 2006).

A step further along the RNAa cascade, RNApolII is recruited to TSS (Chu et al., 2010; Huang et al., 2012; Majid et al., 2010; Matsui et al., 2010; Place et al., 2008; Yue et al., 2010) or possibly stimulated to progress downstream of it (Liu et al., 2013). In case of *Foxg1*-mRNA, the RNApolII enrichement profile of the gene, in baseline conditions as well as upon miR-αFoxg1.0650 and .1694 delivery (Supplementary Figure S14 and Figure 4.10F,G), suggests that the former mechanism applies.

miR-αFoxg1.1694 worked also *in vivo* (Figure 4.11). Here, the cumulative *Foxg1* expression gain was about +68%, albeit only 1/6 of Foxg1-expressing cells were targeted. This means that the actual expression gain in targeted $Foxg1^{+}$ cells might be not far from 6*68%, i.e. about +400%. This suggests that, in a therapeutic scenario, saRNA expression should be dampened to restore physiological *Foxg1*-mRNA expression levels, possibly via a weaker promoter or a tunable transactivating system. Moreover, the employment of more advanced AAV drivers (Deverman et al., 2016) might help targeting the almost totality of telencephalic neural cells.

In summary, we have selected a set of artificial miRNA eliciting a gentle *Foxg1* transactivation, specifically in cortico-cerebral cells. Their delivery elicited an appreciable

biological outcome, while complying with endogenous gene tuning. They stimulated RNApolII recruitment, possibly via Ago1. One of these miRNAs worked promisingly *in vivo*, even though its therapeutic employment still requires further optimization. As recently shown, hemizygosity for specific genes and polygenic chromosomal segments underlies a huge number of neuropathological entitites (Barøy et al., 2013; Carvill and Mefford, 2013; Lal et al., 2015; Lee et al., 2015; Silva et al., 2015), for which no cure are presently available. Based on results reported above, RNAa might be a simple and scalable approach for fixing this class of problems.

****

In the last part of the work, I tested the portability of RNAa to other haploinsufficient genes. Friedreich ataxia (FRDA) is an autosomal recessive inherited neurodegenerative disorder for which there is no known effective treatment or cure. Neurodegenerative pathology occurs primarily in the large sensory neurons of the dorsal root ganglia and cerebellum (Koeppen, 2011). In 96% of patients with FRDA, a homozygous GAA triplet repeat expansion is found in the first intron of the frataxin (*FXN*) gene. A number of repeats ranging from 70 to 1000 triggers epigenetic changes in the gene, which eventually causes frataxin transcriptional repression (Campuzano et al., 1996; Herman et al., 2006; Rai et al., 2008). In case of FRDA fibroblasts, saRNAs upregulated *FXN*-mRNA up to +65%, so almost restoring *FXN* expression levels found in healthy fibroblasts (Fig. 4.14). This is a result of obvious therapeutic interest. We also assayed the possibility to enhance the outcome of FXN-RNAa, by treating FRDA fibroblasts simultaneously with HDAC inhibitors and saRNAs (Figures 4.15 and 4.16). This last approach was poorly fruitful. As the combination of the two treatments did not overcome the functional output obtained by the best performing single treatment (Figure 4.16), it is tempting to speculate that RNAa and epigenetic manipulation could share a common molecular pathway. We started to address molecular mechanisms underlying *FXN* RNAa (Figure 4.17), showing that the destabilization of an antisense transcript associated to

FXN-mRNA could be instrumental to it. Now we plan to further assess the outcome of transcriptional *FXN* stimulation in dorsal root ganglia neurons (DRGNs) and neocortical, layer V subcortically projecting neurons (NCxVScPNs) generated from FRDA patient-specific iPSCs. These neurons - in fact - are among the most dramatically damaged because of *FXN* haploinsufficiency. Moreover, to secure the biological relevance of our approach, we intend to assay the ultimate functional impact of our manipulation on mithocondrial activity of treated cells.

Dravet syndrome (DS), is a rare form of childhood-onset epileptic encephalopathy. DS is caused by de novo heterozygous mutations in the sodium channel α1 subunit (SCN1A) gene in about 95% of the patients (Claes et al., 2001; Meisler et al., 2010). These mutations lead to a reduction of *SCN1A* levels, resulting in impaired depolarization of gabaergic interneurons and consequent hyperexcitability of neural tissue. Among 4 candidate saRNAs, we were able to select only one effective molecule, upregulating *Scn1a* by just 20% in murine E16.5 post mitotic neurons. This was not a suprise for us. In case of *Foxg1*-RNAa, for example, starting from four similarly preselected candidate saRNAs working in proliferating neural precursors, we did find only one active in their postmitotic neuronal derivatives (Figure 4.7). Moreover, "neuronal RNAa" reports are definitively rare in literature (Modarresi et al., 2012). No doubt, further screening for additional saRNAs is needed. As a satisfactory *Scn1a*-RNAa effector is available to us, we will investigate molecular mechanisms accounting for *Scn1a* RNAa and assay compliance of saRNA manipulation with endogenous gene tuning. Finally, the availability of $Scn1a^{+/-}$ mice will allow us to further evaluatethe therapeutic impact of our gene manipulation *in vivo*.

****

To sum up, RNA-programmable transactivators (NMHVs) and saRNAs share two key features that make them appealing tools fot therapeutic stimulation of gene transcription.

First, they elicit moderate transcriptional gains that leave gene expression levels within the physiological range. This is not trivial since and exaggerate gene stimulation may give rise to undesired effects. Second, both NMHVs and saRNAs stimulate target genes *only where* these target genes are normally expressed, avoiding detrimental ectopic gene activation.

On the other side, there are some intriguing differences between these two effectors. For example, NMHV transactivating activity is confined to the immediate surroundings of the intended target genomic region. As far as we know, TSSs located at >1kb from the bait target are hardly affected and only those at <0.5kb from such target are reliably stimulated. Conversely, as shown by Diodato et al. 2013, saRNAs may stimulate transcription from a TSS lying as much as 12kb far from the intended saRNA-genomic target. Next, as shown for miR-αFoxg1.1694, saRNAs poorly interfere with endogenous gene regulation, so allowing for fine tuning of gene expression, locked to neuronal activity. As for NMHVs, we still have to elucidate if they are endowed with similar properties. Finally, the particularly small size of saRNAs makes them especially suitable for in vivo delivery. Albeit smaller than CRISPRs, NMHVs are definitively larger than saRNAs. Maybe, some miniaturization might make them more suitable for in vivo applications.

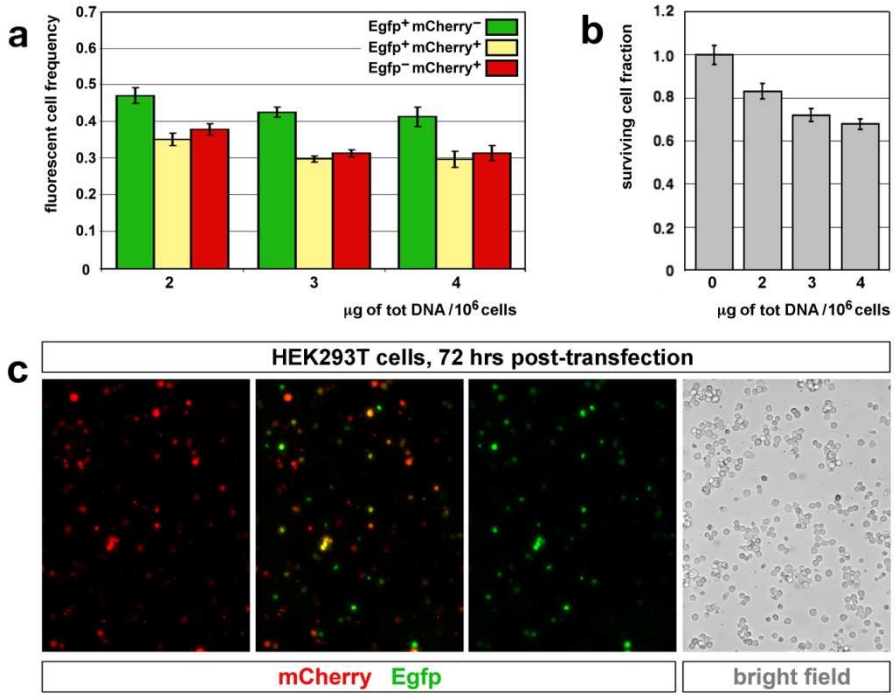
In summary, the scalability of our devices, the gentle gene activation they elicit and selective stimulation of active genes they achieve make these devices promising tools for clean rescue of gene haploisufficiencies. Interestingly, despite their similarities, they display some peculiarities that have to be taken into account, while choosing between the two platforms for therapeutic purposes.

Figures from 4.1 to 4.6 and Supplementary Figures from S1 to S11 were adapted from Fimiani C, Goina E, Mallamaci A. *Upregulating endogenous genes by an RNA-programmable artificial transactivator.* Nucleic Acids Res. 2015 Sep 18; 43(16):7850-64. doi: 10.1093/nar/gkv682

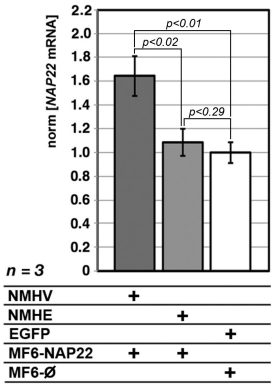
Figures from 4.7 to 4.11 and Supplementary Figures from S12 to S15 were adapted from Fimiani C*,* Goina E, Su Q, Gao G, and Mallamaci A*. RNA activation of haploinsufficient gene Foxg1 in murine neocortex.* Sci Rep. 2016 Dec 20; 6:39311. doi: 10.1038/srep39311

6. SUPPLEMENTARY FIGURES & TABLES

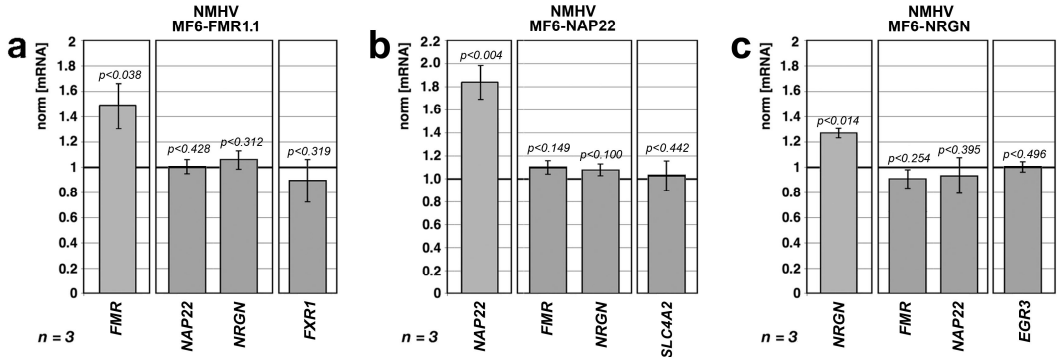
Supplementary Figures to Results 4.1 - *Upregulating endogenous genes by an RNA-programmable artificial transactivator*



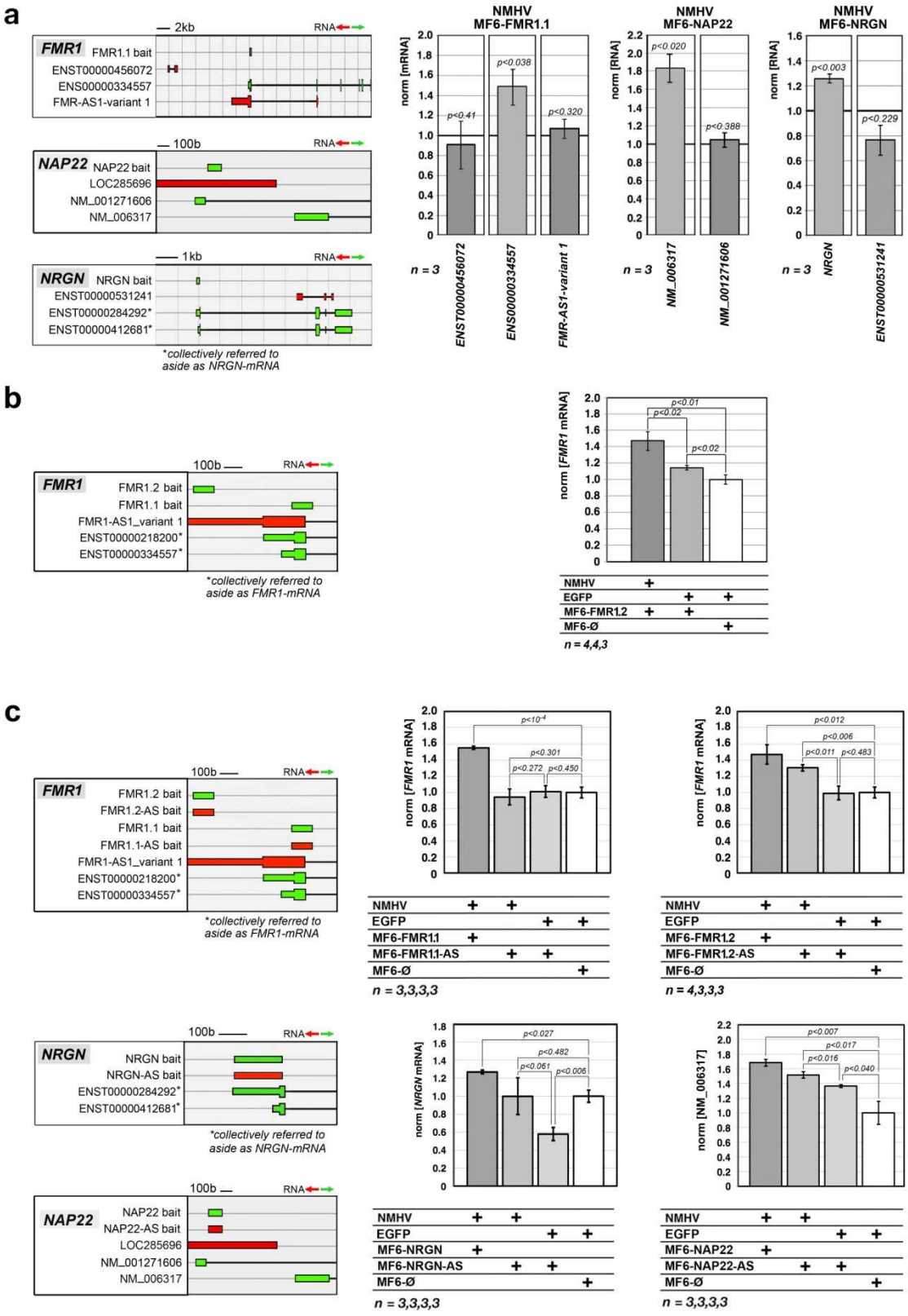
Supplementary Figure S1. Evaluation of HEK293T cell cotransfection efficiency. (a) Absolute frequencies of fluorescent elements, evaluated 72 hour after LipoD co-transfection of HEK293T cells with equimolar amounts of Pgkp1-mCherry (8.0kb) and CMVp-EGFP (4.7kb) plasmids. In *x*, total amounts of DNA delivered to 10^6 cells are indicated. **(b)** Surviving fractions of cells referred to in (a). Data normalized against untransfected cells. **(c)** Dark and bright field pictures of cells referred to in (a), transfected with 2 mg of total DNA /10^6 cells.



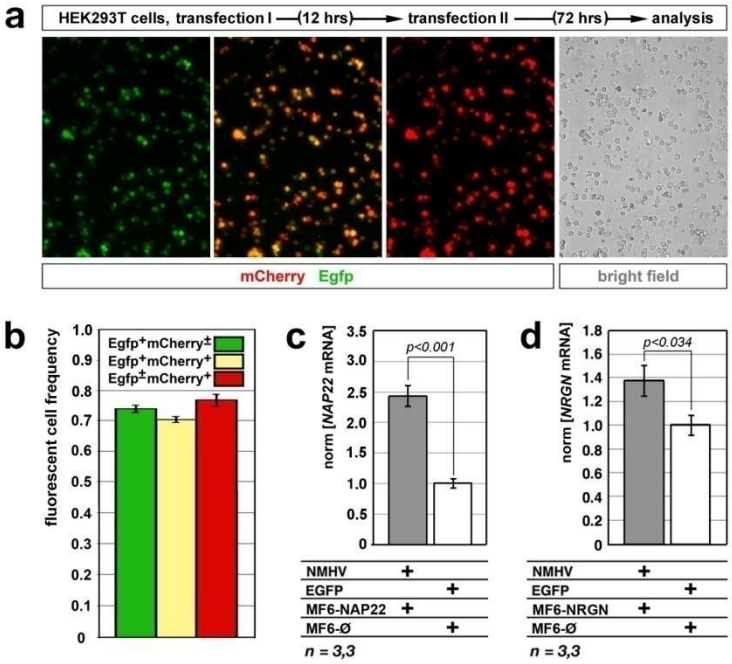
Supplementary Figure S2. Requirement of the VP16 domain for the NMHV function. *NAP22*-mRNA levels in HEK293T cells cotransfected by NMHV, NMHE, EGFP, MF6-NAP22 and MF6-Ø, in different combinations. Results were normalized against *GAPDH* and further normalized against EGFP/MF6-ø controls. Time-frame of the experiments and statistical parameters were as in Figure 4.1.



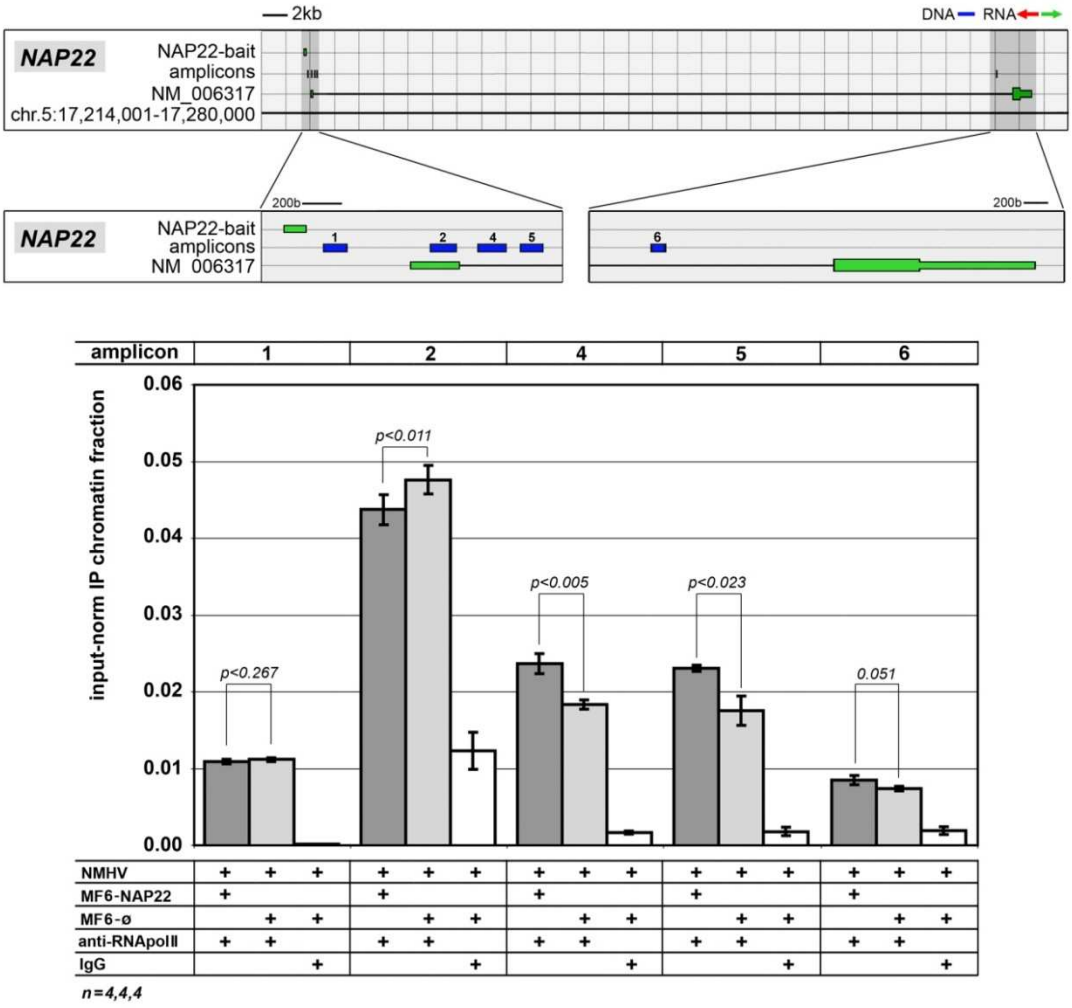
Supplementary Figure S3. Specificity of NMHV-mediated *FMR1, NAP22 and NRGN* transactivation: no perturbation of other active genes and structurally similar, potential offtargets. No aspecific gene upregulation in HEK293T cells expressing NMHV and the MF6-type, FMR1.1 **(a)**, NAP22 **(b)** or NRGN **(c)** baits. *FXR1*, *SLC4A2* and *EGR3* are potential offtargets, with 5' ends displaying remarkable homology to FMR1.1, NAP22 and NRGN baits, respectively (Supplementary Table S5). Results were normalized against *GAPDH* and further normalized against EGFP/MF6-ø controls. Time-frame of the experiments and statistical parameters were as in Figure 4.1.


a
2kb
RNA
FMR1
FMR1.1 bait
ENST00000456072
ENS00000334557
FMR-AS1-variant 1
100b
NAP22
NAP22 bait
LOC285696
NM_001271606
NM_006317
1kb
NRGN
NRGN bait
ENST00000531241
ENST00000284292*
ENST00000412681*
*collectively referred to aside as NRGN-mRNA
NMHV MF6-FMR1.1
NMHV MF6-NAP22
NMHV MF6-NRGN
norm [mRNA]
norm [RNA]
p<0.41
p<0.038
p<0.320
p<0.020
p<0.388
p<0.003
p<0.229
n = 3
ENST00000456072
ENS00000334557
FMR-AS1-variant 1
NM_006317
NM_001271606
NRGN
ENST00000531241
b
100b
RNA
FMR1
FMR1.2 bait
FMR1.1 bait
FMR1-AS1_variant 1
ENST00000218200*
ENST00000334557*
*collectively referred to aside as FMR1-mRNA
norm [FMR1 mRNA]
p<0.01
p<0.02
p<0.02
NMHV
EGFP
MF6-FMR1.2
MF6-Ø
n = 4,4,3
c
100b
RNA
FMR1
FMR1.2 bait
FMR1.2-AS bait
FMR1.1 bait
FMR1.1-AS bait
FMR1-AS1_variant 1
ENST00000218200*
ENST00000334557*
*collectively referred to aside as FMR1-mRNA
norm [FMR1 mRNA]
p<10-4
p<0.301
p<0.272
p<0.450
NMHV
EGFP
MF6-FMR1.1
MF6-FMR1.1-AS
MF6-Ø
n = 3,3,3,3
p<0.012
p<0.006
p<0.011
p<0.483
NMHV
EGFP
MF6-FMR1.2
MF6-FMR1.2-AS
MF6-Ø
n = 4,3,3,3
NRGN
NRGN bait
NRGN-AS bait
ENST00000284292*
ENST00000412681*
*collectively referred to aside as NRGN-mRNA
norm [NRGN mRNA]
p<0.027
p<0.482
p<0.061
p<0.006
NMHV
EGFP
MF6-NRGN
MF6-NRGN-AS
MF6-Ø
n = 3,3,3,3
NAP22
NAP22 bait
NAP22-AS bait
LOC285696
NM_001271606
NM_006317
norm [NM_006317]
p<0.007
p<0.017
p<0.016
p<0.040
NMHV
EGFP
MF6-NAP22
MF6-NAP22-AS
MF6-Ø
n = 3,3,3,3

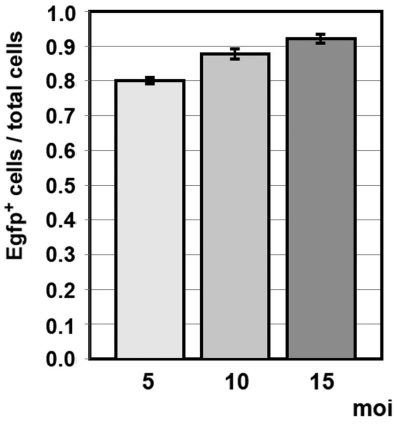
Supplementary Figure S4. Specificity of NMHV-mediated *FMR1*, *NAP22* and *NRGN* transactivation: limited cis-propagation and polarity effects. (a) Absent upregulation of transcripts stemming from TSSs >0.5kb far from bait-targets, in HEK293T cells co-expressing NMHV and the MF6-type, FMR1.1, NAP22 or NRGN baits. **(b)** Upregulation of transcripts originating from *FMR1*-TSSs, being <0.5kb far from bait-target, in HEK293T cells co-expressing NMHV and the *sense*-oriented, MF6-type, FMR1.2 bait. **(c)** Variable modulation of transcripts stemming from TSSs <0.5kb apart from bait-targets, in HEK293T cells co-expressing NMHV and the *antisense*-oriented, MF6-type, FMR1.1-AS, FMR1.2-AS, NRGN-AS or NAP22-AS baits. In each case, transcript upregulation by NMHV and the corresponding sense-oriented bait is shown as a reference. Time-frame of the experiments, data normalization and statistical parameters were as in Figure 4.1.



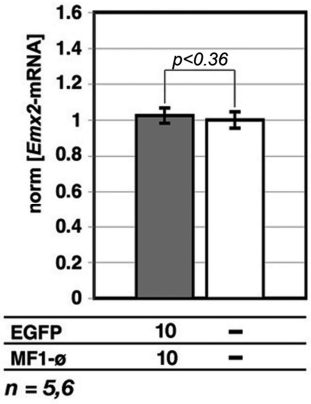
Supplementary Figure S5 Improving the transfection efficiency of HEK293T cells results in a consistent increase of NHMV/MF6-bait-dependent gene transactivation. (a) Dark and bright field pictures of HEK293T cells co-transfected with equimolar amounts of Pgkp1-mCherry (8.0kb) and CMVp-EGFP (4.7kb) plasmids (2.5 mg of total DNA/10^6 cells). Analysis performed 72 hour after completion of the two-steps, Lipofectamine 3000 transfection procedure. (**b**) Absolute frequencies of fluorescent elements, referred to in (**a**). **(c-d).** Upregulation of *NAP22* and *NRGN* mRNAs in HEK293T cells cotransfected with NMHV- and MF6-bait-encoding plasmids, according to the procedure shown in (**a**). Pgkp1-EGFP ("EGFP") and MF6-ø plasmids were used as controls. Results were normalized against *Gapdh* and further normalized against the EGFP/MF6-ø combination. Numbers of biological replicates, *n*, are displayed under the graphs. Bars represent s.e.m.'s.



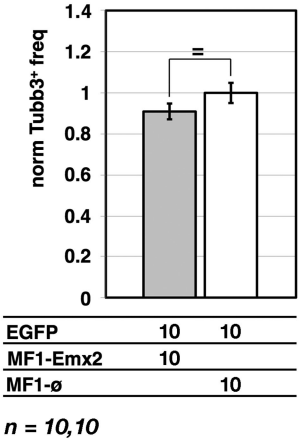
Supplementary Figure S6. Fraction of *NAP22* chromatin immunoprecipitated by anti-RNApolII, in HEK293T cells expressing NMHV/MF6-NAP22 or NMHV/MF6-ø. Graphs refer to results of the experiments described in Figure 4.2d, prior to normalization against NMHV/MF6-ø controls. They include results of additional control tests, run challenging NMHV/MF6-ø cells by IgGs, in place of anti-RNApolII. *n* are numbers of biological replicates. Bars represent s.e.m.'s.



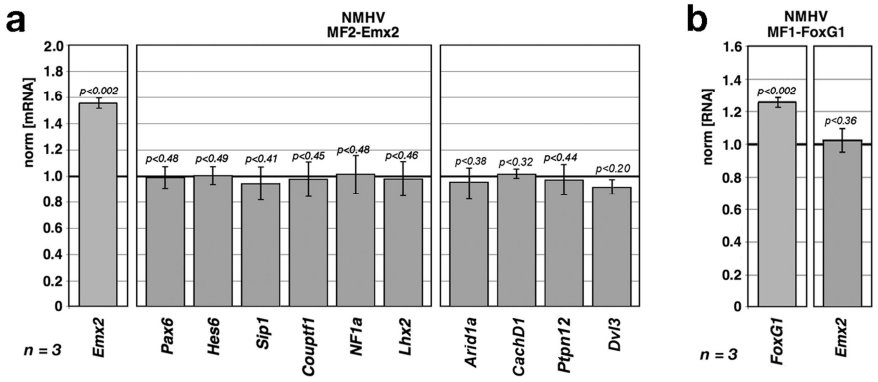
Supplementary Figure S7. Lentivirus dose-dependent infection of rhombo-spinal precursors. Correlation between multiplicity of infection (moi) and effective transduction rate, upon treatment of dissociated E10.5 rhombo-spinal precursors by the constitutive EGFP expressor pCCLsin.PPT.hPGK.EGFP.Wpre (Follenzi and Naldini, 2002), as assessed 4 days upon infection.



Supplementary Figure S8. Unaltered *Emx2* expression upon infection of cortico-cerebral precursors by control lentiviruses. *Emx2*-mRNA levels in uninfected cells and precursors co-infected with the control EGFP- and MF1-∅-encoding lentivectors. Results were normalized against *Gapdh* and further normalized against uninfected cells. Time-frame of the experiments as well as representation of moi's and statistical parameters were as in Figure 4.3.

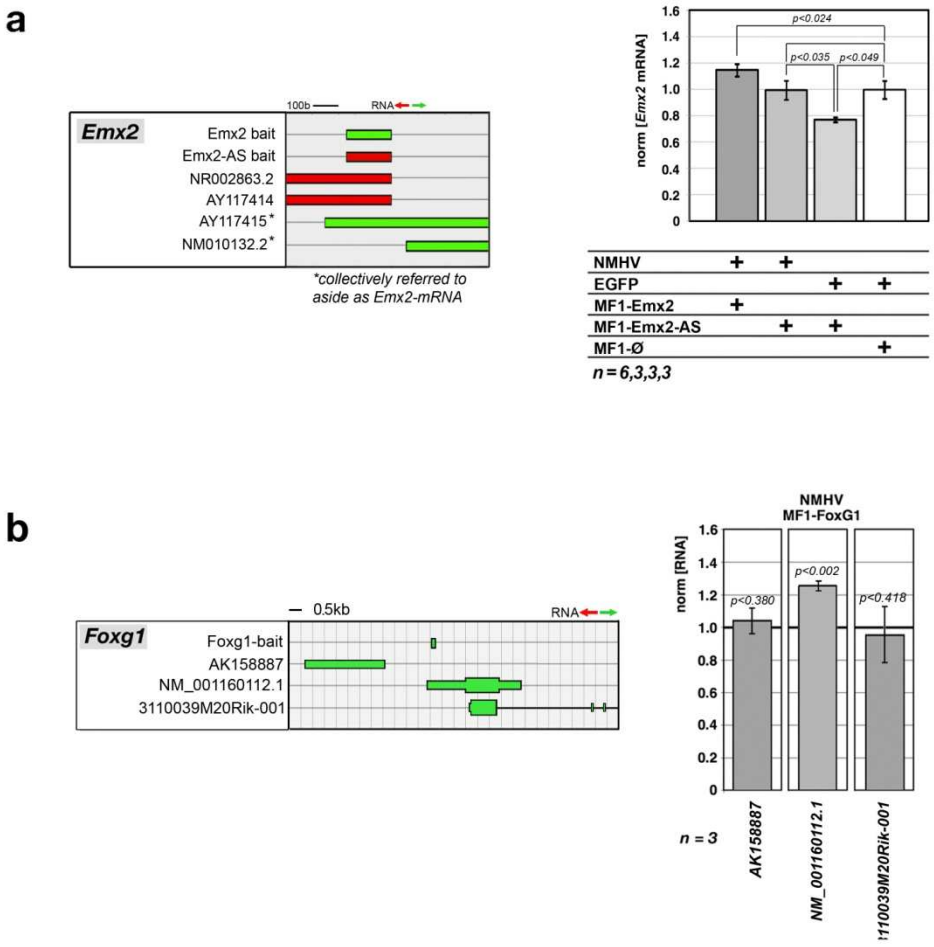


Supplementary Figure S9. Impact of Emx2-bait overexpression on neuronogenesis. No modulation of frequency of Tubb3^{+} neurons in cultures of EGFP/MF1-Emx2-overexpressing precursors, as assayed by immunofluorescence. Results were normalized against EGFP/MF1-ø controls. Time-frame of the experiments as well as representation of moi's and statistical parameters were as in Figure 4.3.



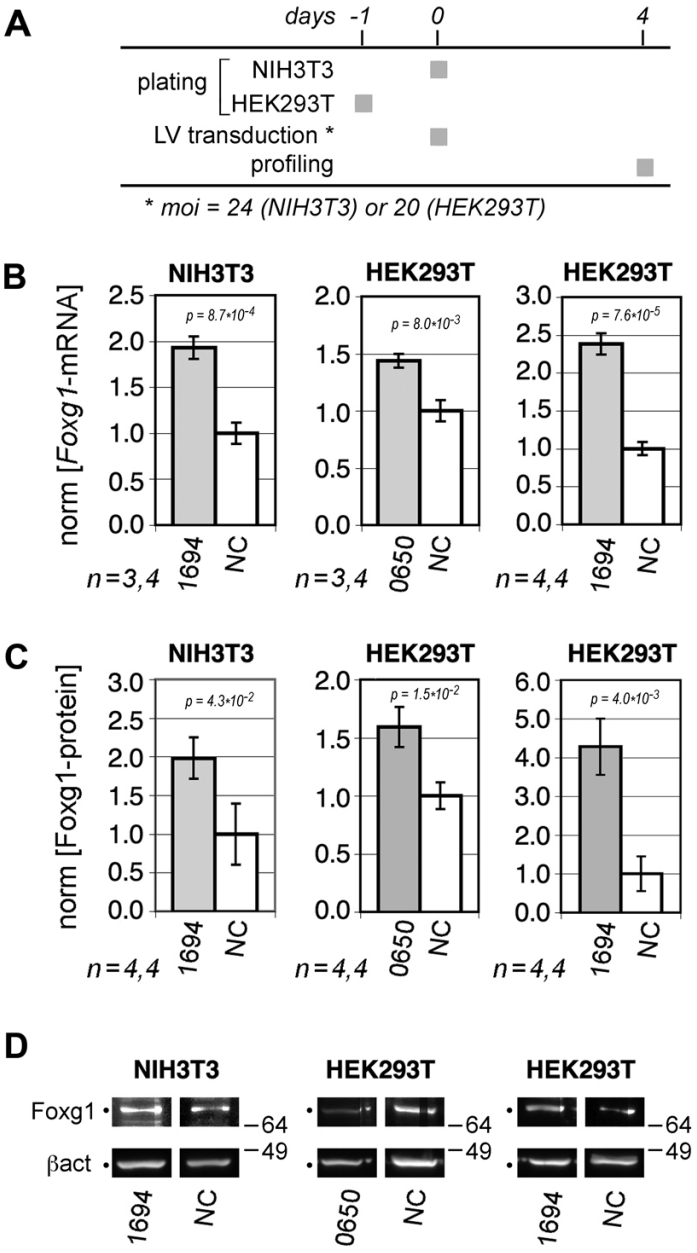
Supplementary Figure S10. Specificity of NMHV-mediated *Emx2* and *FoxG1* transactivation: no perturbation of other active genes and structurally similar, potential offtargets. Absence of aspecific gene transactivation in neural precursors overexpressing *Emx2* **(a)**, upon LV_NMHV / LV_MF2-Emx2 infection, or *FoxG1* **(b)**, upon LV_NMHV / LV_MF1-FoxG1 infection. *Pax6*, *Hes6*, *Sip1*, *Couptf1*, *Nf1a* and *Lhx2* are randomly chosen genes active in cortico-cerebral precursors. *Arid1a, CachD1, Ptpn12 and Dvl3* are potential offtargets, with 5' ends displaying remarkable homology to the Emx2 bait. Results were normalized against *Gapdh* and further normalized against EGFP/MF2-ø and EGFP/MF1-ø controls, respectively.

Time-frame of the experiments as well as representation of moi's and statistical parameters were as in Figure 4.3.



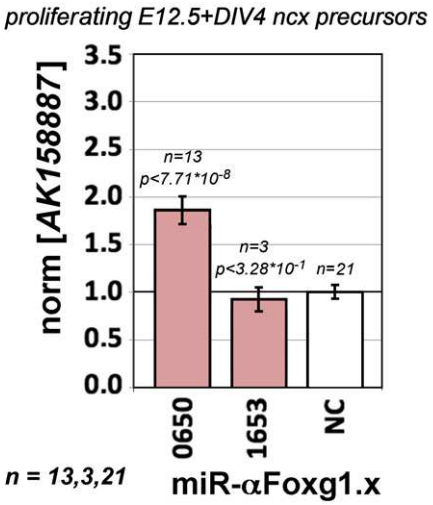
Supplementary Figure S11. Specificity of NMHV-mediated *Emx2* and *FoxG1* transactivation: limited cis-propagation and polarity effects. (a) No upregulation of *Emx2* mRNA, in cortical precursors co-expressing NMHV and the *antisense*-oriented, MF1-type, Emx2-AS bait. *Emx2* mRNA upregulation by NMHV and the corresponding sense-oriented bait is shown as a reference. **(b)** No upregulation of transcripts stemming from TSSs >1.5kb far from the bait-target, in neural precursors co-expressing NMHV and the MF1-type, FoxG1 bait. Time-frame of the experiments, representation of moi's, data normalization and statistical parameters were as in Figure 4.3.

Supplementary Figures to Results 4.2 - *RNA activation of haploinsufficient Foxg1 gene in murine neocortex*

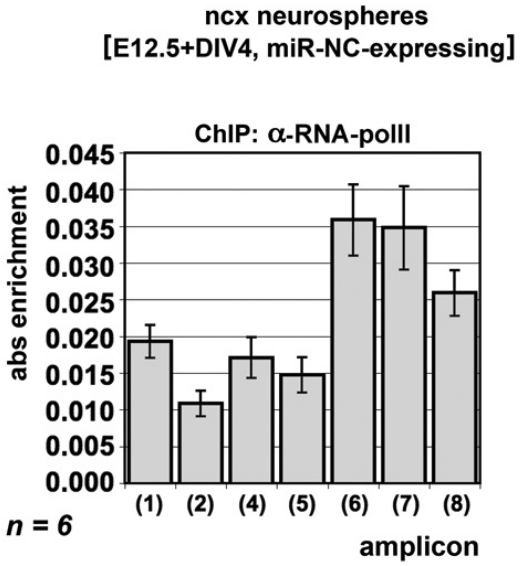


Supplementary Figure S12. Foxg1-RNAa in NIH3T3 and HEK293T cells. (A) Temporal articulation of the assays. **(B)** qRTPCR evaluation of *Foxg1/FOXG1*-mRNA upon saRNA delivery. Values double normalized, against *Gapdh/GAPDH* and controls (NC). **(C)** Western blot evaluation of Foxg1/FOXG1 protein upon saRNA delivery. Values double normalized,

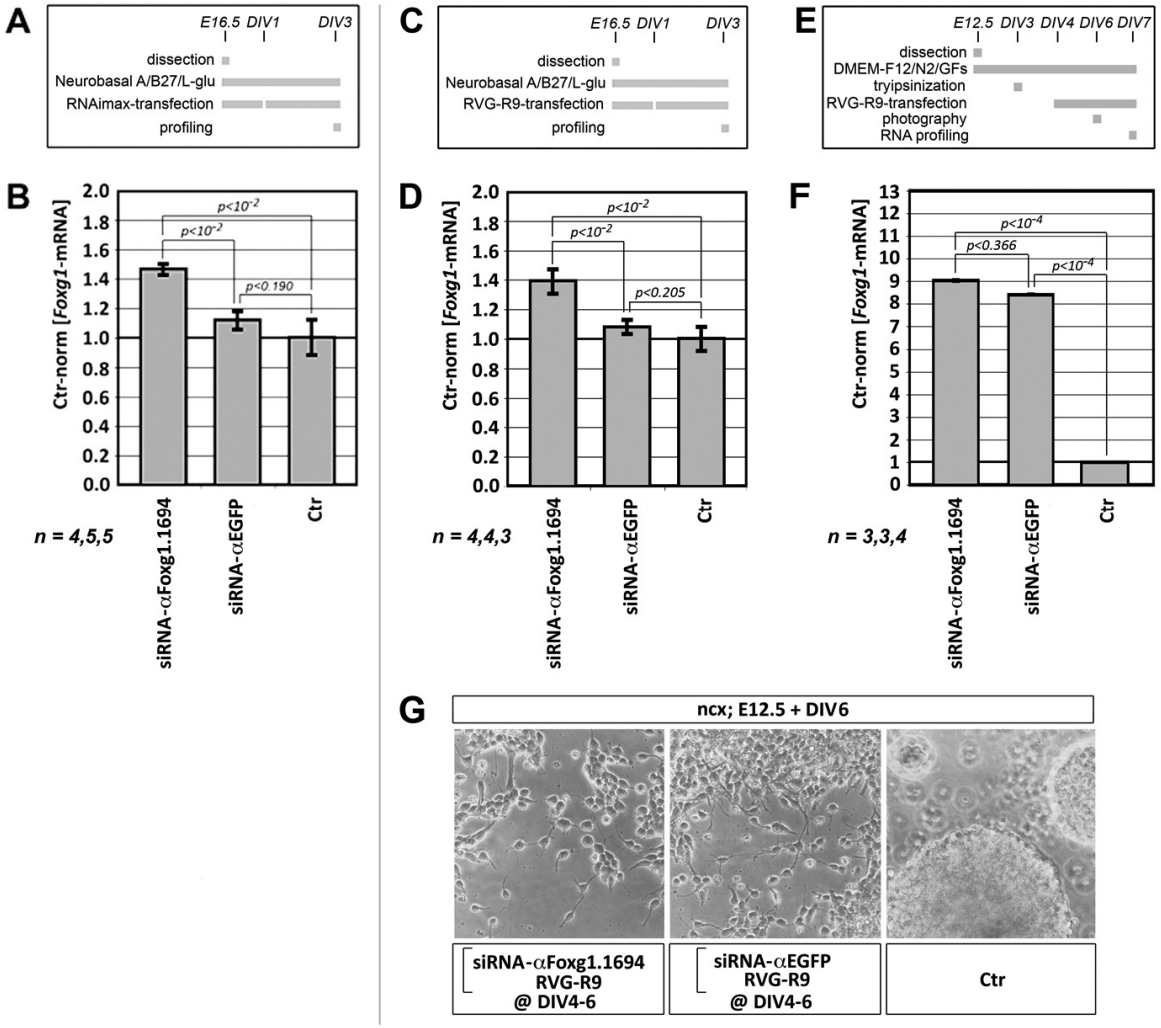
against *βactin/βACTIN* and controls (NC). (**D**) Examples of western blots referred to in (C). Throughout the figure, "1694", "0650" and "NC" stand for miR-αFoxg1.1694, miR-αFoxg1.0650 and miR-NC, respectively. Bars represent sem's . n= number of biological replicates. Evaluation of statistical significance by t-Student assay (one tail, unpaired).



Supplementary Figure S13. Impact of saRNAs on AK158887-ncRNA expression levels. AK158887-ncRNA levels in proliferating neocortical precursors manipulated as in Figure 4.7 B,C. qRTPCR assay performed on amplicon (2) of Figure 4.10A. Values double normalized, against *Gapdh* and control (NC). E, embryonic day. DIV, days in vitro. Bars represent sem's. *n* = number of biological replicates. *p* values calculated by t-Student assay (one-tail, unpaired).

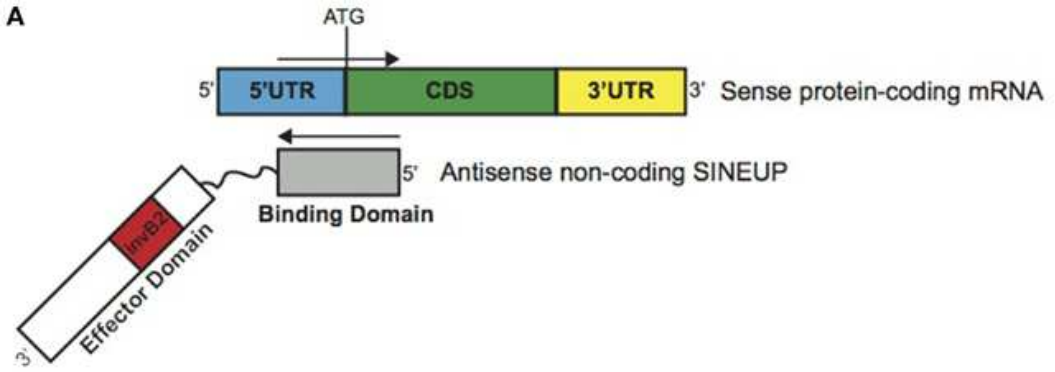


Supplementary Figure S14. Absolute RNApolII enrichment at the *Foxg1* locus in cortico-cerebral precursors in control conditions. qPCR quantification of *Foxg1* chromatin enrichment, upon chromatin immunoprecipitation (ChIP) by antibodies against RNA polymerase II (a-RNA-polII). Evaluation performed in neocortical precursors challenged by miR-NC, according to the protocol shown in Figure 4.7B,C. Values normalized against input chromatin. Bars represent sem's. *n* = number of biological replicates.



Supplementary Figure S15. *Foxg1* stimulation in neocortical cultures treated by chemically synthesized saRNAs. (A,B) *Foxg1*-mRNA expression levels in neocortical differentiating cells treated by siRNA-aFoxg1.1694 or siRNA-aEGFP, according to the RNAimax-based protocol shown in (A). Ctr are untreatd controls. **(C,D)** *Foxg1*-mRNA expression levels in neocortical differentiating cells treated by siRNA-aFoxg1.1694 or siRNA-aEGFP, according to the RVG-9R-based protocol shown in (C). Ctr are untreatd controls. **(E,F)** *Foxg1*-mRNA expression levels in neocortical proliferating precursors treated by siRNA-aFoxg1.1694 or siRNA-aEGFP, according to the RVG-R9-based protocol shown in (E). Ctr are untreatd controls. (**G**) Examples of treated and control neural precursor cells referred to in (E,F). In (B,D,F), values double normalized, against *Gapdh* and control (Ctr). E, embryonic day. DIV, days in vitro. Bars represent sem's. *n* = number of biological replicates. *p* values calculated by t-Student assay (one-tail, unpaired).

Supplementary Figures to Results 4.3 – *Portability of RNA activation (RNAa) to other haploinsufficient genes*



Supplementary Figure S16. Schematic representation of an idealized SINEUP. SINEUP modular structure. SINEUP binding domain (gray): SINEUP sequence reverse-complementary to the region of the protein-coding mRNA surrounding the Kozak-sequence/AUG module. SINEUP effector domain (red): non-mRNA-overlapping portion of SINEUPs (white), containing the inverted SINEB2 element (invB2, red) that stimulates activation of protein synthesis. Structural elements of protein-coding mRNA are shown: 5′ untranslated region (5′UTR, blue), coding sequence (CDS, green) and 3′ untranslated region (3′UTR, yellow). 5′ to 3′ orientation of sense and antisense RNA molecules is indicated. Adapted from Zucchelli et al., 2015.

Supplementary Table S1. Wild type baits I

bait name	bait genomic coordinates	bait length	bait orient-ation vs TSS	bait midpoint distance from TSS	bait CG%	bait cloning oligos - sequence (5'-3')
FMR1.1	hg19_chrX(+)_nt 146,993,634-146,993,748	115b	S	+222b	68%	FMR1b/F - CCCGGATCCCCTCGAGCGCCCGCAGCCCA FMR1b /R - CCCGTCGACCTTGTAGAAAGCGCCATTGGAGCCC
FMR1.2	hg19_chrX(+)_nt 146,993,101-146,993,220	120b	S	-308b	61%	FMR1-UPTSb.S/F - CCCGGATCCCCAGAGAGGCCGAACTGGGATAACC FMR1- UPTSb.S/R - CCCGTCGACGCTGAAGGGCGGTGACAGGTCGCA
NAP22	hg19_chr5(+)_nt 17,217,026-17,217,142	117b	S	+153b	62%	NAP22b/F - CCCGGATCCCGTCGGGAGCGGGCTGGACTG NAP22b/R - CCCGTCGACGTTGGATAAGAAGTGCTCGGGCTCTC
NRGN	hg19_chr11(+)_nt 124,609,848+124,609,995	148b	S	+92b	74%	NRGRb/F - CCCGGATCCCGAGAGCAGAGCTGCTGTTTCGGC NRGRb/R - CCCCTCGAGGGTGCAGCAGTCCATGCTGGTGTC
FMR1.1-AS	hg19_chrX(-)_nt 146,993,634-146,993,748	115b	AS	+222b	68%	FMR1b-AS/F - CCCGGATCCCTTGTAGAAAGCGCCATTGGAGCCC FMR1b-AS/R - CCCGTCGACCCTCGAGCGCCCGCAGCCCA
FMR1.2-AS	hg19_chrX(-)_nt 146,993,101-146,993,220	120b	AS	-308b	61%	FMR1-UPTSb.AS/F - CCCGGATCCGCTGAAGGGCGGTGACAGGTCGCA FMR1- UPTSb.AS/R - CCCGTCGACCCAGAGAGGCCGAACTGGGATAACC
NAP22-AS	hg19_chr5(-)_nt 17,217,026-17,217,142	117b	AS	+153b	62%	NAP22b-AS/F - CCCGGATCCGTTGGATAAGAAGTGCTCGGGCTCTC NAP22b-AS/R - CCCGTCGACCGTCGGGAGCGGGCTGGACTG
NRGN-AS	hg19_chr11(-)_nt 124,609,848+124,609,995	148b	AS	+92b	74%	NRGRb-AS/F - CCCGGATCCGGTGCAGCAGTCCATGCTGGTGTC NRGRb-AS/R - CCCCTCGAGCGAGAGCAGAGCTGCTGTTTCGGC
FMR1.1.60L	hg19_chrX(+)_nt 146,993,634-146,993,698	65b	S	+197b	74%	FMR1b/F - CCCGGATCCCCTCGAGCGCCCGCAGCCCA FMR65/R - CCCGTCGACTCTTCTCTTCAGCCCTGCTAGCGCC
FMR1.1.60R	hg19_chrX_(+)nt 146,993,688-146,993,748	61b	S	+249b	56%	FMR61/F - CCCGGATCCTGAAGAGAAGATGGAGGAGCTGGTGG FMR1b /R - CCCGTCGACCTTGTAGAAAGCGCCATTGGAGCCC
NAP22.60L	hg19_chr5(+)_nt 17,217,026-17,217,090	65b	S	+126b	65%	NAP22b/F - CCCGGATCCCGTCGGGAGCGGGCTGGACTG NAP65/R - CCCGTCGACGTGATGAATGACACCCCCTGGCACC
NAP22.60R	hg19_chr5(+)_nt 17,217,080-17,217,142	63b	S	+181b	54%	NAP63/F - CCCGGATCCTCATTCATCACCTCGAGGCAGCTCCCTA NAP22b/R - CCCGTCGACGTTGGATAAGAAGTGCTCGGGCTCTC

Supplementary Table S2. Wild type baits II

bait name	bait genomic coordinates	bait length	bait orient-ation vs TSS	bait midpoint distance from TSS	bait CG%	bait cloning oligos - sequence (5'-3')
Emx2 (Emx2.179)	mm10_chr19(+)_nt 59,458,457-59,458,635	179b	S	+174b	70%	Emx2.179-S/F - CCCAGATCTGCCGCAGGAGCGAGGGAGCTAGC Emx2.179-S/R - CCCCTCGAGGACTCTTTAAAGTGCGTCAGAGGGAGG
Emx2.120	mm10_chr19(+)_nt 59,458,457-59,458,576	120b	S	+144b	74%	Emx2.179-S/F - CCCAGATCTGCCGCAGGAGCGAGGGAGCTAGC E2b.120/R - GGGCTCGAGGGCCCAGAATGGAACGGAGTCGG
Emx2.60	mm10_chr19(+)_nt 59,458,457-59,458,516	60b	S	+114b	73%	Emx2.179-S/F - CCCAGATCTGCCGCAGGAGCGAGGGAGCTAGC E2b.60/R - GGGCTCGAGCCGCCGACCTCTTGGTGTCTTCGCC
Emx2.30	mm10_chr19(+)_nt 59,458,457-59,458,486	30b	S	+99b	77%	E2b.30/F - GATCTGCCGCAGGAGCGAGGGAGCTAGCCCGGAGCC E2b.30/R - TCGAGGCTCCGGGCTAGCTCCCTCGCTCCTGCGGCA
Emx2-AS	mm10_chr19(-)_nt 59,458,457-59,458,635	179b	AS	+174b	70%	Emx2.179-AS/F - CCCAGATCTGACTCTTTAAAGTGCGTCAGAGGGAGG Emx2.179-AS/R - CCCCTCGAGGCCGCAGGAGCGAGGGAGCTAGC
FoxG1	mm10_chr12_nt 49,383,099-49,383,244	146b	S	+165b	59%	FoxG1.146-S/F - CCCAGATCTAGTACTGCCTAGAAGCTGAAGAGG FoxG1.146-S/R - CCCCTCGAGACCCAAACAGTCCCGAAATAAAGC

Supplementary Table S3. qRTPCR oligos

gene	oligos - sequence (5'-3')
3110039M20Rik-001	RykM20.1/F - CCTGCCCTCCATACTCCAGCTTCTCC RykM20.1/R - CCCGCACTGGGTGAGGCGATCTC
AK158887	AK158887.1108/F - TGGACTGCATTGATTCCTTGGGCAACTAGG AK158887.1250/R - TTGAGCCCCTGGTAAGTAAGACACTCCAG
Arid1a	Arid1a.201/F - GCAGATGGAACACCCAAGACAGAATCCAAATC Arid1a.201/R - TCTCGGGCTCACCACCCAACTCATACA
CachD1	Cachd1-001/F - GTGAACAGCCGAGCCTTCAACCCAGGA Cachd1-001/R - CCCTTCTTCTGAGCTGAAATATTGCCACTTGAT
Couptf1	Couptf1/F - CTTCATGGACCACATCCGCATCTTTCAGGAACAG Couptf1/ - TCACATACTCCTCCAGGGCACACTGTGATTTCTC
Dvl3	Dvl3.ex13/F - CTACATCTTTGGCGACCTCTGTGGTAACAT Dvl3.ex14/R - GGAGCCAGTGTGTCCTGGTCAGAG
EGR3	EGR3.001/F - CGGCAGCAGCGACTCGGTAGTCCATT EGR3.001/R - GCTGGAAGGAGCCGGAGTAAGAGAGTT
Emx2	Emx2.E2S/N2F - GGAAAGGAAGCAGCTGGCTCACAGTCTCAGTCTTAC Emx2.E2S/N2 - RGTGGTGTGTCCCTTTTTTCTTCTGTTGAGAATCTGAGCCTTC
ENST000000531241	ENST531241/F - ATTACCTTTGAAAATGCTCAGTTCTTCTTCGGTC ENST531241/R - TCCTATCTCCTGTGTTTGAGTTCATCCTG
ENST00000456072	ENST456072/F - ATGCCTGCCTTGGTTATGGATGTGACAC ENST56072/R - CTGATCGTAGCTCACTGTAGCCTCAAACTC
FMR1	hFMR1/F - GAAGATTCAATAACAGTTGCATTTGAAAACAACTGG hFMR1/R - GCTCTGGAATACACCTCAACTTCATCAC
FMR-AS1-v1	NR024503/F - CCATTCCTGAAAAGCACTCAAACTGGACTTGAA NR024503/R - GGGCTCCAATGGCGCTTTCTACAAGG
FoxG1	FoxG1.2193/F - TGGAGTGTCAGCGAGGTGCAATGTGG FoxG1.2303/R - TACTGCACACATGGAAATCTGGCAGCC
FXR1	FXR1.001/F - GCGGCTCTAACGGGGCTTTCTACAAGG FXR1.001/R - CTTCATTAAATGGAACCTGGCGTTCTGGTTG
Gapdh	Gapdh.5/F - ATCTTCTTGTGCAGTGCCAGCCTCGTC Gapdh.5/R - GAACATGTAGACCATGTAGTTGAGGTCAATGAAGG
Hes6	Hes6/FI - GGAAGCACGGGGGGACCGCAAG Hes6/RE - TGCACTGGATGTAGCCAGCAGCGAAG
Lhx2	Lhx2/ForM - GGCAAGCCCTTCCTCGGGGCAGCCGCATC Lhx2/RevM - GCACACAACGCTGCCCGGTCACTGCTGATGGACGG
NM_006317 (NAP22-var1)	hNAP22/F - GGGGCTGCATAGGCACCCAGAG hNAP22/R - CCTCGGCCTTCTTGTCTTTCTCCTTG
Nf1a	Nf1a/F - GGCCTTACTTCTCACACCCAGCCATCCGTTAC Nf1a/R - GTGCACCTTGCCTTGACTGCTTCCATTGG
NM_001271606 (NAP22-var2)	Nap22/F2 - CTCACCCCAACCTCGCTGCCAG Nap22/R2 - GGCCTTCTTGTCTTTCTCCTTGGCTTTC
NRGR	hNRGR/F2 - GGAGACTAGGCCAGAACTGAGCATTTTCAA hNRGR/R2 - CAGGGAAGTCTCGTCGCTGCGAAG
Pax6	Pax6/ForM -CCAAGGGCGGTGAGCAGATGTGTGAGATCTTCTATTCTAG Pax6/RevM - CCCGTTGACAAAGACACCACCAAGCTGATTCACTC
Ptpn12	Ptpn12.001/FN - GCCTTTGGCGAATACAGTCATAGACTTCTGGA Ptpn12.001/R - CTTTTTCCTTCCCATCTCAAATTCTCGACAGGC
SCL4A2	SCL4A2/F - CTCCCTCTCCTTCCGCAGTCTCCT SCL4A2/R - CAGAGATGACCATCTGCTCCACCAC
Sip1	Sip1/F2 - CGAGAGGCATATGGTGACGCACAAG Sip1/R1 - CACTGTGAATTCTCAGGTGTTCTTTCAGGT

Supplementary Table S4. ChIP oligos

ChIP amplicon	oligos - sequences (5'-3')
NAP22_amplicon 1	NapIP/F - GAGAAGTCCACGGACAGCCCAGG NapIP/R - GTGCCCCGCCAACGTTTCCTAAATG
*NAP22*_amplicon 2	Nap225UTR/F - GCTCCAACTGGCTCCTCGCTCC Nap225UTR/R - GTGCCTATGCAGCCCCTGAGTTAG
*NAP22*_amplicon 3	Nap22i1/F - TCCCTTCATGCAGCGGGCAGCAG Nap22i1/R - CCCTCCACCATGCGAGCGGC
*NAP22*_amplicon 4	Nap22i3/F - GGTGACGGGAGGAATTGCCGAATG Nap22i3/R - CTTTCTCCCAGGCTGGTAAGGGCT
*NAP22*_amplicon X	NAP22-midIN/F - CCTTACATTGTAAACTATCAGCTAGGGTTGAAGT NAP22-midIN/R - GGTATACATTGGAAATATGTTCATGTATAGAATCTCAC
*NAP22*_amplicon 5	Nap22i2/F - CAGTTCTGCCAGTGGACCTGACCTG Nap22i2/R - GTCCCATAAATGAGAAAAGCCCAGGAG
SLC4A2	SLC4IP/F2 - GCTATTGGTCACACTGGCCCAGAGG SLC4IP/R2 - CTGAGGCCGCAGGAGGAAGTCCAT
Emx2	Emx2.Fint - ATTTACCAGGCTTCGGAGGAAGCTG Emx2.Rint - CATGGAAGTGTTCGCTTCTTCACTAGTA
CachD1	CachdIP/F - AAAGTTTGGCGGGCTGCGCCTCC CachdIP/R - CCGGCCTTACGGTCTCCTCTTCCT
Dvl3	Dvl3IP/F - CCGTACCTGGTGAAGCTGCCCCT Dvl3IP/R - CCAAAATCGTCGTCCATAGACTTGAAGAAG
Ptpn12	PtpnIP/F - GGGACTTCATGGTGAGTGTCCGTTCT PtpnIP/R - CCTGTCCTCGCACCGCACACAAA

Supplementary Table S5. Off-target/on-target comparisons

off-target gene (on-target gene)	off-target sequence location: - hg19 coordinates - distance from off-target gene TSS, relative orientation	off-target vs on-target comparison	gap density	homology
SLC4A2 (*MAP2*)	- chr.7(-):150759353-150759431 - circa -0.3kb, antisense	off 1 GGGTCTGAGACGGGTTGCTGGGTGAGAGACCCA-GGGTTCTCAAAGTTCCTCAACCGCTG 59 on 22 GGGTCTGAGAAGGGTAGCT-GGTG-----CCAGGGGGTGTCA---TTCATC-ACCTC-G 69 off 60 AGGCTAAGCTACCTAGGTCT 79 on 70 AGGC--AGCTCCCTAAGTCT 87	15/80 (19%)	57/80 (71%)
FNIP1 (*FNIP1*)	- chr.3(+):180,630,471-180,630,524 - circa +0.3kb, sense	off 1 AACATGGCGGAGCTGACGGTGGAGGTTCGCGGCTCTAACGGGGCTTTCTACAAG 54 on 62 AAGATGGAGGAGCTGGTGGTGGAAGTGCGGGGCTCCAATGGCGCTTTCTACAAG 115	0/54 (0%)	44/54 (81%)
EGFR (*NRGN*)	- chr.8(+):22,550,683-22,550,780 - circa +0.05kb, sense	off 5 GGGTGCCTCAGCTGGTGCGGTATGAGGCTGGGTCGT-GGG-GGGGGTGGGGCGTGTGCGG 62 on 121 GGGT-CCTCTGCGGGGACG--A--AGGCTGG--CGCAGGGCGGGGGGTGGGGTCTGT--- 73 off 63 GGGGTG--GGGTGGGGGCTGGGCTGGGG 88 on 72 GTGGTGCCGGGGTGGGGGCT---CTGGGG 48 off 59 GCGGGGGGGTGGGGTGGGGGCTGG-GCTGGG-GGGGGATCT 96 on 89 GC-GGGGGTGGGGTCTGTG-TGGTGCGGGGTGGGGGCTCT 52 off 31 GCTGG-GTCGTGGGGGGGGTGGGGCGTGTGCGGGG-GGTGGGGTGGGGGCTGGGCTGGGG 88 on 133 GCTGGTGTCG----GGGGGT----CCTCTGCGGGGACGAAGGCT-GGCGCAGGGCGGGGG 83 off 89 GGGGATCT 96 on 82 TGGGGTCT 75	4/40 (10%) 11/68 (16%)	31/40 (78%) 46/68 (68%)

Supplementary Table S6. Off-target/on-target comparisons

off-target gene (on-target gene)	off-target sequence location: - mm10 coordinates - distance from off-target gene TSS, relative orientation	off-target vs on-target comparison	gap density	homology
Aridle (*Emx2*)	- chr.4(+):133754037-133754110 - -circa 0.4kb, antisense	off 4 AGGAGGGAGGGAGC--G---GGGGGGGAGGGGG--GAC-CGGGGACG--GGCGGGCGGGC 53 on 6 AGGAGCGAGGGAGCTAGCCCGGAGCGCAGGGCGAAGACACCAAGAGGTCGGCGGCCGGGC 65 off 54 GGGCGGGCTGGAGG 67 on 66 GGGC-GGCTGGAGG 78	11/74 (15%)	54/74 (73%)
Cachd1 (*Emx2*)	- chr.4(+):100776869-100776966 - circa +0.2kb, antisense	off 5 GGAAAGCGAAGGCGGCGC--C-GCTCCGCCGGTGCTCTC-AGCCGCCCGCCCGGCCTGCG 60 on 110 GGAA--CGGAGTCGGCGCTACTGCCCCGGCTGTGC-CTCCAGCCGCCCGCCCGGCC-GC- 56 off 61 GGCG-CCGC--G--GTCTTCGAGCCGCTGC-CGCCGGGC 93 on 55 --CGACCTCTTGGTGTCTTC--GCC-CTGCGCTCCGGGC 22	20/99 (20%)	72/99 (73%)
Ptpn13 (*Emx2*)	- chr.5(+):21,055,747-21,055,837 - circa +0.01kb, sense	off 5 CCCG-C-GTCCCCCCCGCCGCCCGCCCGCGCGCCGCAGCGCCCGCT--CCGTCTTC-CCC 59 on 88 CCCGGCTGTGCCTCCAGCCGCCCGCCCG---GCCGC--CGACCTCTTGGTGTCTTCGCCC 34 off 60 AGCTCGCTCCGGCC---CGCCCTCCCTCC 85 on 33 TG--CGCTCCGGGCTAGCTCCCTCGCTCC 7	15/89 (17%)	63/89 (71%)
Dvl3 (*Emx2*)	- chr.16(+):20,517,023 -20,517,140 - circa +0.15kb, sense	off 6 GCGGGCGGCGCTGGGACCCGG-GAGC-GGCCGGAGA-AC-AAGGGAGCT-GGCGGCCCGG 60 on 10 GCGAG-GGAGCTAG--CCCGGAGCGCAGGGCGAAGACACCAAG--AGGTCGGCGGCCGGG 64 off 61 CCGGCGGCTGAGTGGGGCTGAGCAGCGGGCCGCGCCG-AGCGCCGAGCTC 109 on 65 CGGGCGGCTG--GAGGC--A-CAGCCGG--G-GCAGTAGCGCCGA-CTC 104	21/110 (19%)	77/110 (70%)

Supplementary Table S7. Mutant, NAP22.60L-derivative baits.

bait	*sequence (5′ → 3′)*
NAP22.60L	CGTCGGGAGCGGGCTGGACTGGGGTCTGAGAAGGGTAGCTGGTGCCAGGGGGTGTCATTCATCAC
NAP22.60L.mut30.1	CGTCGGGAGCGGGCTGGACTGGGACTCAGAGGAAACGATCAACGCCAGGGGGTGTCATTCATCAC
NAP22.60L.mut30.2	CGTCGGGAGCGGGCTAAGTCAAAACCTGAGAAGGGTAGCTAACATTGAAAGGTGTCATTCATCAC
NAP22.60L.mut30.3	CGTCGGGAGCGAATCAAGCTGGGGTCTGAAGGAAACAGCTGGTGCCAAAAAACATCATTCATCAC
NAP22.60L.mut30.4	CGTCGGGAGTAAATTGGACTGGGACTCAAGAAGGGTAATCAATGCCAGGGGACACTATTCATCAC
NAP22.60L.mut15.1	CGTCGGGAGCGGGCTGGACTGGGGTCTCTCTTCCCATGCTGGTGCCAGGGGGTGTCATTCATCAC
NAP22.60L.mut15.2	CGTCGGGAGCGGGCTGGAGACCCGTCTGAGAAGGGTAGCTGGACGGTGGGGGTGTCATTCATCAC
NAP22.60L.mut15.3	CGTCGGGAGCGGGGACGACTGGGGTCTGAGTTCCGTAGCTGGTGCCAGCCCGTGTCATTCATCAC
NAP22.60L.mut15.4	CGTCGGGAGCGCCGTGGACTGGGGTGAGAGAAGGGTAGGAGGTGCCAGGGGCACTCATTCATCAC
NAP22.60L.mut15.5	CGTCGGGAGCCCGCTGGACTGCCGTCTGAGAACCGTAGCTGGTCGCAGGGGGTGAGATTCATCAC
NAP22.60L.mut15.6	CGTCGCGAGCGCGCTGGTCTGGGCTCTGACAAGGGAAGCTGCTGCCACGGGGTCTCATTGATCAC

Supplementary Table S8

artificial miRNAs

name (miR-αFoxg.)	*sequence (5' - 3')*	*genomic target coord**	*Block-it score***	*off-target numbers ****	*human vs mouse target difference*****
0650	TAAACTTCCCAGTAAGAGGTC	chr12(+): 49,379,719-49,379,739	5/5	0,0	1 sub
0755	TACTGTTCTCGCAAACCTAAT	chr12(-): 49,379,746-49,379,766	NA	0,0	0
1653	TTGTGAAGTTGAAAGTCTCTG	chr12(+): 49,380,664-49,380,684	5/5	0,0	1 ins
1694	TTCAAATCCAATTTGCACCCA	chr12(-): 49,380,612-49,380,632	5/5	0,0	0
2273	TTGTATTCAAGGAACAACTCC	chr12(-): 49,381,265-49,381,285	4.5/5	0,0	4 sub
2764	AAATGATTCGGTGTAACCGGA	chr12(+): 49,381,769-49,381,789	5/5	0,0	0
3700	TTCCCAGGGATTGGAATTTAG	chr12(+): 49,382,712-49,382,732	4.5/5	0,0	0
3795	AGGATTTGTGATCTGTGTGCT	chr12(-): 49,382,686-49,382,706	NA	0,0	6 sub, 1 ins

* UCSC Genome Browser GRCm38/mm10

** scores attributed by the running version of Block-it software (09.16.2016); NA, not available [here, the candidate miRNA, selected by a past version of Block-it software (2012), could not be re-harvested by the current version of this software, as falling under the 3/5 threshold]

*** as evaluated by Blastn (NCBI, "*somehow similar sequence*") and Blat (UCSC), on mouse transcriptome and genome, respectively

**** sub, substitution; ins, insertion

GapmeRs

name	*sequence (5'-3')**
αAK158887-1.1 GapmeR	AGTTACTCTTTAGCGT
Negative Control A GapmeR	AACACGTCTATACGC

* underlined, LNA

Morpholinos

name	*Sequence*
α-Ago1 morpholino	GTCCCGCTTCCATCCCATATACCCG
α-GFP morpholino	ACAGCTCCTCGCCCTTGCTCACCAT

siRNAs

name	*Sequence*
siRNA-aFoxg1.0650	5' pUAAACUUCCCAGUAAGAGGUCGdTdT 3' 3' dTdTAUUUGAAGGGUCAUUCUCCAGCp 5'
siRNA-aFoxg1.1694	5' pUUCAAAUCCAAUUUGCACCCAGdTdT 3' 3' dTdTAAGUUUAGGUUAAACGUGGGUCp 5'
siRNA-aGFP	5' pGAACUUCAGGGUCAGCUUGdTdT 3' 3' dTdTCUUGAAGUCCCAGUCGAACp 5'

polypeptide

name	*sequence (N-C)*
RVG-R9 peptide	YTIWMPENPRPGTPCDIFTNSRGKRASNGGGGRRRRRRRRR

DNA oligos

name	*sequence (5'-3')*
mAK567Fw	GAGGCGACCGCTTCTGAACTGAGTAT
mAK727Rev	TATAGACTTCCCTGAGAGCACAAACATCAA
mAKintFw	TGCCATTATGTGTGAGTCTCTCTAGGG
mAKintRev	GTAGCAAAGCTAGATCCACTAGCACCC
mAK2110Fw	GTTGGCTCTAGGGAAGGCAGACTTCA
mAK2225Rev	ATGCACAGGACGGTTTGTGACCTCTTG

mAK2408Fw	CTGCTCGAATGAAGTGCGCTGTGTAAGC
mAK2565Rev	CTCAGCTCTCATCCACTACCTACTCACTC
mFoxg1 127Fw	TAGAAGCTGAAGAGGAGGTGGAGTGC
mFoxg1 215Rev	CAGACCCAAACAGTCCCGAAATAAAGC
mFoxCDS1085Fw	GACAAGAAGAACGGCAAGTACGAGAAGC
mFoxCDS1144Rev	GAACTCATAGATGCCATTGAGCGTCAGG
mFoxg1cdsFw	CGACCCTGCCCTGTGAGTCTTTAAG
mFoxg1cdsRev	GGGTTGGAAGAAGACCCCTGATTTTGATG
mFoxg1 2193Fw	TGGAGTGTCAGCGAGGTGCAATGTGG
mFoxg1 2303Rev	TACTGCACACATGGAAATCTGGCAGCC
mGAPDHFw	ATCTTCTTGTGCAGTGCCAGCCTCGTC
mGAPDHRev	GAACATGTAGACCATGTAGTTGAGGTCAATGAAGG

Supplementary Table S9

artificial miRNAs

name (miR-αFXN.)	*sequence (5' - 3')*	*genomic target coord**	*Block-it score***	*off-target numbers ****
304	AATAGTGCTAAGCTGGGAAGT	chr9(+): 69,035,641-69,035,661	5/5	0,0
546	ATTTACACAAGGCATCCGTCT	chr9(+): 69,035,399-69,035,419	5/5	0,0
387	TGATCTGACAGATTAAGGGAG	chr9(-): 69,030,582 - 69,030,602	5/5	0,0
1694	TAAGCAGCAACTGTCATTAGC	chr9(-): 69,020,039-69,020,059	5/5	0,0

* UCSC Genome Browser GRCh38/hg38

** scores attributed by the running version of Block-it software (Dec 21, 2016);

*** as evaluated by Blastn (NCBI, "*somehow similar sequence*") and Blat (UCSC), on human transcriptome and genome, respectively

DNA oligos

name	*sequence (5'-3')*
hFX/F1	GTGATCAACAAGCAGACGCCAAACAAGCA
hFX/R1	GTACACCCAGTTTTTCCCAGTCCAGTCA
hGAPDH/RT1	GGGTCTACATGGCAACTGT
FAST-RT	CCAAGCAGCCTCAATTTGTG
FASTF1p	GTGGGGGAGCAGCTAGAGG
FASTR1p	CACTTCCCAGCAAGACAGC
N-FASTF1	CAGCTAGAGGTTAGACCTCAG
N-FASTR1	CAGCAGCTCCCAAGTTCCTC

Supplementary Table S10

artificial miRNAs

name (miR-αScn1a.)	*sequence (5' - 3')*	*genomic target coord**	*Block-it score***	*off-target numbers ****
201.1	TTAGCTTTCATGCTTCTGGTC	Chr2(-): 66,441,037-66,441,057	5/5	0,0
201.2	TTTACTGCACACTCCAAGAGA	Chr2(-): 66,441,082-66,441,102	5/5	0,0
001.1	TAGTGTGACAATTCAATGGCT	Chr2(-): 66,410,807-66,410,827	5/5	0,0
001.2	TTTGCATGTGAATTCGGACCA	Chr2(-): 66,409,726-66,409,746	5/5	0,0

* UCSC Genome Browser GRCm38/mm10

** scores attributed by the running version of Block-it software (Dec 21, 2016);

*** as evaluated by Blastn (NCBI, "*somehow similar sequence*") and Blat (UCSC), on human transcriptome and genome, respectively

**** sub, substitution; ins, insertion

DNA oligos

name	*sequence (5'-3')*
mScn1a/F	TGTGCCCATTGCTGTGGGAGAGTCT
mScn1a/R	TCTGAGGAGCTACTGCTTTCGTTGAGTTT
mGAPDH/F	ATCTTCTTGTGCAGTGCCAGCCTCGTC
mGAPDH/R	GAACATGTAGACCATGTAGTTGAGGTCAATGAAGG

7. BIBLIOGRAPHY

Acampora, D., Boyl, P.P., Signore, M., Martinez-Barbera, J.P., Ilengo, C., Puelles, E., Annino, A., Reichert, H., Corte, G., and Simeone, A. (2001). OTD/OTX2 functional equivalence depends on 5' and 3' UTR-mediated control of Otx2 mRNA for nucleo-cytoplasmic export and epiblast-restricted translation. Dev. Camb. Engl. *128*, 4801–4813.

Adinolfi, S., Trifuoggi, M., Politou, A.S., Martin, S., and Pastore, A. (2002). A structural approach to understanding the iron-binding properties of phylogenetically different frataxins. Hum. Mol. Genet. *11*, 1865–1877.

Al-Mahdawi, S., Pinto, R.M., Ismail, O., Varshney, D., Lymperi, S., Sandi, C., Trabzuni, D., and Pook, M. (2008). The Friedreich ataxia GAA repeat expansion mutation induces comparable epigenetic changes in human and transgenic mouse brain and heart tissues. Hum. Mol. Genet. *17*, 735–746.

Aman, T.K., Grieco-Calub, T.M., Chen, C., Rusconi, R., Slat, E.A., Isom, L.L., and Raman, I.M. (2009). Regulation of persistent Na current by interactions between beta subunits of voltage-gated Na channels. J. Neurosci. Off. J. Soc. Neurosci. *29*, 2027–2042.

Amir, R.E., Van den Veyver, I.B., Wan, M., Tran, C.Q., Francke, U., and Zoghbi, H.Y. (1999). Rett syndrome is caused by mutations in X-linked MECP2, encoding methyl-CpG-binding protein 2. Nat. Genet. *23*, 185–188.

Ariani, F., Hayek, G., Rondinella, D., Artuso, R., Mencarelli, M.A., Spanhol-Rosseto, A., Pollazzon, M., Buoni, S., Spiga, O., Ricciardi, S., et al. (2008). FOXG1 is responsible for the congenital variant of Rett syndrome. Am. J. Hum. Genet. *83*, 89–93.

Atluri, P., Fleck, M.W., Shen, Q., Mah, S.J., Stadfelt, D., Barnes, W., Goderie, S.K., Temple, S., and Schneider, A.S. (2001). Functional Nicotinic Acetylcholine Receptor Expression in Stem and Progenitor Cells of the Early Embryonic Mouse Cerebral Cortex. Dev. Biol. *240*, 143–156.

Auerbach, D.S., Jones, J., Clawson, B.C., Offord, J., Lenk, G.M., Ogiwara, I., Yamakawa, K., Meisler, M.H., Parent, J.M., and Isom, L.L. (2013). Altered cardiac electrophysiology and SUDEP in a model of Dravet syndrome. PloS One *8*, e77843.

Bahi-Buisson, N., Nectoux, J., Girard, B., Van Esch, H., De Ravel, T., Boddaert, N., Plouin, P., Rio, M., Fichou, Y., Chelly, J., et al. (2010). Revisiting the phenotype associated with FOXG1 mutations: two novel cases of congenital Rett variant. Neurogenetics *11*, 241–249.

Barøy, T., Misceo, D., Strømme, P., Stray-Pedersen, A., Holmgren, A., Rødningen, O.K., Blomhoff, A., Helle, J.R., Stormyr, A., Tvedt, B., et al. (2013). Haploinsufficiency of two histone modifier genes on 6p22.3, ATXN1 and JARID2, is associated with intellectual disability. Orphanet J. Rare Dis. *8*, 3.

Bechi, G., Scalmani, P., Schiavon, E., Rusconi, R., Franceschetti, S., and Mantegazza, M. (2012). Pure haploinsufficiency for Dravet syndrome Na(V)1.1 (SCN1A) sodium channel truncating mutations. Epilepsia *53*, 87–100.

Beerli, R.R., and Barbas, C.F. (2002). Engineering polydactyl zinc-finger transcription factors. Nat. Biotechnol. *20*, 135–141.

Beerli, R.R., Segal, D.J., Dreier, B., and Barbas, C.F. (1998). Toward controlling gene expression at will: specific regulation of the erbB-2/HER-2 promoter by using polydactyl zinc finger proteins constructed from modular building blocks. Proc. Natl. Acad. Sci. U. S. A. *95*, 14628–14633.

Beerli, R.R., Dreier, B., and Barbas, C.F. (2000). Positive and negative regulation of endogenous genes by designed transcription factors. Proc. Natl. Acad. Sci. U. S. A. *97*, 1495–1500.

Benjamini, Y., Hochberg, Y. (1995). Controlling the False Discovery Rate: A Practical and Powerful Approach to Multiple Testing. J. R. Stat. Soc. Ser. B 289–300.

Bhakta, M.S., Henry, I.M., Ousterout, D.G., Das, K.T., Lockwood, S.H., Meckler, J.F., Wallen, M.C., Zykovich, A., Yu, Y., Leo, H., et al. (2013). Highly active zinc-finger nucleases by extended modular assembly. Genome Res. *23*, 530–538.

Bitterman, K.J., Anderson, R.M., Cohen, H.Y., Latorre-Esteves, M., and Sinclair, D.A. (2002). Inhibition of silencing and accelerated aging by nicotinamide, a putative negative regulator of yeast sir2 and human SIRT1. J. Biol. Chem. *277*, 45099–45107.

Blau, J., Xiao, H., McCracken, S., O'Hare, P., Greenblatt, J., and Bentley, D. (1996). Three functional classes of transcriptional activation domain. Mol. Cell. Biol. *16*, 2044–2055.

Boch, J., Scholze, H., Schornack, S., Landgraf, A., Hahn, S., Kay, S., Lahaye, T., Nickstadt, A., and Bonas, U. (2009). Breaking the code of DNA binding specificity of TAL-type III effectors. Science *326*, 1509–1512.

Bogdanove, A.J., and Voytas, D.F. (2011). TAL effectors: customizable proteins for DNA targeting. Science *333*, 1843–1846.

van Bokhoven, H. (2011). Genetic and epigenetic networks in intellectual disabilities. Annu. Rev. Genet. *45*, 81–104.

Bourguignon, C., Li, J., and Papalopulu, N. (1998). XBF-1, a winged helix transcription factor with dual activity, has a role in positioning neurogenesis in Xenopus competent ectoderm. Dev. Camb. Engl. *125*, 4889–4900.

Brancaccio, M., Pivetta, C., Granzotto, M., Filippis, C., and Mallamaci, A. (2010). Emx2 and Foxg1 inhibit gliogenesis and promote neuronogenesis. Stem Cells Dayt. Ohio *28*, 1206–1218.

Bredenkamp, N., Seoighe, C., and Illing, N. (2007). Comparative evolutionary analysis of the FoxG1 transcription factor from diverse vertebrates identifies conserved recognition sites for microRNA regulation. Dev. Genes Evol. *217*, 227–233.

Brunetti-Pierri, N., Paciorkowski, A.R., Ciccone, R., Della Mina, E., Bonaglia, M.C., Borgatti, R., Schaaf, C.P., Sutton, V.R., Xia, Z., Jelluma, N., et al. (2011). Duplications of FOXG1 in 14q12 are associated with developmental epilepsy, mental retardation, and severe speech impairment. Eur. J. Hum. Genet. EJHG *19*, 102–107.

Campuzano, V., Montermini, L., Moltò, M.D., Pianese, L., Cossée, M., Cavalcanti, F., Monros, E., Rodius, F., Duclos, F., Monticelli, A., et al. (1996). Friedreich's ataxia: autosomal recessive disease caused by an intronic GAA triplet repeat expansion. Science *271*, 1423–1427.

Carey, J., Lowary, P.T., and Uhlenbeck, O.C. (1983). Interaction of R17 coat protein with synthetic variants of its ribonucleic acid binding site. Biochemistry (Mosc.) *22*, 4723–4730.

Carlson, D.F., Fahrenkrug, S.C., and Hackett, P.B. (2012). Targeting DNA With Fingers and TALENs. Mol. Ther. Nucleic Acids *1*, e3.

Carpenter, B., Hill, K.J., Charalambous, M., Wagner, K.J., Lahiri, D., James, D.I., Andersen, J.S., Schumacher, V., Royer-Pokora, B., Mann, M., et al. (2004). BASP1 is a transcriptional cosuppressor for the Wilms' tumor suppressor protein WT1. Mol. Cell. Biol. *24*, 537–549.

Carvill, G.L., and Mefford, H.C. (2013). Microdeletion syndromes. Curr. Opin. Genet. Dev. *23*, 232–239.

Castaldo, I., Pinelli, M., Monticelli, A., Acquaviva, F., Giacchetti, M., Filla, A., Sacchetti, S., Keller, S., Avvedimento, V.E., Chiariotti, L., et al. (2008). DNA methylation in intron 1 of the frataxin gene is related to GAA repeat length and age of onset in Friedreich ataxia patients. J. Med. Genet. *45*, 808–812.

Catterall, W.A., Kalume, F., and Oakley, J.C. (2010). NaV1.1 channels and epilepsy. J. Physiol. *588*, 1849–1859.

Ceulemans, B. (2011). Overall management of patients with Dravet syndrome. Dev. Med. Child Neurol. *53 Suppl 2*, 19–23.

Chan, P.K., Torres, R., Yandim, C., Law, P.P., Khadayate, S., Mauri, M., Grosan, C., Chapman-Rothe, N., Giunti, P., Pook, M., et al. (2013). Heterochromatinization induced by GAA-repeat hyperexpansion in Friedreich's ataxia can be reduced upon HDAC inhibition by vitamin B3. Hum. Mol. Genet. *22*, 2662–2675.

Chavez, A., Scheiman, J., Vora, S., Pruitt, B.W., Tuttle, M., P R Iyer, E., Lin, S., Kiani, S., Guzman, C.D., Wiegand, D.J., et al. (2015). Highly efficient Cas9-mediated transcriptional programming. Nat. Methods *12*, 326–328.

Chavez, A., Tuttle, M., Pruitt, B.W., Ewen-Campen, B., Chari, R., Ter-Ovanesyan, D., Haque, S.J., Cecchi, R.J., Kowal, E.J.K., Buchthal, J., et al. (2016). Comparison of Cas9 activators in multiple species. Nat. Methods *13*, 563–567.

Cheah, C.S., Yu, F.H., Westenbroek, R.E., Kalume, F.K., Oakley, J.C., Potter, G.B., Rubenstein, J.L., and Catterall, W.A. (2012). Specific deletion of NaV1.1 sodium channels in inhibitory interneurons causes

seizures and premature death in a mouse model of Dravet syndrome. Proc. Natl. Acad. Sci. U. S. A. *109*, 14646–14651.

Cheng, A.W., Wang, H., Yang, H., Shi, L., Katz, Y., Theunissen, T.W., Rangarajan, S., Shivalila, C.S., Dadon, D.B., and Jaenisch, R. (2013). Multiplexed activation of endogenous genes by CRISPR-on, an RNA-guided transcriptional activator system. Cell Res. *23*, 1163–1171.

Chial, H.J., Giddings, T.H., Siewert, E.A., Hoyt, M.A., and Winey, M. (1999). Altered dosage of the Saccharomyces cerevisiae spindle pole body duplication gene, NDC1, leads to aneuploidy and polyploidy. Proc. Natl. Acad. Sci. U. S. A. *96*, 10200–10205.

Cho, D.H., Thienes, C.P., Mahoney, S.E., Analau, E., Filippova, G.N., and Tapscott, S.J. (2005). Antisense transcription and heterochromatin at the DM1 CTG repeats are constrained by CTCF. Mol. Cell *20*, 483–489.

Christian, M., Cermak, T., Doyle, E.L., Schmidt, C., Zhang, F., Hummel, A., Bogdanove, A.J., and Voytas, D.F. (2010). Targeting DNA double-strand breaks with TAL effector nucleases. Genetics *186*, 757–761.

Chu, Y., Yue, X., Younger, S.T., Janowski, B.A., and Corey, D.R. (2010). Involvement of argonaute proteins in gene silencing and activation by RNAs complementary to a non-coding transcript at the progesterone receptor promoter. Nucleic Acids Res. *38*, 7736–7748.

Claes, L., Del-Favero, J., Ceulemans, B., Lagae, L., Van Broeckhoven, C., and De Jonghe, P. (2001). De novo mutations in the sodium-channel gene SCN1A cause severe myoclonic epilepsy of infancy. Am. J. Hum. Genet. *68*, 1327–1332.

Clark, K.L., Halay, E.D., Lai, E., and Burley, S.K. (1993). Co-crystal structure of the HNF-3/fork head DNA-recognition motif resembles histone H5. Nature *364*, 412–420.

Codazzi, F., Hu, A., Rai, M., Salerno Scarzella, F., Mangiameli, E., Pelizzoni, I., Grohovaz, F., and Pandolfo, M. (2016). Friedreich ataxia induced pluripotent stem cell-derived neurons show a cellular phenotype that is corrected by a benzamide HDAC inhibitor. Hum. Mol. Genet.

Condò, I., Ventura, N., Malisan, F., Tomassini, B., and Testi, R. (2006). A pool of extramitochondrial frataxin that promotes cell survival. J. Biol. Chem. *281*, 16750–16756.

Condò, I., Ventura, N., Malisan, F., Rufini, A., Tomassini, B., and Testi, R. (2007). In vivo maturation of human frataxin. Hum. Mol. Genet. *16*, 1534–1540.

Cong, L., Zhou, R., Kuo, Y.-C., Cunniff, M., and Zhang, F. (2012). Comprehensive interrogation of natural TALE DNA-binding modules and transcriptional repressor domains. Nat. Commun. *3*, 968.

Cong, L., Ran, F.A., Cox, D., Lin, S., Barretto, R., Habib, N., Hsu, P.D., Wu, X., Jiang, W., Marraffini, L.A., et al. (2013). Multiplex genome engineering using CRISPR/Cas systems. Science *339*, 819–823.

Copley, R.R. (2004). Evolutionary convergence of alternative splicing in ion channels. Trends Genet. TIG *20*, 171–176.

Cossée, M., Campuzano, V., Koutnikova, H., Fischbeck, K., Mandel, J.L., Koenig, M., Bidichandani, S.I., Patel, P.I., Moltè, M.D., Cañizares, J., et al. (1997). Frataxin fracas. Nat. Genet. *15*, 337–338.

De Biase, I., Chutake, Y.K., Rindler, P.M., and Bidichandani, S.I. (2009). Epigenetic silencing in Friedreich ataxia is associated with depletion of CTCF (CCCTC-binding factor) and antisense transcription. PloS One *4*, e7914.

Deltcheva, E., Chylinski, K., Sharma, C.M., Gonzales, K., Chao, Y., Pirzada, Z.A., Eckert, M.R., Vogel, J., and Charpentier, E. (2011). CRISPR RNA maturation by trans-encoded small RNA and host factor RNase III. Nature *471*, 602–607.

Deng, W., Shi, X., Tjian, R., Lionnet, T., and Singer, R.H. (2015). CASFISH: CRISPR/Cas9-mediated in situ labeling of genomic loci in fixed cells. Proc. Natl. Acad. Sci. U. S. A. *112*, 11870–11875.

Depienne, C., Trouillard, O., Saint-Martin, C., Gourfinkel-An, I., Bouteiller, D., Carpentier, W., Keren, B., Abert, B., Gautier, A., Baulac, S., et al. (2009). Spectrum of SCN1A gene mutations associated with Dravet syndrome: analysis of 333 patients. J. Med. Genet. *46*, 183–191.

Deverman, B.E., Pravdo, P.L., Simpson, B.P., Kumar, S.R., Chan, K.Y., Banerjee, A., Wu, W.-L., Yang, B., Huber, N., Pasca, S.P., et al. (2016). Cre-dependent selection yields AAV variants for widespread gene transfer to the adult brain. Nat. Biotechnol. *34*, 204–209.

Diodato, A., Pinzan, M., Granzotto, M., and Mallamaci, A. (2013). Promotion of cortico-cerebral precursors expansion by artificial pri-miRNAs targeted against the Emx2 locus. Curr. Gene Ther. *13*, 152–161.

Dittenhafer-Reed, K.E., Feldman, J.L., and Denu, J.M. (2011). Catalysis and mechanistic insights into sirtuin activation. Chembiochem Eur. J. Chem. Biol. *12*, 281–289.

Dou, C.L., Li, S., and Lai, E. (1999). Dual role of brain factor-1 in regulating growth and patterning of the cerebral hemispheres. Cereb. Cortex N. Y. N 1991 *9*, 543–550.

Doudna, J.A., and Charpentier, E. (2014). Genome editing. The new frontier of genome engineering with CRISPR-Cas9. Science *346*, 1258096.

Dravet, C. (2011). Dravet syndrome history. Dev. Med. Child Neurol. *53 Suppl 2*, 1–6.

Dravet, C., Bureau, M., Oguni, H., Fukuyama, Y., and Cokar, O. (2005). Severe myoclonic epilepsy in infancy: Dravet syndrome. Adv. Neurol. *95*, 71–102.

Drubin, D.G., Jones, H.D., and Wertman, K.F. (1993). Actin structure and function: roles in mitochondrial organization and morphogenesis in budding yeast and identification of the phalloidin-binding site. Mol. Biol. Cell *4*, 1277–1294.

Dürr, A., Cossee, M., Agid, Y., Campuzano, V., Mignard, C., Penet, C., Mandel, J.L., Brice, A., and Koenig, M. (1996). Clinical and genetic abnormalities in patients with Friedreich's ataxia. N. Engl. J. Med. *335*, 1169–1175.

Eagleson, K.L., Schlueter McFadyen-Ketchum, L.J., Ahrens, E.T., Mills, P.H., Does, M.D., Nickols, J., and Levitt, P. (2007). Disruption of Foxg1 expression by knock-in of cre recombinase: effects on the development of the mouse telencephalon. Neuroscience *148*, 385–399.

Engel, N., Thorvaldsen, J.L., and Bartolomei, M.S. (2006). CTCF binding sites promote transcription initiation and prevent DNA methylation on the maternal allele at the imprinted H19/Igf2 locus. Hum. Mol. Genet. *15*, 2945–2954.

Escayg, A., and Goldin, A.L. (2010). Sodium channel SCN1A and epilepsy: mutations and mechanisms. Epilepsia *51*, 1650–1658.

Escayg, A., Heils, A., MacDonald, B.T., Haug, K., Sander, T., and Meisler, M.H. (2001). A novel SCN1A mutation associated with generalized epilepsy with febrile seizures plus--and prevalence of variants in patients with epilepsy. Am. J. Hum. Genet. *68*, 866–873.

Faghihi, M.A., Kocerha, J., Modarresi, F., Engström, P.G., Chalk, A.M., Brothers, S.P., Koesema, E., St Laurent, G., and Wahlestedt, C. (2010). RNAi screen indicates widespread biological function for human natural antisense transcripts. PloS One *5*.

Falcone, C., Filippis, C., Granzotto, M., and Mallamaci, A. (2015). *Emx2* expression levels in NSCs modulate astrogenesis rates by regulating *E gf R* and *F gf9*: *Emx2* Limits Astrogenesis Repressing *EgfR* and *Fgf9*. Glia *63*, 412–422.

Fehr, S., Wilson, M., Downs, J., Williams, S., Murgia, A., Sartori, S., Vecchi, M., Ho, G., Polli, R., Psoni, S., et al. (2013). The CDKL5 disorder is an independent clinical entity associated with early-onset encephalopathy. Eur. J. Hum. Genet. EJHG *21*, 266–273.

Filippova, G.N., Thienes, C.P., Penn, B.H., Cho, D.H., Hu, Y.J., Moore, J.M., Klesert, T.R., Lobanenkov, V.V., and Tapscott, S.J. (2001). CTCF-binding sites flank CTG/CAG repeats and form a methylation-sensitive insulator at the DM1 locus. Nat. Genet. *28*, 335–343.

Filippova, G.N., Cheng, M.K., Moore, J.M., Truong, J.-P., Hu, Y.J., Nguyen, D.K., Tsuchiya, K.D., and Disteche, C.M. (2005). Boundaries between chromosomal domains of X inactivation and escape bind CTCF and lack CpG methylation during early development. Dev. Cell *8*, 31–42.

Fimiani, C., Goina, E., and Mallamaci, A. (2015). Upregulating endogenous genes by an RNA-programmable artificial transactivator. Nucleic Acids Res. *43*, 7850–7864.

Florian, C., Bahi-Buisson, N., and Bienvenu, T. (2012). FOXG1-Related Disorders: From Clinical Description to Molecular Genetics. Mol. Syndromol. *2*, 153–163.

Follenzi, A., and Naldini, L. (2002). Generation of HIV-1 derived lentiviral vectors. Methods Enzymol. *346*, 454–465.

Frank-Kamenetskii, M.D., and Mirkin, S.M. (1995). Triplex DNA structures. Annu. Rev. Biochem. *64*, 65–95.

Garg, A., Lohmueller, J.J., Silver, P.A., and Armel, T.Z. (2012). Engineering synthetic TAL effectors with orthogonal target sites. Nucleic Acids Res. *40*, 7584–7595.

Gasiunas, G., and Siksnys, V. (2013). RNA-dependent DNA endonuclease Cas9 of the CRISPR system: Holy Grail of genome editing? Trends Microbiol. *21*, 562–567.

Gibson, T.J., Koonin, E.V., Musco, G., Pastore, A., and Bork, P. (1996). Friedreich's ataxia protein: phylogenetic evidence for mitochondrial dysfunction. Trends Neurosci. *19*, 465–468.

Gilbert, L.A., Larson, M.H., Morsut, L., Liu, Z., Brar, G.A., Torres, S.E., Stern-Ginossar, N., Brandman, O., Whitehead, E.H., Doudna, J.A., et al. (2013). CRISPR-mediated modular RNA-guided regulation of transcription in eukaryotes. Cell *154*, 442–451.

Gilbert, L.A., Horlbeck, M.A., Adamson, B., Villalta, J.E., Chen, Y., Whitehead, E.H., Guimaraes, C., Panning, B., Ploegh, H.L., Bassik, M.C., et al. (2014). Genome-Scale CRISPR-Mediated Control of Gene Repression and Activation. Cell *159*, 647–661.

Gong, B., Rhodes, K.J., Bekele-Arcuri, Z., and Trimmer, J.S. (1999). Type I and type II Na(+) channel alpha-subunit polypeptides exhibit distinct spatial and temporal patterning, and association with auxiliary subunits in rat brain. J. Comp. Neurol. *412*, 342–352.

Gonzalez, B., Schwimmer, L.J., Fuller, R.P., Ye, Y., Asawapornmongkol, L., and Barbas, C.F. (2010). Modular system for the construction of zinc-finger libraries and proteins. Nat. Protoc. *5*, 791–810.

Gordon, D., Merrick, D., Auld, V., Dunn, R., Goldin, A.L., Davidson, N., and Catterall, W.A. (1987). Tissue-specific expression of the RI and RII sodium channel subtypes. Proc. Natl. Acad. Sci. U. S. A. *84*, 8682–8686.

Gordon, D.M., Shi, Q., Dancis, A., and Pain, D. (1999). Maturation of frataxin within mammalian and yeast mitochondria: one-step processing by matrix processing peptidase. Hum. Mol. Genet. *8*, 2255–2262.

Goss, K.H., Risinger, M.A., Kordich, J.J., Sanz, M.M., Straughen, J.E., Slovek, L.E., Capobianco, A.J., German, J., Boivin, G.P., and Groden, J. (2002). Enhanced tumor formation in mice heterozygous for Blm mutation. Science *297*, 2051–2053.

Grabczyk, E., Mancuso, M., and Sammarco, M.C. (2007). A persistent RNA.DNA hybrid formed by transcription of the Friedreich ataxia triplet repeat in live bacteria, and by T7 RNAP in vitro. Nucleic Acids Res. *35*, 5351–5359.

Greene, E., Entezam, A., Kumari, D., and Usdin, K. (2005). Ancient repeated DNA elements and the regulation of the human frataxin promoter. Genomics *85*, 221–230.

Guerrini, R., and Parrini, E. (2012). Epilepsy in Rett syndrome, and CDKL5- and FOXG1-gene-related encephalopathies. Epilepsia *53*, 2067–2078.

Gupta, A., Christensen, R.G., Rayla, A.L., Lakshmanan, A., Stormo, G.D., and Wolfe, S.A. (2012). An optimized two-finger archive for ZFN-mediated gene targeting. Nat. Methods *9*, 588–590.

Gürlebeck, D., Szurek, B., and Bonas, U. (2005). Dimerization of the bacterial effector protein AvrBs3 in the plant cell cytoplasm prior to nuclear import. Plant J. Cell Mol. Biol. *42*, 175–187.

Gustincich, S., Zucchelli, S., and Mallamaci, A. (2016). The Yin and Yang of nucleic acid-based therapy in the brain. Prog. Neurobiol.

Hamasaki, T., Leingärtner, A., Ringstedt, T., and O'Leary, D.D.M. (2004). EMX2 regulates sizes and positioning of the primary sensory and motor areas in neocortex by direct specification of cortical progenitors. Neuron *43*, 359–372.

Hanashima, C., Shen, L., Li, S.C., and Lai, E. (2002). Brain factor-1 controls the proliferation and differentiation of neocortical progenitor cells through independent mechanisms. J. Neurosci. Off. J. Soc. Neurosci. *22*, 6526–6536.

Hanashima, C., Li, S.C., Shen, L., Lai, E., and Fishell, G. (2004). Foxg1 suppresses early cortical cell fate. Science *303*, 56–59.

Hanashima, C., Fernandes, M., Hebert, J.M., and Fishell, G. (2007). The role of Foxg1 and dorsal midline signaling in the generation of Cajal-Retzius subtypes. J. Neurosci. Off. J. Soc. Neurosci. *27*, 11103–11111.

Harkin, L.A., McMahon, J.M., Iona, X., Dibbens, L., Pelekanos, J.T., Zuberi, S.M., Sadleir, L.G., Andermann, E., Gill, D., Farrell, K., et al. (2007). The spectrum of SCN1A-related infantile epileptic encephalopathies. Brain J. Neurol. *130*, 843–852.

Hatini, V., Tao, W., and Lai, E. (1994). Expression of winged helix genes, BF-1 and BF-2, define adjacent domains within the developing forebrain and retina. J Neurobiol *25*, 1293–1309.

Heins, N., Cremisi, F., Malatesta, P., Gangemi, R.M., Corte, G., Price, J., Goudreau, G., Gruss, P., and Götz, M. (2001). Emx2 promotes symmetric cell divisions and a multipotential fate in precursors from the cerebral cortex. Mol. Cell. Neurosci. *18*, 485–502.

Herman, D., Jenssen, K., Burnett, R., Soragni, E., Perlman, S.L., and Gottesfeld, J.M. (2006). Histone deacetylase inhibitors reverse gene silencing in Friedreich's ataxia. Nat. Chem. Biol. *2*, 551–558.

Hilton, I.B., D'Ippolito, A.M., Vockley, C.M., Thakore, P.I., Crawford, G.E., Reddy, T.E., and Gersbach, C.A. (2015). Epigenome editing by a CRISPR-Cas9-based acetyltransferase activates genes from promoters and enhancers. Nat. Biotechnol. *33*, 510–517.

Hsu, P.D., Scott, D.A., Weinstein, J.A., Ran, F.A., Konermann, S., Agarwala, V., Li, Y., Fine, E.J., Wu, X., Shalem, O., et al. (2013). DNA targeting specificity of RNA-guided Cas9 nucleases. Nat. Biotechnol. *31*, 827–832.

Hu, J., Lei, Y., Wong, W.-K., Liu, S., Lee, K.-C., He, X., You, W., Zhou, R., Guo, J.-T., Chen, X., et al. (2014). Direct activation of human and mouse Oct4 genes using engineered TALE and Cas9 transcription factors. Nucleic Acids Res.

Huang, V., Place, R.F., Portnoy, V., Wang, J., Qi, Z., Jia, Z., Yu, A., Shuman, M., Yu, J., and Li, L.-C. (2012). Upregulation of Cyclin B1 by miRNA and its implications in cancer. Nucleic Acids Res. *40*, 1695–1707.

Janowski, B.A., Younger, S.T., Hardy, D.B., Ram, R., Huffman, K.E., and Corey, D.R. (2007). Activating gene expression in mammalian cells with promoter-targeted duplex RNAs. Nat. Chem. Biol. *3*, 166–173.

Jiao, J., Yang, Y., Shi, Y., Chen, J., Gao, R., Fan, Y., Yao, H., Liao, W., Sun, X.-F., and Gao, S. (2013). Modeling Dravet syndrome using induced pluripotent stem cells (iPSCs) and directly converted neurons. Hum. Mol. Genet. *22*, 4241–4252.

Jinek, M., Chylinski, K., Fonfara, I., Hauer, M., Doudna, J.A., and Charpentier, E. (2012). A programmable dual-RNA-guided DNA endonuclease in adaptive bacterial immunity. Science *337*, 816–821.

Johnson, D., Horsley, S.W., Moloney, D.M., Oldridge, M., Twigg, S.R., Walsh, S., Barrow, M., Njølstad, P.R., Kunz, J., Ashworth, G.J., et al. (1998). A comprehensive screen for TWIST mutations in patients with craniosynostosis identifies a new microdeletion syndrome of chromosome band 7p21.1. Am. J. Hum. Genet. *63*, 1282–1293.

Kacser, H., and Burns, J.A. (1981). The molecular basis of dominance. Genetics *97*, 639–666.

Kaestner, K.H., Lee, K.H., Schlöndorff, J., Hiemisch, H., Monaghan, A.P., and Schütz, G. (1993). Six members of the mouse forkhead gene family are developmentally regulated. Proc. Natl. Acad. Sci. U. S. A. *90*, 7628–7631.

Kalderon, D., Richardson, W.D., Markham, A.F., and Smith, A.E. (1984). Sequence requirements for nuclear location of simian virus 40 large-T antigen. Nature *311*, 33–38.

Kay, S., Boch, J., and Bonas, U. (2005). Characterization of AvrBs3-like effectors from a Brassicaceae pathogen reveals virulence and avirulence activities and a protein with a novel repeat architecture. Mol. Plant-Microbe Interact. MPMI *18*, 838–848.

Kay, S., Hahn, S., Marois, E., Hause, G., and Bonas, U. (2007). A bacterial effector acts as a plant transcription factor and induces a cell size regulator. Science *318*, 648–651.

Kearns, N.A., Genga, R.M.J., Enuameh, M.S., Garber, M., Wolfe, S.A., and Maehr, R. (2014). Cas9 effector-mediated regulation of transcription and differentiation in human pluripotent stem cells. Development *141*, 219–223.

Kearns, N.A., Pham, H., Tabak, B., Genga, R.M., Silverstein, N.J., Garber, M., and Maehr, R. (2015). Functional annotation of native enhancers with a Cas9-histone demethylase fusion. Nat. Methods *12*, 401–403.

Kelly, T.K., Karsten, S.L., Geschwind, D.H., and Kornblum, H.I. (2009). Cell lineage and regional identity of cultured spinal cord neural stem cells and comparison to brain-derived neural stem cells. PloS One *4*, e4213.

Khonsari, H., Schneider, M., Al-Mahdawi, S., Chianea, Y.G., Themis, M., Parris, C., Pook, M.A., and Themis, M. (2016). Lentivirus-meditated frataxin gene delivery reverses genome instability in Friedreich ataxia patient and mouse model fibroblasts. Gene Ther.

Kim, J.-H., Sedlak, M., Gao, Q., Riley, C.P., Regnier, F.E., and Adamec, J. (2010). Oxidative stress studies in yeast with a frataxin mutant: a proteomics perspective. J. Proteome Res. *9*, 730–736.

Kim, S., Lee, M.J., Kim, H., Kang, M., and Kim, J.-S. (2011). Preassembled zinc-finger arrays for rapid construction of ZFNs. Nat. Methods *8*, 7.

Klug, A. (2010). The discovery of zinc fingers and their applications in gene regulation and genome manipulation. Annu. Rev. Biochem. *79*, 213–231.

Kobayashi, N., Boyer, T.G., and Berk, A.J. (1995). A class of activation domains interacts directly with TFIIA and stimulates TFIIA-TFIID-promoter complex assembly. Mol. Cell. Biol. *15*, 6465–6473.

Koeppen, A.H. (2011). Friedreich's ataxia: pathology, pathogenesis, and molecular genetics. J. Neurol. Sci. *303*, 1–12.

Koeppen, A.H., and Mazurkiewicz, J.E. (2013). Friedreich ataxia: neuropathology revised. J. Neuropathol. Exp. Neurol. *72*, 78–90.

Konermann, S., Brigham, M.D., Trevino, A.E., Joung, J., Abudayyeh, O.O., Barcena, C., Hsu, P.D., Habib, N., Gootenberg, J.S., Nishimasu, H., et al. (2015). Genome-scale transcriptional activation by an engineered CRISPR-Cas9 complex. Nature *517*, 583–588.

Kortüm, F., Das, S., Flindt, M., Morris-Rosendahl, D.J., Stefanova, I., Goldstein, A., Horn, D., Klopocki, E., Kluger, G., Martin, P., et al. (2011). The core FOXG1 syndrome phenotype consists of postnatal microcephaly, severe mental retardation, absent language, dyskinesia, and corpus callosum hypogenesis. J. Med. Genet. *48*, 396–406.

Koutnikova, H., Campuzano, V., and Koenig, M. (1998). Maturation of wild-type and mutated frataxin by the mitochondrial processing peptidase. Hum. Mol. Genet. *7*, 1485–1489.

Kumar, P., Wu, H., McBride, J.L., Jung, K.-E., Kim, M.H., Davidson, B.L., Lee, S.K., Shankar, P., and Manjunath, N. (2007). Transvascular delivery of small interfering RNA to the central nervous system. Nature *448*, 39–43.

Kumari, D., Biacsi, R.E., and Usdin, K. (2011). Repeat expansion affects both transcription initiation and elongation in friedreich ataxia cells. J. Biol. Chem. *286*, 4209–4215.

Ladd, P.D., Smith, L.E., Rabaia, N.A., Moore, J.M., Georges, S.A., Hansen, R.S., Hagerman, R.J., Tassone, F., Tapscott, S.J., and Filippova, G.N. (2007). An antisense transcript spanning the CGG repeat region of FMR1 is upregulated in premutation carriers but silenced in full mutation individuals. Hum. Mol. Genet. *16*, 3174–3187.

Lal, D., Ruppert, A.-K., Trucks, H., Schulz, H., de Kovel, C.G., Kasteleijn-Nolst Trenité, D., Sonsma, A.C.M., Koeleman, B.P., Lindhout, D., Weber, Y.G., et al. (2015). Burden Analysis of Rare Microdeletions Suggests a Strong Impact of Neurodevelopmental Genes in Genetic Generalised Epilepsies. PLOS Genet. *11*, e1005226.

Larson, M.H., Gilbert, L.A., Wang, X., Lim, W.A., Weissman, J.S., and Qi, L.S. (2013). CRISPR interference (CRISPRi) for sequence-specific control of gene expression. Nat. Protoc. *8*, 2180–2196.

Le Guen, T., Bahi-Buisson, N., Nectoux, J., Boddaert, N., Fichou, Y., Diebold, B., Desguerre, I., Raqbi, F., Daire, V.C., Chelly, J., et al. (2011). A FOXG1 mutation in a boy with congenital variant of Rett syndrome. Neurogenetics *12*, 1–8.

LeCuyer, K.A., Behlen, L.S., and Uhlenbeck, O.C. (1995a). Mutants of the bacteriophage MS2 coat protein that alter its cooperative binding to RNA. Biochemistry (Mosc.) *34*, 10600–10606.

LeCuyer, K.A., Behlen, L.S., and Uhlenbeck, O.C. (1995b). Mutants of the bacteriophage MS2 coat protein that alter its cooperative binding to RNA. Biochemistry (Mosc.) *34*, 10600–10606.

Lee, B.H., Smith, T., and Paciorkowski, A.R. (2015). Autism spectrum disorder and epilepsy: Disorders with a shared biology. Epilepsy Behav. *47*, 191–201.

Li, L.-C., Okino, S.T., Zhao, H., Pookot, D., Place, R.F., Urakami, S., Enokida, H., and Dahiya, R. (2006). Small dsRNAs induce transcriptional activation in human cells. Proc. Natl. Acad. Sci. U. S. A. *103*, 17337–17342.

Li, Y., Moore, R., Guinn, M., and Bleris, L. (2012). Transcription activator-like effector hybrids for conditional control and rewiring of chromosomal transgene expression. Sci. Rep. *2*, 897.

Libby, R.T., Hagerman, K.A., Pineda, V.V., Lau, R., Cho, D.H., Baccam, S.L., Axford, M.M., Cleary, J.D., Moore, J.M., Sopher, B.L., et al. (2008). CTCF cis-regulates trinucleotide repeat instability in an epigenetic manner: a novel basis for mutational hot spot determination. PLoS Genet. *4*, e1000257.

Libri, V., Yandim, C., Athanasopoulos, S., Loyse, N., Natisvili, T., Law, P.P., Chan, P.K., Mohammad, T., Mauri, M., Tam, K.T., et al. (2014). Epigenetic and neurological effects and safety of high-dose nicotinamide in patients with Friedreich's ataxia: an exploratory, open-label, dose-escalation study. Lancet Lond. Engl. *384*, 504–513.

Lin, Y.S., Ha, I., Maldonado, E., Reinberg, D., and Green, M.R. (1991). Binding of general transcription factor TFIIB to an acidic activating region. Nature *353*, 569–571.

Liu, M., Roth, A., Yu, M., Morris, R., Bersani, F., Rivera, M.N., Lu, J., Shioda, T., Vasudevan, S., Ramaswamy, S., et al. (2013). The IGF2 intronic miR-483 selectively enhances transcription from IGF2 fetal promoters and enhances tumorigenesis. Genes Dev. *27*, 2543–2548.

Liu, Q., Segal, D.J., Ghiara, J.B., and Barbas, C.F. (1997). Design of polydactyl zinc-finger proteins for unique addressing within complex genomes. Proc. Natl. Acad. Sci. U. S. A. *94*, 5525–5530.

Liu, Y., Lopez-Santiago, L.F., Yuan, Y., Jones, J.M., Zhang, H., O'Malley, H.A., Patino, G.A., O'Brien, J.E., Rusconi, R., Gupta, A., et al. (2013c). Dravet syndrome patient-derived neurons suggest a novel epilepsy mechanism. Ann. Neurol. *74*, 128–139.

Long, Y.-S., Zhao, Q.-H., Su, T., Cai, Y.-L., Zeng, Y., Shi, Y.-W., Yi, Y.-H., Chang, H.-H., and Liao, W.-P. (2008). Identification of the promoter region and the 5'-untranslated exons of the human voltage-gated sodium channel Nav1.1 gene (SCN1A) and enhancement of gene expression by the 5'-untranslated exons. J. Neurosci. Res. *86*, 3375–3381.

Lykke-Andersen, J., Shu, M.D., and Steitz, J.A. (2000). Human Upf proteins target an mRNA for nonsense-mediated decay when bound downstream of a termination codon. Cell *103*, 1121–1131.

Maeder, M.L., Thibodeau-Beganny, S., Osiak, A., Wright, D.A., Anthony, R.M., Eichtinger, M., Jiang, T., Foley, J.E., Winfrey, R.J., Townsend, J.A., et al. (2008). Rapid "open-source" engineering of customized zinc-finger nucleases for highly efficient gene modification. Mol. Cell *31*, 294–301.

Maeder, M.L., Linder, S.J., Reyon, D., Angstman, J.F., Fu, Y., Sander, J.D., and Joung, J.K. (2013a). Robust, synergistic regulation of human gene expression using TALE activators. Nat. Methods *10*, 243–245.

Maeder, M.L., Linder, S.J., Cascio, V.M., Fu, Y., Ho, Q.H., and Joung, J.K. (2013). CRISPR RNA-guided activation of endogenous human genes. Nat. Methods *10*, 977–979.

Majid, S., Dar, A.A., Saini, S., Yamamura, S., Hirata, H., Tanaka, Y., Deng, G., and Dahiya, R. (2010). MicroRNA-205-directed transcriptional activation of tumor suppressor genes in prostate cancer. Cancer *116*, 5637–5649.

Mali, P., Yang, L., Esvelt, K.M., Aach, J., Guell, M., DiCarlo, J.E., Norville, J.E., and Church, G.M. (2013a). RNA-guided human genome engineering via Cas9. Science *339*, 823–826.

Mali, P., Yang, L., Esvelt, K.M., Aach, J., Guell, M., DiCarlo, J.E., Norville, J.E., and Church, G.M. (2013b). RNA-Guided Human Genome Engineering via Cas9. Science *339*, 823–826.

Mallamaci, A. (2011). Molecular bases of cortico-cerebral regionalization. Prog. Brain Res. *189*, 37–64.

Mallamaci, A., Iannone, R., Briata, P., Pintonello, L., Mercurio, S., Boncinelli, E., and Corte, G. (1998). EMX2 protein in the developing mouse brain and olfactory area. Mech. Dev. *77*, 165–172.

Marraffini, L.A., and Sontheimer, E.J. (2010). Self versus non-self discrimination during CRISPR RNA-directed immunity. Nature *463*, 568–571.

Martelli, A., Schmucker, S., Reutenauer, L., Mathieu, J.R.R., Peyssonnaux, C., Karim, Z., Puy, H., Galy, B., Hentze, M.W., and Puccio, H. (2015). Iron regulatory protein 1 sustains mitochondrial iron loading and function in frataxin deficiency. Cell Metab. *21*, 311–322.

Martynoga, B., Morrison, H., Price, D.J., and Mason, J.O. (2005). Foxg1 is required for specification of ventral telencephalon and region-specific regulation of dorsal telencephalic precursor proliferation and apoptosis. Dev. Biol. *283*, 113–127.

Matsui, M., Sakurai, F., Elbashir, S., Foster, D.J., Manoharan, M., and Corey, D.R. (2010). Activation of LDL receptor expression by small RNAs complementary to a noncoding transcript that overlaps the LDLR promoter. Chem. Biol. *17*, 1344–1355.

Matsui, M., Chu, Y., Zhang, H., Gagnon, K.T., Shaikh, S., Kuchimanchi, S., Manoharan, M., Corey, D.R., and Janowski, B.A. (2013). Promoter RNA links transcriptional regulation of inflammatory pathway genes. Nucleic Acids Res. *41*, 10086–10109.

Meisler, M.H., O'Brien, J.E., and Sharkey, L.M. (2010). Sodium channel gene family: epilepsy mutations, gene interactions and modifier effects. J. Physiol. *588*, 1841–1848.

Mencarelli, M.A., Kleefstra, T., Katzaki, E., Papa, F.T., Cohen, M., Pfundt, R., Ariani, F., Meloni, I., Mari, F., and Renieri, A. (2009). 14q12 Microdeletion syndrome and congenital variant of Rett syndrome. Eur. J. Med. Genet. *52*, 148–152.

Mendenhall, E.M., Williamson, K.E., Reyon, D., Zou, J.Y., Ram, O., Joung, J.K., and Bernstein, B.E. (2013). Locus-specific editing of histone modifications at endogenous enhancers. Nat. Biotechnol. *31*, 1133–1136.

Mercer, A.C., Gaj, T., Fuller, R.P., and Barbas, C.F. (2012). Chimeric TALE recombinases with programmable DNA sequence specificity. Nucleic Acids Res. *40*, 11163–11172.

Meshorer, E., and Misteli, T. (2006). Chromatin in pluripotent embryonic stem cells and differentiation. Nat. Rev. Mol. Cell Biol. *7*, 540–546.

Modarresi, F., Faghihi, M.A., Lopez-Toledano, M.A., Fatemi, R.P., Magistri, M., Brothers, S.P., van der Brug, M.P., and Wahlestedt, C. (2012). Inhibition of natural antisense transcripts in vivo results in gene-specific transcriptional upregulation. Nat. Biotechnol. *30*, 453–459.

Montermini, L., Richter, A., Morgan, K., Justice, C.M., Julien, D., Castellotti, B., Mercier, J., Poirier, J., Capozzoli, F., Bouchard, J.P., et al. (1997). Phenotypic variability in Friedreich ataxia: role of the associated GAA triplet repeat expansion. Ann. Neurol. *41*, 675–682.

Moore, F.E., Reyon, D., Sander, J.D., Martinez, S.A., Blackburn, J.S., Khayter, C., Ramirez, C.L., Joung, J.K., and Langenau, D.M. (2012). Improved somatic mutagenesis in zebrafish using transcription activator-like effector nucleases (TALENs). PloS One *7*, e37877.

Moran, O., Conti, F., and Tammaro, P. (2003). Sodium channel heterologous expression in mammalian cells and the role of the endogenous beta1-subunits. Neurosci. Lett. *336*, 175–179.

Morgan, A.R., and Wells, R.D. (1968). Specificity of the three-stranded complex formation between double-stranded DNA and single-stranded RNA containing repeating nucleotide sequences. J. Mol. Biol. *37*, 63–80.

Morris, K.V., Santoso, S., Turner, A.-M., Pastori, C., and Hawkins, P.G. (2008). Bidirectional transcription directs both transcriptional gene activation and suppression in human cells. PLoS Genet. *4*, e1000258.

Moscou, M.J., and Bogdanove, A.J. (2009). A simple cipher governs DNA recognition by TAL effectors. Science *326*, 1501.

Mulley, J.C., Scheffer, I.E., Petrou, S., Dibbens, L.M., Berkovic, S.F., and Harkin, L.A. (2005). SCN1A mutations and epilepsy. Hum. Mutat. *25*, 535–542.

Muñoz Bodnar, A., Bernal, A., Szurek, B., and López, C.E. (2013). Tell me a tale of TALEs. Mol. Biotechnol. *53*, 228–235.

Muroya, K., Hasegawa, T., Ito, Y., Nagai, T., Isotani, H., Iwata, Y., Yamamoto, K., Fujimoto, S., Seishu, S., Fukushima, Y., et al. (2001). GATA3 abnormalities and the phenotypic spectrum of HDR syndrome. J. Med. Genet. *38*, 374–380.

Muzio, L., and Mallamaci, A. (2005). Foxg1 confines Cajal-Retzius neuronogenesis and hippocampal morphogenesis to the dorsomedial pallium. J. Neurosci. Off. J. Soc. Neurosci. *25*, 4435–4441.

Muzio, L., Soria, J.M., Pannese, M., Piccolo, S., and Mallamaci, A. (2005). A mutually stimulating loop involving emx2 and canonical wnt signalling specifically promotes expansion of occipital cortex and hippocampus. Cereb Cortex *15*, 2021–2028.

Nelles, D.A., Fang, M.Y., O'Connell, M.R., Xu, J.L., Markmiller, S.J., Doudna, J.A., and Yeo, G.W. (2016). Programmable RNA Tracking in Live Cells with CRISPR/Cas9. Cell *165*, 488–496.

Neul, J.L., Kaufmann, W.E., Glaze, D.G., Christodoulou, J., Clarke, A.J., Bahi-Buisson, N., Leonard, H., Bailey, M.E.S., Schanen, N.C., Zappella, M., et al. (2010). Rett syndrome: revised diagnostic criteria and nomenclature. Ann. Neurol. *68*, 944–950.

Neuteboom, L.W., Lindhout, B.I., Saman, I.L., Hooykaas, P.J.J., and van der Zaal, B.J. (2006). Effects of different zinc finger transcription factors on genomic targets. Biochem. Biophys. Res. Commun. *339*, 263–270.

Ogiwara, I., Miyamoto, H., Morita, N., Atapour, N., Mazaki, E., Inoue, I., Takeuchi, T., Itohara, S., Yanagawa, Y., Obata, K., et al. (2007). Nav1.1 localizes to axons of parvalbumin-positive inhibitory interneurons: a circuit basis for epileptic seizures in mice carrying an Scn1a gene mutation. J. Neurosci. Off. J. Soc. Neurosci. *27*, 5903–5914.

Ogiwara, I., Iwasato, T., Miyamoto, H., Iwata, R., Yamagata, T., Mazaki, E., Yanagawa, Y., Tamamaki, N., Hensch, T.K., Itohara, S., et al. (2013). Nav1.1 haploinsufficiency in excitatory neurons ameliorates seizure-associated sudden death in a mouse model of Dravet syndrome. Hum. Mol. Genet. *22*, 4784–4804.

Ohmori, I., Ohtsuka, Y., Ouchida, M., Ogino, T., Maniwa, S., Shimizu, K., and Oka, E. (2003). Is phenotype difference in severe myoclonic epilepsy in infancy related to SCN1A mutations? Brain Dev. *25*, 488–493.

Okuno, H. (2011). Regulation and function of immediate-early genes in the brain: Beyond neuronal activity markers. Neurosci. Res. *69*, 175–186.

Onorati, M., Binetti, M., Conti, L., Camnasio, S., Calabrese, G., Albieri, I., Di Febo, F., Toselli, M., Biella, G., Martynoga, B., et al. (2010). Preservation of positional identity in fetus-derived neural stem (NS) cells from different mouse central nervous system compartments. Cell. Mol. Life Sci. CMLS.

Orlando, S.J., Santiago, Y., DeKelver, R.C., Freyvert, Y., Boydston, E.A., Moehle, E.A., Choi, V.M., Gopalan, S.M., Lou, J.F., Li, J., et al. (2010). Zinc-finger nuclease-driven targeted integration into mammalian genomes using donors with limited chromosomal homology. Nucleic Acids Res. *38*, e152.

Pandolfo, M., and Manto, M. (2013). Cerebellar and afferent ataxias. Contin. Minneap. Minn *19*, 1312–1343.

Papa, F.T., Mencarelli, M.A., Caselli, R., Katzaki, E., Sampieri, K., Meloni, I., Ariani, F., Longo, I., Maggio, A., Balestri, P., et al. (2008). A 3 Mb deletion in 14q12 causes severe mental retardation, mild facial dysmorphisms and Rett-like features. Am. J. Med. Genet. A. *146A*, 1994–1998.

Peng, H., Begg, G.E., Harper, S.L., Friedman, J.R., Speicher, D.W., and Rauscher, F.J. (2000). Biochemical analysis of the Kruppel-associated box (KRAB) transcriptional repression domain. J. Biol. Chem. *275*, 18000–18010.

Perdue, M.L., Garcia, M., Beck, J., Brugh, M., and Swayne, D.E. (1996). An Arg-Lys insertion at the hemagglutinin cleavage site of an H5N2 avian influenza isolate. Virus Genes *12*, 77–84.

Perez-Pinera, P., Ousterout, D.G., Brunger, J.M., Farin, A.M., Glass, K.A., Guilak, F., Crawford, G.E., Hartemink, A.J., and Gersbach, C.A. (2013). Synergistic and tunable human gene activation by combinations of synthetic transcription factors. Nat. Methods *10*, 239–242.

Peters, J.M., Colavin, A., Shi, H., Czarny, T.L., Larson, M.H., Wong, S., Hawkins, J.S., Lu, C.H.S., Koo, B.-M., Marta, E., et al. (2016). A Comprehensive, CRISPR-based Functional Analysis of Essential Genes in Bacteria. Cell *165*, 1493–1506.

Pintaudi, M., Calevo, M.G., Vignoli, A., Parodi, E., Aiello, F., Baglietto, M.G., Hayek, Y., Buoni, S., Renieri, A., Russo, S., et al. (2010). Epilepsy in Rett syndrome: clinical and genetic features. Epilepsy Behav. EB *19*, 296–300.

Place, R.F., Li, L.-C., Pookot, D., Noonan, E.J., and Dahiya, R. (2008). MicroRNA-373 induces expression of genes with complementary promoter sequences. Proc. Natl. Acad. Sci. U. S. A. *105*, 1608–1613.

Plasterer, H.L., Deutsch, E.C., Belmonte, M., Egan, E., Lynch, D.R., and Rusche, J.R. (2013). Development of frataxin gene expression measures for the evaluation of experimental treatments in Friedreich's ataxia. PloS One *8*, e63958.

Portnoy, V., Huang, V., Place, R.F., and Li, L.-C. (2011). Small RNA and transcriptional upregulation. Wiley Interdiscip. Rev. RNA *2*, 748–760.

Portnoy, V., Lin, S.H.S., Li, K.H., Burlingame, A., Hu, Z.-H., Li, H., and Li, L.-C. (2016). saRNA-guided Ago2 targets the RITA complex to promoters to stimulate transcription. Cell Res. *26*, 320–335.

Punga, T., and Bühler, M. (2010). Long intronic GAA repeats causing Friedreich ataxia impede transcription elongation. EMBO Mol. Med. *2*, 120–129.

Puspasari, N., Rowley, S.M., Gordon, L., Lockhart, P.J., Ioannou, P.A., Delatycki, M.B., and Sarsero, J.P. (2011). Long range regulation of human FXN gene expression. PloS One *6*, e22001.

Qi, L.S., Larson, M.H., Gilbert, L.A., Doudna, J.A., Weissman, J.S., Arkin, A.P., and Lim, W.A. (2013). Repurposing CRISPR as an RNA-guided platform for sequence-specific control of gene expression. Cell *152*, 1173–1183.

Raciti, M., Granzotto, M., Duc, M.D., Fimiani, C., Cellot, G., Cherubini, E., and Mallamaci, A. (2013). Reprogramming fibroblasts to neural-precursor-like cells by structured overexpression of pallial patterning genes. Mol. Cell. Neurosci. *57*, 42–53.

Rai, M., Soragni, E., Jenssen, K., Burnett, R., Herman, D., Coppola, G., Geschwind, D.H., Gottesfeld, J.M., and Pandolfo, M. (2008). HDAC inhibitors correct frataxin deficiency in a Friedreich ataxia mouse model. PloS One *3*, e1958.

Rajeswari, M.R. (2012). DNA triplex structures in neurodegenerative disorder, Friedreich's ataxia. J. Biosci. *37*, 519–532.

Ran, F.A., Hsu, P.D., Lin, C.-Y., Gootenberg, J.S., Konermann, S., Trevino, A.E., Scott, D.A., Inoue, A., Matoba, S., Zhang, Y., et al. (2013). Double nicking by RNA-guided CRISPR Cas9 for enhanced genome editing specificity. Cell *154*, 1380–1389.

Reetz, K., Dogan, I., Costa, A.S., Dafotakis, M., Fedosov, K., Giunti, P., Parkinson, M.H., Sweeney, M.G., Mariotti, C., Panzeri, M., et al. (2015). Biological and clinical characteristics of the European Friedreich's Ataxia Consortium for Translational Studies (EFACTS) cohort: a cross-sectional analysis of baseline data. Lancet Neurol. *14*, 174–182.

Romaniuk, P.J., Lowary, P., Wu, H.N., Stormo, G., and Uhlenbeck, O.C. (1987). RNA binding site of R17 coat protein. Biochemistry (Mosc.) *26*, 1563–1568.

Römer, P., Hahn, S., Jordan, T., Strauss, T., Bonas, U., and Lahaye, T. (2007). Plant pathogen recognition mediated by promoter activation of the pepper Bs3 resistance gene. Science *318*, 645–648.

Roth, M., Bonev, B., Lindsay, J., Lea, R., Panagiotaki, N., Houart, C., and Papalopulu, N. (2010). FoxG1 and TLE2 act cooperatively to regulate ventral telencephalon formation. Dev. Camb. Engl. *137*, 1553–1562.

Sakamoto, N., Ohshima, K., Montermini, L., Pandolfo, M., and Wells, R.D. (2001). Sticky DNA, a self-associated complex formed at long GAA*TTC repeats in intron 1 of the frataxin gene, inhibits transcription. J. Biol. Chem. *276*, 27171–27177.

Sander, J.D., Dahlborg, E.J., Goodwin, M.J., Cade, L., Zhang, F., Cifuentes, D., Curtin, S.J., Blackburn, J.S., Thibodeau-Beganny, S., Qi, Y., et al. (2011). Selection-free zinc-finger-nuclease engineering by context-dependent assembly (CoDA). Nat. Methods *8*, 67–69.

Sandi, C., Sandi, M., Anjomani Virmouni, S., Al-Mahdawi, S., and Pook, M.A. (2014). Epigenetic-based therapies for Friedreich ataxia. Front. Genet. *5*, 165.

Sansom, S.N., Griffiths, D.S., Faedo, A., Kleinjan, D.-J., Ruan, Y., Smith, J., van Heyningen, V., Rubenstein, J.L., and Livesey, F.J. (2009). The level of the transcription factor Pax6 is essential for controlling the balance between neural stem cell self-renewal and neurogenesis. PLoS Genet. *5*, e1000511.

Sapranauskas, R., Gasiunas, G., Fremaux, C., Barrangou, R., Horvath, P., and Siksnys, V. (2011). The Streptococcus thermophilus CRISPR/Cas system provides immunity in Escherichia coli. Nucleic Acids Res. *39*, 9275–9282.

Scala, E., Ariani, F., Mari, F., Caselli, R., Pescucci, C., Longo, I., Meloni, I., Giachino, D., Bruttini, M., Hayek, G., et al. (2005). CDKL5/STK9 is mutated in Rett syndrome variant with infantile spasms. J. Med. Genet. *42*, 103–107.

Schatz, P.J., Pillus, L., Grisafi, P., Solomon, F., and Botstein, D. (1986). Two functional alpha-tubulin genes of the yeast Saccharomyces cerevisiae encode divergent proteins. Mol. Cell. Biol. *6*, 3711–3721.

Scheffer, I.E., Wallace, R., Mulley, J.C., and Berkovic, S.F. (2001). Clinical and molecular genetics of myoclonic-astatic epilepsy and severe myoclonic epilepsy in infancy (Dravet syndrome). Brain Dev. *23*, 732–735.

Schmucker, S., and Puccio, H. (2010). Understanding the molecular mechanisms of Friedreich's ataxia to develop therapeutic approaches. Hum. Mol. Genet. *19*, R103-110.

Schmucker, S., Argentini, M., Carelle-Calmels, N., Martelli, A., and Puccio, H. (2008). The in vivo mitochondrial two-step maturation of human frataxin. Hum. Mol. Genet. *17*, 3521–3531.

Schmucker, S., Martelli, A., Colin, F., Page, A., Wattenhofer-Donzé, M., Reutenauer, L., and Puccio, H. (2011). Mammalian frataxin: an essential function for cellular viability through an interaction with a preformed ISCU/NFS1/ISD11 iron-sulfur assembly complex. PloS One *6*, e16199.

Schornack, S., Minsavage, G.V., Stall, R.E., Jones, J.B., and Lahaye, T. (2008). Characterization of AvrHah1, a novel AvrBs3-like effector from Xanthomonas gardneri with virulence and avirulence activity. New Phytol. *179*, 546–556.

Schwartz, J.C., Younger, S.T., Nguyen, N.-B., Hardy, D.B., Monia, B.P., Corey, D.R., and Janowski, B.A. (2008). Antisense transcripts are targets for activating small RNAs. Nat. Struct. Mol. Biol. *15*, 842–848.

Segal, D.J., Dreier, B., Beerli, R.R., and Barbas, C.F. (1999). Toward controlling gene expression at will: selection and design of zinc finger domains recognizing each of the 5'-GNN-3' DNA target sequences. Proc. Natl. Acad. Sci. U. S. A. *96*, 2758–2763.

Segal, D.J., Crotty, J.W., Bhakta, M.S., Barbas, C.F., and Horton, N.C. (2006). Structure of Aart, a designed six-finger zinc finger peptide, bound to DNA. J. Mol. Biol. *363*, 405–421.

Seidman, J.G., and Seidman, C. (2002). Transcription factor haploinsufficiency: when half a loaf is not enough. J. Clin. Invest. *109*, 451–455.

Seltzer, L.E., and Paciorkowski, A.R. (2014). Genetic disorders associated with postnatal microcephaly. Am. J. Med. Genet. C Semin. Med. Genet. *166C*, 140–155.

Shen, L., Nam, H.-S., Song, P., Moore, H., and Anderson, S.A. (2006). FoxG1 haploinsufficiency results in impaired neurogenesis in the postnatal hippocampus and contextual memory deficits. Hippocampus *16*, 875–890.

Shoichet, S.A., Kunde, S.-A., Viertel, P., Schell-Apacik, C., von Voss, H., Tommerup, N., Ropers, H.-H., and Kalscheuer, V.M. (2005). Haploinsufficiency of novel FOXG1B variants in a patient with severe mental retardation, brain malformations and microcephaly. Hum. Genet. *117*, 536–544.

Siegenthaler, J.A., Tremper-Wells, B.A., and Miller, M.W. (2008). Foxg1 haploinsufficiency reduces the population of cortical intermediate progenitor cells: effect of increased p21 expression. Cereb. Cortex N. Y. N 1991 *18*, 1865–1875.

Silva, A.M., Brown, J.M., Buckle, V.J., Wade-Martins, R., and Lufino, M.M.P. (2015). Expanded GAA repeats impair FXN gene expression and reposition the FXN locus to the nuclear lamina in single cells. Hum. Mol. Genet. *24*, 3457–3471.

Spigoni, G., Gedressi, C., and Mallamaci, A. (2010). Regulation of Emx2 Expression by Antisense Transcripts in Murine Cortico-Cerebral Precursors. PLoS ONE *5*, e8658.

Spring, K., Ahangari, F., Scott, S.P., Waring, P., Purdie, D.M., Chen, P.C., Hourigan, K., Ramsay, J., McKinnon, P.J., Swift, M., et al. (2002). Mice heterozygous for mutation in Atm, the gene involved in ataxia-telangiectasia, have heightened susceptibility to cancer. Nat. Genet. *32*, 185–190.

Stehling, O., Sheftel, A.D., and Lill, R. (2009). Chapter 12 Controlled expression of iron-sulfur cluster assembly components for respiratory chain complexes in mammalian cells. Methods Enzymol. *456*, 209–231.

Stringer, K.F., Ingles, C.J., and Greenblatt, J. (1990). Direct and selective binding of an acidic transcriptional activation domain to the TATA-box factor TFIID. Nature *345*, 783–786.

Suls, A., Claeys, K.G., Goossens, D., Harding, B., Van Luijk, R., Scheers, S., Deprez, L., Audenaert, D., Van Dyck, T., Beeckmans, S., et al. (2006). Microdeletions involving the SCN1A gene may be common in SCN1A-mutation-negative SMEI patients. Hum. Mutat. *27*, 914–920.

Takizawa, T., and Meshorer, E. (2008). Chromatin and nuclear architecture in the nervous system. Trends Neurosci. *31*, 343–352.

Tanenbaum, M.E., Gilbert, L.A., Qi, L.S., Weissman, J.S., and Vale, R.D. (2014). A protein-tagging system for signal amplification in gene expression and fluorescence imaging. Cell *159*, 635–646.

Tao, W., and Lai, E. (1992). Telencephalon-restricted expression of BF-1, a new member of the HNF-3/fork head gene family, in the developing rat brain. Neuron *8*, 957–966.

Thakore, P.I., D'Ippolito, A.M., Song, L., Safi, A., Shivakumar, N.K., Kabadi, A.M., Reddy, T.E., Crawford, G.E., and Gersbach, C.A. (2015). Highly specific epigenome editing by CRISPR-Cas9 repressors for silencing of distal regulatory elements. Nat. Methods *12*, 1143–1149.

Tourtellotte, W.G., and Milbrandt, J. (1998). Sensory ataxia and muscle spindle agenesis in mice lacking the transcription factor Egr3. Nat. Genet. *20*, 87–91.

Tsou, A.Y., Paulsen, E.K., Lagedrost, S.J., Perlman, S.L., Mathews, K.D., Wilmot, G.R., Ravina, B., Koeppen, A.H., and Lynch, D.R. (2011). Mortality in Friedreich ataxia. J. Neurol. Sci. *307*, 46–49.

Urlinger, S., Baron, U., Thellmann, M., Hasan, M.T., Bujard, H., and Hillen, W. (2000). Exploring the sequence space for tetracycline-dependent transcriptional activators: novel mutations yield expanded range and sensitivity. Proc. Natl. Acad. Sci. U. S. A. *97*, 7963–7968.

Urnov, F.D., Miller, J.C., Lee, Y.-L., Beausejour, C.M., Rock, J.M., Augustus, S., Jamieson, A.C., Porteus, M.H., Gregory, P.D., and Holmes, M.C. (2005). Highly efficient endogenous human gene correction using designed zinc-finger nucleases. Nature *435*, 646–651.

Vaquero, A., Scher, M., Lee, D., Erdjument-Bromage, H., Tempst, P., and Reinberg, D. (2004). Human SirT1 interacts with histone H1 and promotes formation of facultative heterochromatin. Mol. Cell *16*, 93–105.

Vaquero, A., Scher, M., Erdjument-Bromage, H., Tempst, P., Serrano, L., and Reinberg, D. (2007). SIRT1 regulates the histone methyl-transferase SUV39H1 during heterochromatin formation. Nature *450*, 440–444.

Vojta, A., Dobrinić, P., Tadić, V., Bočkor, L., Korać, P., Julg, B., Klasić, M., and Zoldoš, V. (2016). Repurposing the CRISPR-Cas9 system for targeted DNA methylation. Nucleic Acids Res. *44*, 5615–5628.

Wells, R.D. (2008). DNA triplexes and Friedreich ataxia. FASEB J. Off. Publ. Fed. Am. Soc. Exp. Biol. *22*, 1625–1634.

Westenbroek, R.E., Merrick, D.K., and Catterall, W.A. (1989). Differential subcellular localization of the RI and RII Na+ channel subtypes in central neurons. Neuron *3*, 695–704.

Xiao, H., Pearson, A., Coulombe, B., Truant, R., Zhang, S., Regier, J.L., Triezenberg, S.J., Reinberg, D., Flores, O., and Ingles, C.J. (1994). Binding of basal transcription factor TFIIH to the acidic activation domains of VP16 and p53. Mol. Cell. Biol. *14*, 7013–7024.

Xuan, S., Baptista, C.A., Balas, G., Tao, W., Soares, V.C., and Lai, E. (1995). Winged helix transcription factor BF-1 is essential for the development of the cerebral hemispheres. Neuron *14*, 1141–1152.

Yamakawa, K. (2011). Molecular and cellular basis: insights from experimental models of Dravet syndrome. Epilepsia *52 Suppl 2*, 70–71.

Yang, H., Wang, H., Shivalila, C.S., Cheng, A.W., Shi, L., and Jaenisch, R. (2013). One-step generation of mice carrying reporter and conditional alleles by CRISPR/Cas-mediated genome engineering. Cell *154*, 1370–1379.

Yeung, A., Bruno, D., Scheffer, I.E., Carranza, D., Burgess, T., Slater, H.R., and Amor, D.J. (2009). 4.45 Mb microduplication in chromosome band 14q12 including FOXG1 in a girl with refractory epilepsy and intellectual impairment. Eur. J. Med. Genet. *52*, 440–442.

Yu, F.H., Mantegazza, M., Westenbroek, R.E., Robbins, C.A., Kalume, F., Burton, K.A., Spain, W.J., McKnight, G.S., Scheuer, T., and Catterall, W.A. (2006). Reduced sodium current in GABAergic interneurons in a mouse model of severe myoclonic epilepsy in infancy. Nat. Neurosci. *9*, 1142–1149.

Yue, X., Schwartz, J.C., Chu, Y., Younger, S.T., Gagnon, K.T., Elbashir, S., Janowski, B.A., and Corey, D.R. (2010). Transcriptional regulation by small RNAs at sequences downstream from 3' gene termini. Nat. Chem. Biol. *6*, 621–629.

Zalatan, J.G., Lee, M.E., Almeida, R., Gilbert, L.A., Whitehead, E.H., La Russa, M., Tsai, J.C., Weissman, J.S., Dueber, J.E., Qi, L.S., et al. (2015). Engineering complex synthetic transcriptional programs with CRISPR RNA scaffolds. Cell *160*, 339–350.

Zhang, F., Cong, L., Lodato, S., Kosuri, S., Church, G.M., and Arlotta, P. (2011a). Efficient construction of sequence-specific TAL effectors for modulating mammalian transcription. Nat. Biotechnol. *29*, 149–153.

Zhang, H., Yang, B., Mu, X., Ahmed, S.S., Su, Q., He, R., Wang, H., Mueller, C., Sena-Esteves, M., Brown, R., et al. (2011b). Several rAAV Vectors Efficiently Cross the Blood–brain Barrier and Transduce Neurons and Astrocytes in the Neonatal Mouse Central Nervous System. Mol. Ther. *19*, 1440–1448.

Zhao, Y., Dai, Z., Liang, Y., Yin, M., Ma, K., He, M., Ouyang, H., and Teng, C.-B. (2014). Sequence-specific inhibition of microRNA via CRISPR/CRISPRi system. Sci. Rep. *4*, 3943.

Zhou, Y., Zhu, S., Cai, C., Yuan, P., Li, C., Huang, Y., and Wei, W. (2014). High-throughput screening of a CRISPR/Cas9 library for functional genomics in human cells. Nature *509*, 487–491.

Zhu, H., Joliot, V., and Prywes, R. (1994). Role of transcription factor TFIIF in serum response factor-activated transcription. J. Biol. Chem. *269*, 3489–3497.

Zucchelli, S., Fasolo, F., Russo, R., Cimatti, L., Patrucco, L., Takahashi, H., Jones, M.H., Santoro, C., Sblattero, D., Cotella, D., et al. (2015). SINEUPs are modular antisense long non-coding RNAs that increase synthesis of target proteins in cells. Front. Cell. Neurosci. *9*, 174.